

Final Report

FEASIBILITY STUDY OF SCANNING CELESTIAL ATTITUDE SYSTEM (SCADS)
FOR EARTH RESOURCES TECHNOLOGY SATELLITE (ERTS)

Contract No. NAS5-21552

August, 1971

Prepared for:

National Aeronautics and Space Administration
Goddard Space Flight Center
Greenbelt, Maryland

CONTROL DATA CORPORATION
Navigation and Space Systems
3101 East 80th Street
Minneapolis, Minnesota 55420

RD 1102

(NASA-CR-122361) FEASIBILITY STUDY OF
SCANNING CELESTIAL ATTITUDE SYSTEM (SCADS)
FOR EARTH RESOURCES TECHNOLOGY SATELLITE
(ERTS) Final Report (Control Data Corp.)
Aug. 1971 122 p

Reproduced by
**NATIONAL TECHNICAL
INFORMATION SERVICE**
U S Department of Commerce
Springfield VA 22151



N72-18657

Unclas
19511

Final Report

FEASIBILITY STUDY OF SCANNING CELESTIAL ATTITUDE SYSTEM (SCADS)
FOR EARTH RESOURCES TECHNOLOGY SATELLITE (ERTS)

Contract No. NAS5-21552

August, 1971

Prepared for:

National Aeronautics and Space Administration
Goddard Space Flight Center
Greenbelt, Maryland

CONTROL DATA CORPORATION
Navigation and Space Systems
3101 East 80th Street
Minneapolis, Minnesota 55420

RD 1102

ABSTRACT

The principal purpose of this study is to investigate the feasibility of using the Scanning Celestial Attitude Determination System (SCADS) during Earth Resources Technology Satellite (ERTS) missions to compute an accurate spacecraft attitude by use of stellar measurements. The spacecraft is that designed by G. E. Corporation, and is local-vertical-stablized.

A heuristic discussion of the SCADS concept is first given. Two concepts are introduced: a passive system which contains no moving parts, and an active system in which the reticle is caused to rotate about the sensor's axis. Later it is shown that the aperture diameter may be one inch for the passive system, and two inches for the active system.

A quite complete development of the equations of attitude motions is then given. These equations are used to generate the true attitude which in turn is used to compute the transit times of detectable stars and to determine the errors associated with the SCADS attitude.

The stray light problem which originates because of direct sunlight, earth-reflected sunlight, and spacecraft-reflected sunlight is then considered. It is shown that a location aboard the spacecraft's lower sensor ring does exist which minimizes the stray light problem and also provides a favorable location for the SCADS sensor.

A more complete discussion of the analytical foundation of SCADS concept and its use for the geometries particular to this study is then given. Also given are salient design parameters for the passive and active systems.

An error analysis indicates the errors of the passive and active systems (two head sensor) to be on the order of 0.04° and 0.02° , respectively. These errors are associated with a worst-case attitude control and a worst-case stellar background.

Finally, suggestions are given which might reduce these attitude errors. The suggestions involve changes in the slit-pattern and method of data reduction.

FOREWORD

This final report represents a complete technical documentation of all efforts performed under Contract NAS5-21552, and does not require supplementation by interim reports. It represents eight man-months of funded effort.

The study was performed by the Systems Analysis Group of Navigation and Space Systems, Control Data Corporation. Mr. C. B. Grosch was project engineer. Other participants were W. V. Berge and L. J. Wilson.

Control Data Corporation would like to acknowledge the assistance of Henry Hoffman and Gilbert Fleisher (Project Technical Officer) of NASA Goddard. They defined the problem and suggested several of the general methods used to obtain the solution given herein.

TABLE OF CONTENTS

Title Page	i
Abstract	ii
Foreword	iii
Table of Contents	iv
List of Tables and Figures	v
INTRODUCTION	1
Transit Rate	2
Model	5
Orbit	7
Attitude Parameters	8
SYMBOLS	10
SYSTEMS OF COORDINATES	12
EQUATIONS OF MOTION	17
SENSOR LOCATION ABOARD THE SPACECRAFT	30
EQUATIONS IMPLIED BY A MEASURED TRANSIT TIME	39
THE ATTITUDE MODEL	42
Constant Yaw, Pitch, and Roll Mode	44
Good Geometry	44
Weighting of Measurements	48
Estimation of Angular Velocity from Flywheel Outputs	49
DETERMINATION OF ATTITUDE	56
STELLAR AVAILABILITY AND DETECTABILITY	59
RESULTS	69
Passive System	72
Active System	78
AREAS FOR ADDITIONAL INVESTIGATIONS	84
Instrumentation	84
Star Identification	86
Analysis	86
CONCLUDING REMARKS	87
Instrumentation	87
Data Reduction	88
Error Analysis	89
REFERENCES	90
APPENDIX A: ANGULAR MOMENTUM OF A BODY COMPOSED OF CONNECTED RIGID SECTIONS	91
APPENDIX B: INERTIA TENSOR OF THE SOLAR ARRAY	95
APPENDIX C: THE SKEW-SYMMETRIC MATRIX $\mathbf{A}\mathbf{A}'$ AND THE ANGULAR VELOCITY	101
APPENDIX D: THE EXTERNAL TORQUE	108
APPENDIX E: DETERMINATION OF APPROXIMATE INGRESS, EGRESS, AND TRANSIT TIME	111

LIST OF TABLES AND FIGURES

Table I:	Methods of Increasing Data Rate	4
Table II:	Advantages and Disadvantages of a Passive System with Respect to an Active System	6
Table III:	Orbital Parameters	8
Table IV:	Attitude Parameters	9
Table V:	Instrumentation Parameters	60
Table VI:	$m_T(P)$ and $\sigma_T(m_T(P))$	65
Table VII:	Parameters Which Define the Chosen Error in the Constant Attitude ($t_0 = 0$)	71
Table VIII:	Standard Deviation of Yaw, Pitch, and Roll Errors, Number of Stars Transited, and Number of Transits. Attitude Errors in Degrees x 100. $\Omega = 0$.	83
Figure 1:	Schematic of Radial Slit Instrumentation.	3
Figure 2:	Orientation of Optical Axis and Slit with Respect to the Spacecraft.	14
Figure 3:	Geometry of Solar Panels, Optic Origin, and Optic Axis Direction.	31
Figure 4:	Minimum Angle Between Optical Axis and Solar Panel Envelope as a Function of Sensor Location and Optical Axis Elevation.	36
Figure 5:	Minimum Angle Between Optical Axis of Each Head and Solar Panel as a Function of Solar Panel Angle.	37
Figure 6:	Viewing Geometry as seen from the Spacecraft.	38
Figure 7:	The Slit and Its Relationship to the Spacecraft.	40
Figure 8:	Yaw, and Two Approximations of Yaw as a Function of Time.	43
Figure 9:	The Preferred Direction.	46
Figure 10:	The Preferred Axes for the Single-Head Sensor.	46
Figure 11:	Placement of Three Stars to Yield the Optimum Geometry for the Single Head.	47
Figure 12:	The Two-Head Sensor Geometry.	47
Figure 13:	Method of Weighting to More Utilize Those Measurements Nearest to the Time at Which the Attitude is Desired.	50
Figure 14:	Estimated Pitch Rate and True Pitch Rate as a Function of Time. $1640 \leq t \leq 2400$ Seconds.	56
Figure 15:	Iterative Method of Obtaining Instrumentation Parameters.	61

LIST OF TABLES AND FIGURES - continued

Figure 16:	Slit Pattern for Passive System.	63
Figure 17:	Slit Pattern for Active System.	64
Figure 18:	Detection Probability as a Function of Stellar Magnitude and Instrumentation Spin Period.	66
Figure 19:	Average Number of Transits/Second for Passive System and Active System.	68
Figure 20:	Method Used to Compute True Attitude and Star Sensor Attitude.	70
Figure 21:	True Yaw and Pitch as a Function of Time.	73
Figure 22:	True Yaw, Error in Control Yaw, Yaw Flywheel Angular Momentum, and Yaw External Torque.	74
Figure 23:	Cumulative Distribution Function of Roll Error. Passive System, One and Two Heads.	75
Figure 24:	Yaw and Pitch, and Two Estimates of Yaw and Pitch for $960 \leq t \leq 1380$ Seconds.	76
Figure 25:	Yaw and Pitch, and Two Estimates of Yaw and Pitch for $1640 \leq t \leq 2040$ Seconds.	77
Figure 26:	Cumulative Distribution Functions of Roll and Yaw Errors: Two Heads.	79
Figure 27:	Cumulative Distribution Functions of Roll and Yaw Errors: Single Head.	80
Figure 28:	Estimated Yaw, $\tilde{\psi}$, and ψ .	81
Figure 29:	Possible Improvement of Slit Pattern for the Active System.	85
Figure 30:	Possible Improvement of Slit Pattern for the Passive System.	85

INTRODUCTION

Consider a nearly local-vertical-stabilized satellite orbiting the earth. Let S_4 denote the local-vertical¹ system of coordinates which is associated with the instantaneous satellite position. Also, let S_7 be a system of coordinates fixed in some portion of the satellite (S_4 and S_7 will be defined more precisely in the next sections). The orientation of S_7 with respect to S_4 may be defined by three angles ψ , θ , φ which will be called yaw, pitch, and roll, respectively. The general problem is to determine the satellite's yaw, pitch, and roll at any given time by utilizing a particular set of onboard stellar measurements.

Suppose an optical system is constructed so as to provide a set of viewing directions which lie on a curve $\hat{d}(\eta)$, $\eta_1 \leq \eta \leq \eta_2$. Where $\hat{d}(\eta)$ is a unit vector whose components with respect to S_7 are known if η were given.

Since S_7 is changing orientation with respect to an inertial system, the curve of viewing directions $\hat{d}(\eta)$ will intermittently sweep across a star. This event is called a transit and the instant of its occurrence is called a transit time.

At any transit time, which is produced by a known star,² the spacecraft's attitude is constrained. This constraint is generated as follows:

- (1) The direction to the star resolved in S_7 is known except for a single parameter, η .
- (2) This direction may be resolved in S_4 by introducing yaw, pitch, and roll at the measured time. Thus, the direction resolved in S_4 is known except for four parameters: η , $\psi(t_i)$, $\theta(t_i)$, $\varphi(t_i)$, where t_i is the i^{th} measured transit time.

¹It is assumed that the satellite's position is a known function of time; hence, the orientation of S_4 with respect to a preferred inertial system is known.

²The problem of identifying the transited star is not trivial. However, it will not be considered here. A discussion of the problem and its solution for two particular geometries may be found in References 1 and 2.

- (3) Since the star is identified, its direction with respect to S_4 is readily computable with the aid of the star catalog and the satellite's known position.
- (4) Equating these two directions to the star yields two independent equations in the unknowns η , $\psi(t_i)$, $\theta(t_i)$, $\varphi(t_i)$.
- (5) The parasitic unknown, η , may be eliminated from these two equations to obtain one equation in the unknowns $\psi(t_i)$, $\theta(t_i)$, and $\varphi(t_i)$.

The equation generated at Step (5) will be called the constraint equation implied by the measured transit time. The ease with which η may be eliminated from the two equations obtained at Step (4) is dependent upon the functional form of $\hat{d}(\eta)$. The elimination is particularly simple if the directions $\hat{d}(\eta)$ lie on a right circular cone. Fortunately, the instrumentation of forming $\hat{d}(\eta)$ to lie on such a cone is simple. Even more simplification is obtained if $\hat{d}(\eta)$ lies in a plane. This type of configuration is assumed in this study, and is pictured schematically in Figure 1. Because of the instrumentation, we call the optical element which generates the viewing directions, $\hat{d}(\eta)$, a slit; and the portion of a plane which contains $\hat{d}(\eta)$ a slit-plane.

Two problems, which are given considerable attention later in the study, may be noted. The first may be called the transit-rate problem; the second, the modeling problem.

Transit Rate

Our discussion thus far defined a slit-plane to have a fixed orientation with respect to S_7 . Such a system will be called a passive system. At any instant of time, a star may or may not lie in this plane. If a star is not detected, no information is obtained. Transits will be gathered, however, since S_7 changes orientation with respect to an inertial system. But, this change in orientation is rather slow (approximately one revolution/orbital period); so, too few transits tend to be gathered. Some methods of overcoming this difficulty are listed in Table I. Also listed is the qualitative effect of each change.

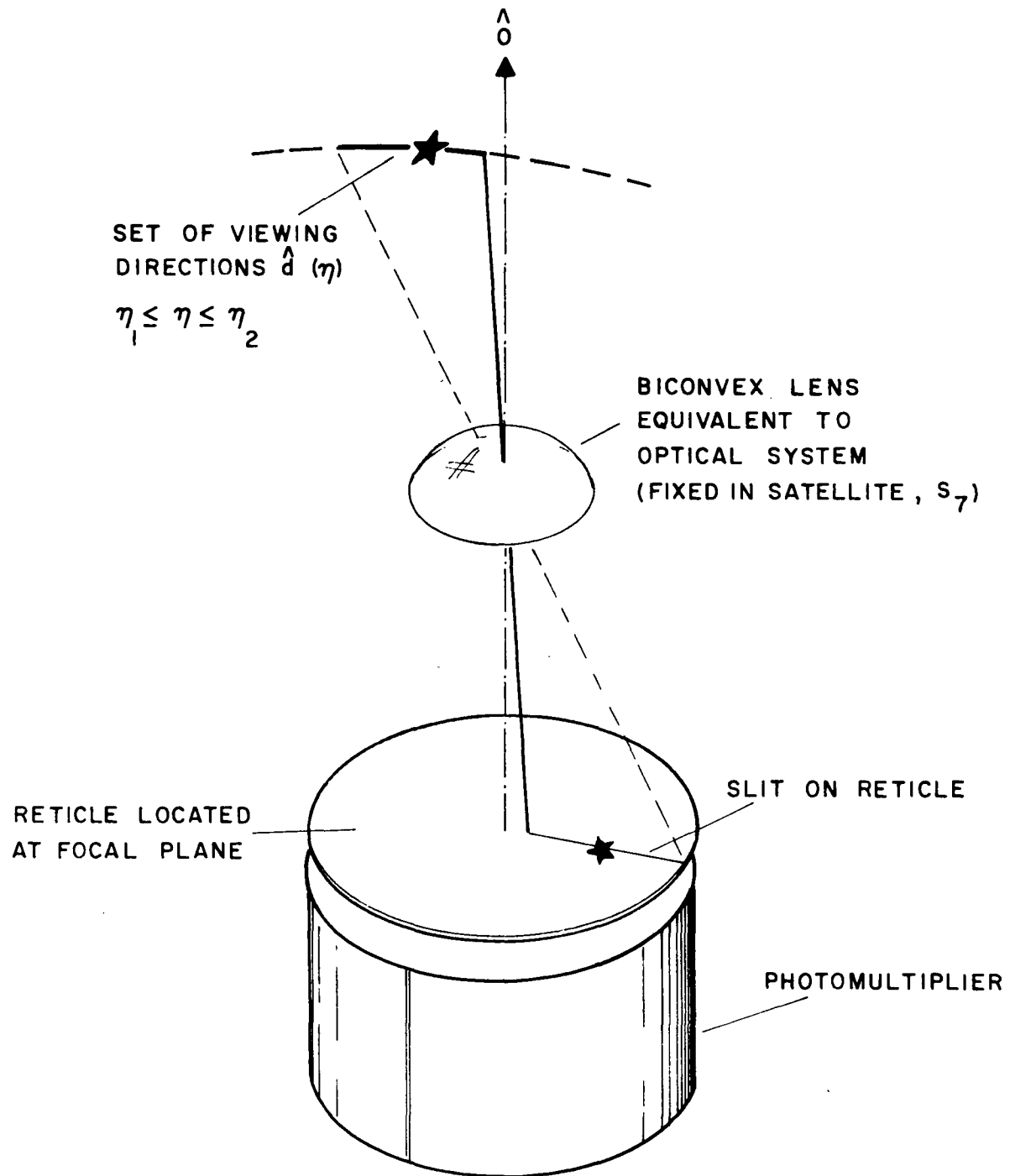


Figure 1: Schematic of Radial Slit Instrumentation.

TABLE I
METHODS OF INCREASING DATA RATE

Parameter Change	Qualitative Effect
1. Increase field of view	Adds more stars, more background noise, increases optical inaccuracies or adds to optical costs, adds more weight.
2. Increase number of slits	Adds more transits/star, more background noise, greater fabrication difficulties, complicates star identification, increases possibility of near simultaneous transits (since only one photo-detector is used).
3. Increase number of sensor heads	Makes for better stellar geometry, adds candidate stars, increases cost, size, weight, power requirements; but, reduces size, etc., of each individual head.
4. Sense dimmer stars	Adds candidate stars, complicates star identification, increases optical aperture, puts more load on optics and electronics in terms of accuracy and sensitivity, increases probability of false transits.
5. Rotate the reticle about the optical axis	Adds more transits/star, requires an angle encoder or its equivalent to sense orientation of reticle with respect to S_7 , increases optical aperture, increases cost, decreases reliability.

Parameter changes 2 and 3 can be used very effectively for the passive system. Hence, the recommended passive system consists of two heads, in which each sensor head possesses 5 slits (Figures 6 and 16).

Parameter change 5 yields a configuration which will be called an "active" system. This term is used because the reticle is made to rotate within the instrument. In this case, the viewing directions are specified as $\hat{d}(\eta, t)$ or $\hat{d}(\eta, \theta)$, where t is time and θ is an angle encoder reading. Again, \hat{d} is known except for a single parameter η so the previous discussion still holds for the active system.

The advantages and disadvantages of a passive system with respect to an active system for a nearly local-vertical-stabilized satellite are given in Table II.

A major question, which is answered in this study, is the accuracy with which the passive and active systems can determine the spacecraft's attitude. Another important question--What is the optimum spin rate if an active system is to be used?--is also dealt with.

Model

The second major concern is the attitude model which dictates the form of the yaw, pitch, and roll motion which is to be used in reducing the data. The need for such a model arises because the basic constraint simply yields one equation in $\psi(t_i)$, $\theta(t_i)$, $\phi(t_i)$ which are yaw, pitch, and roll at the measured transit time. Since only one transit time is, in general, gathered at t_i and perhaps no transit times are gathered at a time at which an attitude estimate is desired; a time-dependent characterization of yaw, pitch, and roll must be given beforehand. This attitude model may then be used to couple the constraint equations. So as not to yield an unwieldy or ill-conditioned numerical problem, the functional form of the attitude model must contain only a few unknown parameters.

TABLE II
ADVANTAGES AND DISADVANTAGES OF A PASSIVE SYSTEM
WITH RESPECT TO AN ACTIVE SYSTEM

Passive Advantages	Passive Disadvantages
<ol style="list-style-type: none"> 1. <u>Size</u>. The optical aperture tends to be smaller since the slits scan slowly with respect to the stellar background. Also, no drive or read-out mechanism of the driven reticle is required. 2. <u>Power</u>. 3. <u>Weight</u>. 4. <u>Reliability</u>. 5. <u>Cost</u>. 6. <u>Onboard Storage</u>. Since fewer transits are gathered per unit time, less total onboard storage is required. 7. <u>More Nearly Uniform Stellar Distribution</u>. Since the scan is slow, dim stars can be detected. As the spin rate of the active system is increased, only the brighter stars are detected. More transits may be gathered per orbital period, but the rate tends to be less and less uniform as the spin rate is increased. 	<ol style="list-style-type: none"> 1. <u>Model</u>. Since the star transits are gathered more slowly, the transits used to compute the attitude are necessarily spread over a longer time interval. Thus, a more complete model of the attitude motion may be required. 2. <u>Analysis</u>. More difficult. 3. <u>Data Reduction</u>. 4. <u>Attitude Error</u>. Greater RMS error over all cases in one orbital period.

A second model is necessary in this study, this is the "real-world" model. This study uses the attitude dynamics as governed by the ERTS spacecraft designed by General Electric Corporation. A rather complete development, including all major effects, of the equations of motion is given. This resulting ninth order system of differential equations is solved numerically to obtain the real world attitude. It is felt that the resulting real world attitude model is a faithful simulation of the physical problem, except for the attitude control law. That is, the control system has a horizon sensor and a rate gyro. Outputs from these sensors are processed and commands sent to three flywheels and three jets. The main attitude control is via the flywheels. The jets are used primarily during initial attitude acquisition. In this study, some liberty is taken in that it is assumed that yaw, pitch, and roll are somehow measured (with errors). These measured values are then used to command the flywheels via a control function which is a linear function of the measured yaw, pitch, and roll and their measured rates.

The spacecraft orbits and attitude characteristics will now be briefly defined. Further explanation is given in the text.

Orbit

One particular class of the low altitude, sun synchronous orbits has been assumed in this study. The orbital parameters of this class are given in Table III. The qualitative effect upon this study of the choice of orbit is as follows:

- (1) As the orbital altitude is lowered, a greater portion of the stellar field is obscured by the earth; and earth reflected sunlight becomes a greater problem. In addition, the time derivative of the true anomaly is greater which, considered by itself, implies a greater number of stellar transits per second for the passive system. One probably cannot consider a passive system for a synchronous (24 hr.) orbit.

- (2) Since the orbit is sun synchronous, the sun's direction, as viewed from the spacecraft, is constrained. This constraint can be used to avoid direct and scattered sunlight entering the sensors.

TABLE III
ORBITAL PARAMETERS

Parameter	Value
a	4563 nautical miles
e	0
i	99.08°
Ω	152.5° + Right Asc. of sun (9:30 a.m.)
$\dot{\Omega}$	1°/day
Period	6196.015 sec
Height	492.35 nautical miles
True anomaly rate, $\dot{\nu}$	0.0581°/sec

Attitude Parameters

The spacecraft is that designed by General Electric Corporation for the ERTS missions. It is attitude stabilized by jets and flywheels; however, in this study only the flywheels are used for stabilization.

A dynamic equivalent of the spacecraft's configuration is given in Figure 1B.* The spacecraft is composed of five rigid sections:

- (1) main body,
- (2) solar array, and
- (3) three flywheels.

*Figure 1 of Appendix B.

The solar array rotates about a fixed axis. The angle of rotation is chosen so as to maximize the received solar energy. Important spacecraft attitude parameters are given in Table IV.

TABLE IV
ATTITUDE PARAMETERS

Spacecraft Parameters			
Solar array mass = 2.33 slugs			
Solar array size = 3' x 8'			
Array rotation rate and acceleration $\dot{\beta} = \dot{\gamma}, \ddot{\beta} = 0$			
Principal moments of spacecraft without array			
$A_o = 256 \text{ slug ft}^2$			
$B_o = 217 \text{ slug ft}^2$			
$C_o = 96.5 \text{ slug ft}^2$			
Average value of principal moments with array			
$A_1 = 289.757$			
$B_1 = 231.674$			
$C_1 = 167.537$			
(See Appendix B for further explanation)			
External Torque			
Maximum magnitude = $1.15 \times 10^{-4} \text{ ft lbs}$			
Minimum magnitude = $4.71 \times 10^{-5} \text{ ft lbs}$			
(See Appendix D)			
Attitude			
	Yaw, ψ	Pitch, θ	Roll, ϕ
max. (deg x 100)	85.2	38.6	42.8
min. (deg x 100)	-144.7	-75.8	-76.1
(See Figure 21)			

SYMBOLS

A_o, B_o, C_o	principal moments of inertia of spacecraft without solar array
A_1, B_1, C_1	average value of principal moments of total spacecraft
a, e, Ω, ω, i	orbital elements of spacecraft's trajectory
D_j	angular momentum of all three flywheels resolved in the direction \hat{i}_j , $j = 1$; \hat{j}_j , $j = 2$; \hat{k}_j , $j = 3$
\bar{H}	angular momentum with respect to an inertial system of the spacecraft
h_1, h_2, h_3	components of a star in the coordinate system S_3
M_s	mass of solar array
T_1, T_2, T_3	components of external torque in the system S_7
β	angle which defines orientation of solar array with respect to the spacecraft
β_i	angle between yaw axis, \hat{k}_j , and projection of the i^{th} sensor optical axis in the yaw-roll plane (\hat{i}_j, \hat{j}_j)
γ_{ij}	angle defining orientation of slit j with respect to its optical axis
ψ	true yaw
θ	true pitch
φ	true roll
$\Delta\psi, \Delta\theta, \Delta\varphi$	error in the measurement of yaw, pitch, and roll by the attitude control system
$\tilde{\psi}, \tilde{\theta}, \tilde{\varphi}$	estimates of yaw, pitch, and roll obtained by use of the star sensor system
v	true anomaly of spacecraft
η	slit-curve is written as a function of this parameter
σ_i	angle between i^{th} sensor optical axis and pitch axis
$\Phi(M, S)$	inertia tensor of the set of masses, M , computed with respect to the coordinate system, S

$\bar{\omega}_{ij}$ angular velocity of the coordinate system S_j with respect to the coordinate system S_i

Coordinate systems:

S_1 celestial system

S_4 local geocentric system

S_7 spacecraft fixed system

S_{10ij} system associated with i^{th} head and j^{th} slit

In general:

A' is the transpose of a matrix A

\hat{U} implies \hat{U} a unit vector

$\langle x \rangle$ is the average value of $x(t)$ in a given time interval

\cdot equals $\frac{d}{dt}$

\bar{U} implies \bar{U} a vector with three components

SYSTEMS OF COORDINATES

To aid in later discussion, a set of fundamental coordinate systems, S_i , will now be introduced. A triad of orthonormal right-handed vectors associated with each system, S_i , will be denoted by $(\hat{i}_i, \hat{j}_i, \hat{k}_i)$. Also, S_{i+1} and S_i will be such that one of the following relations is satisfied:

$$\hat{i}_{i+1} = \hat{i}_i, \hat{j}_{i+1} = \hat{j}_i, \hat{k}_{i+1} = \hat{k}_i .$$

S_1 - the celestial system, \hat{i}_1 in the direction of the First Point of Aries, \hat{k}_1 in the direction of the north pole. This system is needed because stars have their directions catalogued with respect to this system.

S_3 - the orbital plane system. It will be assumed that the orbital plane precesses uniformly.

$$\hat{i}_1 \rightarrow \hat{i}_2 \quad \text{rotation } \Omega \text{ about } \hat{k}_1 = \hat{k}_2$$

$$\hat{k}_2 \rightarrow \hat{k}_3' \quad \text{rotation } i \text{ about } \hat{i}_2 = \hat{i}_3'$$

$$\hat{i}_3' = -\hat{k}_3, \hat{k}_3' = -\hat{j}_3, \hat{j}_3' = \hat{i}_3 .$$

Ω is the argument of the ascending node, i is the orbital inclination.

S_4 - the local geocentric system or desired attitude system.

$$\hat{i}_3 \rightarrow \hat{i}_4 \quad \text{rotation } -\nu \text{ about } \hat{j}_3 = \hat{j}_4 .$$

Now,

\hat{j}_4 is in the negative orbital normal direction

\hat{k}_4 is a direction from the spacecraft to the earth's center

\hat{i}_4 is such that the orbital velocity has a positive component along \hat{i}_4

v is the true anomaly of the spacecraft.

In practice, the desired spacecraft attitude may be that of a local geodetic (vertical) system rather than of a local geocentric system. For this case another system, whose orientation with respect to S_4 depends upon the latitude and altitude of the spacecraft, must be introduced. This refinement will not be used here.

S_7 - spacecraft fixed system. This system is defined to be parallel to the principal axes of the main frame of the spacecraft, (the portion of the spacecraft not including the solar panels). The orientation of S_7 with respect to S_4 is determined by roll, pitch, and yaw as follows:

$\hat{i}_4 \rightarrow \hat{i}_5$ rotation ψ (yaw) about $\hat{k}_4 = \hat{k}_5$

$\hat{i}_5 \rightarrow \hat{i}_6$ rotation θ (pitch) about $\hat{j}_5 = \hat{j}_6$

$\hat{j}_6 \rightarrow \hat{j}_7$ rotation φ (roll) about $\hat{i}_6 = \hat{i}_7$.

The nominal and desired values of ψ , θ , and φ are zero. However, because of various errors in the attitude control system, these angles may vary between -1° and 1° .

S_{9i} - the i^{th} head system (see Figure 2)

$\hat{k}_7 \rightarrow \hat{k}_{8i}$ rotation β_i about $\hat{j}_7 = \hat{j}_8$

$\hat{j}_8 \rightarrow \hat{j}_{9i}$ rotation σ_i about $\hat{i}_{8i} = \hat{i}_{9i}$.

The direction \hat{j}_{9i} will be the direction of the optical axis of the i^{th} head, and the angle σ_i will be called the cant angle of this head.

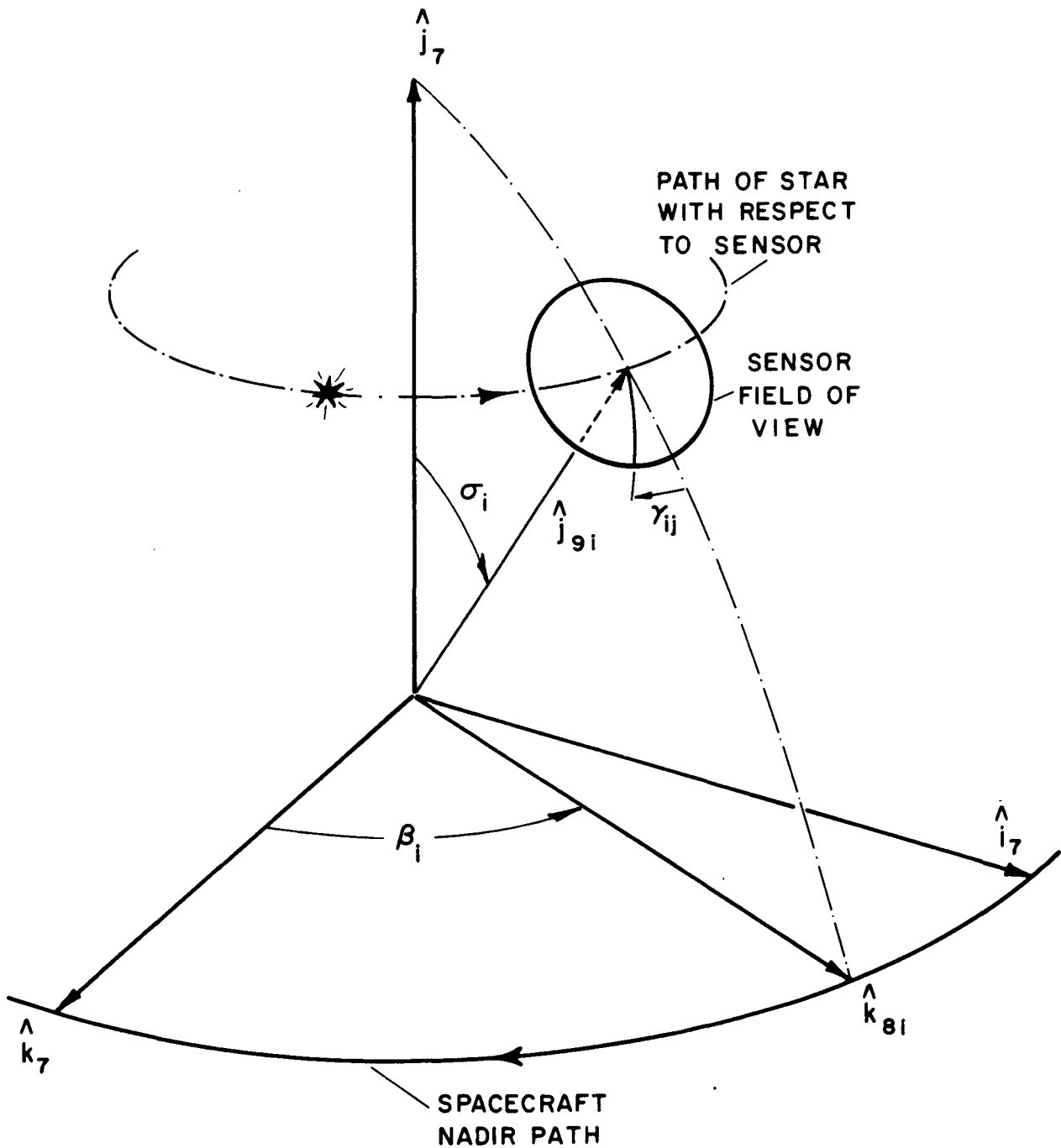


Figure 2: Orientation of Optical Axis and Slit With Respect to S_7 . The Two Sensor Recommended Configuration has $\sigma_1 = \sigma_2 = 62^\circ$, $\beta_1 = 113^\circ$, $\beta_2 = 247^\circ$.

s_{10ij} - the i^{th} head, j^{th} slit system,

$\hat{k}_{9i} \rightarrow \hat{k}_{10ij}$ rotation γ_{ij} about $\hat{j}_{9i} = \hat{j}_{10i}$.

The j^{th} slit-plane of the i^{th} head has \hat{i}_{10ij} as its normal.

The various coordinate transformations may now be written

$$\begin{pmatrix} \hat{i}_3 \\ \hat{j}_3 \\ \hat{k}_3 \end{pmatrix} = T(i, \Omega) \begin{pmatrix} \hat{i}_1 \\ \hat{j}_1 \\ \hat{k}_1 \end{pmatrix},$$

where

$$T(i, \Omega) = \begin{pmatrix} -\sin \Omega \cos i & \cos \Omega \cos i & \sin i \\ -\sin \Omega \sin i & \cos \Omega \sin i & -\cos i \\ -\cos \Omega & -\sin \Omega & 0 \end{pmatrix}$$

$$\begin{pmatrix} \hat{i}_4 \\ \hat{j}_4 \\ \hat{k}_4 \end{pmatrix} = B(-\nu) \begin{pmatrix} \hat{i}_3 \\ \hat{j}_3 \\ \hat{k}_3 \end{pmatrix},$$

where

$$B(-\nu) = \begin{pmatrix} \cos \nu & 0 & \sin \nu \\ 0 & 1 & 0 \\ -\sin \nu & 0 & \cos \nu \end{pmatrix}.$$

$$\begin{pmatrix} \hat{i}_7 \\ \hat{j}_7 \\ \hat{k}_7 \end{pmatrix} = C(\varphi, \theta, \psi) \begin{pmatrix} \hat{i}_4 \\ \hat{j}_4 \\ \hat{k}_4 \end{pmatrix},$$

where for small φ , θ , and ψ

$$C(\varphi, \theta, \psi) = \begin{pmatrix} 1 & \psi & -\theta \\ -\psi & 1 & \varphi \\ \theta & -\varphi & 1 \end{pmatrix}.$$

$$\begin{pmatrix} \hat{i}_{9i} \\ \hat{j}_{9i} \\ \hat{k}_{9i} \end{pmatrix} = S(\sigma_i, \beta_i) \begin{pmatrix} \hat{i}_7 \\ \hat{j}_7 \\ \hat{k}_7 \end{pmatrix},$$

where

$$S(\sigma_i, \beta_i) = \begin{pmatrix} \cos \beta_i & 0 & -\sin \beta_i \\ \sin \sigma_i \sin \beta_i & \cos \sigma_i & \sin \sigma_i \cos \beta_i \\ \cos \sigma_i \sin \beta_i & -\sin \sigma_i & \cos \sigma_i \cos \beta_i \end{pmatrix}.$$

And finally,

$$\begin{pmatrix} \hat{i}_{10ij} \\ \hat{j}_{10i} \\ \hat{k}_{10ij} \end{pmatrix} = B(\gamma_{ij}) \begin{pmatrix} \hat{i}_{9i} \\ \hat{j}_{9i} \\ \hat{k}_{9i} \end{pmatrix}.$$

So the transformation from the celestial triad to the slit triad is

$$\begin{pmatrix} \hat{i}_{10ij} \\ \hat{j}_{10i} \\ \hat{k}_{10ij} \end{pmatrix} = B(\gamma_{ij}) S(\sigma_i, \beta_i) C(\varphi, \theta, \psi) B(-\nu) T(i, \Omega) \begin{pmatrix} \hat{i}_1 \\ \hat{j}_1 \\ \hat{k}_1 \end{pmatrix}. \quad (1)$$

EQUATIONS OF MOTION

A development of the equations of motion will now be given. This development uses, as a starting point, an expression for the angular momentum of the spacecraft. The writer believes that this method is easier to follow than that outlined by Pringle (Reference [3]) which uses the kinetic energy as a starting point. Assume the following:

1. The spacecraft is composed of five rigid sections as follows:
 - a. main body,
 - b. three symmetric flywheels mounted such that the spin axis of each flywheel has a fixed direction with respect to the main body, and
 - c. solar array.
2. The only factor which causes a change in the moments of inertia of the spacecraft is the rotation of the solar array.
3. The center of mass of the solar array is fixed with respect to the main body.

Thus, from the results of Appendix A, we can write

$$\bar{H} = \Phi(T, S_7) \bar{\omega}_{17} + \sum_{i=1}^4 \Phi(m_i, S_{mi}) \bar{\omega}_{7mi}, \quad (2)$$

where

- | | |
|---------------------|------------------------------------------------------------------------------------------------------------------------------------------------------------------------------------------------------------------------------------------------------------------|
| \bar{H} | angular momentum of the spacecraft. |
| $\Phi(T, S_7)$ | inertia tensor of the spacecraft computed with respect to S_7 , S_7 is a system with origin at the center of mass of the total spacecraft. The unit vectors \hat{i}_7 , \hat{j}_7 , and \hat{k}_7 are parallel to the principal axes of the main body. |
| $\bar{\omega}_{17}$ | angular velocity of S_7 with respect to S_1 (the celestial system). |
| $\Phi(m_i, S_{mi})$ | inertia tensor of the set (m_i) computed with respect to S_{mi} , S_{mi} being a system with a origin at the center of mass of m_i . |

m_i $i = 1, 2, 3$ denotes the three flywheels.

m_4 denotes the solar array.

$\bar{\omega}_{7mi}$ angular velocity of S_{mi} with respect to S_7 .

Let

$$\Phi(m_i, S_{mi}) \bar{\omega}_{7mi} = d_i \hat{i}_{mi}, \quad i = 1, 2, 3$$

where

d_i magnitude, with respect to S_7 , of the angular momentum of the i^{th} flywheel.

\hat{i}_{mi} spin direction of the flywheel.

Now, let the direction of the spin axis of the i^{th} flywheel be resolved along the principal axes the main body. So,

$$\hat{i}_{mi} = b_{1i} \hat{i}_7 + b_{2i} \hat{j}_7 + b_{3i} \hat{k}_7,$$

where b_{ji} are given and $b_{j1}^2 + b_{j2}^2 + b_{j3}^2 = 1$. The flywheels are mounted so that $b_{ii} \approx 1$, $b_{ij} \approx 0$, $i \neq j$. Let

$$D_j = \sum_{i=1}^3 d_i b_{ji}.$$

Hence,

$$\sum_{i=1}^3 \Phi(m_i, S_{mi}) \bar{\omega}_{7mi} = \begin{pmatrix} D_1 \\ D_2 \\ D_3 \end{pmatrix}. \quad (3)$$

Here D_j are the components of the angular momentum of the three flywheels in the S_7 system. These components are known (with errors) since the direction, moment of inertia, and spin rate of the flywheels are known.

The inertia tensor of the total system may be written

$$\Phi(T, S_7) = \begin{pmatrix} A_o & 0 & 0 \\ 0 & B_o & 0 \\ 0 & 0 & C_o \end{pmatrix} + M_s \begin{pmatrix} 0 & 0 & 0 \\ 0 & 0 & 0 \\ 0 & 0 & H^2 \end{pmatrix} + \Phi_s, \quad (4)$$

where

$\Phi_s = \Phi(m_4, S_{m4})$ and is computed with respect to axes parallel to S_7 ,

M_s mass of the solar array,

H distance between solar array center of mass and origin of S_7 , and

A_o, B_o, C_o principal moments of inertia of the total spacecraft without the solar array.

The first term in Equation (4) arises by consideration of the spacecraft body without the solar array. The moments A_o, B_o , and C_o are constant by Assumption 2. The second term follows from the parallel axes theorem (Figure 1B).^{*} Finally, the third term is simply the inertia tensor of the solar array computed with the origin at its center of mass.

Hence, Equation (2) becomes

$$\bar{H} = \Phi(T, S_7) (\bar{\omega}_{17} + \bar{\omega}_{7m4}) - \begin{pmatrix} A_o & 0 & 0 \\ 0 & B_o & 0 \\ 0 & 0 & C_o + M_s H^2 \end{pmatrix} \bar{\omega}_{7m4} + \begin{pmatrix} D_1 \\ D_2 \\ D_3 \end{pmatrix}; \quad (5)$$

here \bar{H} , $\Phi(T, S_7)$, $\bar{\omega}_{17}$, $\bar{\omega}_{7m4}$, D_1 , D_2 , and D_3 must be resolved in S_7 .

^{*}Figure 1 of Appendix B.

In order to equate the time derivative of \bar{H} and the external torques, it is convenient to resolve \bar{H} in the inertial system S_1 . This transformation has been given as

$$\begin{pmatrix} \hat{i}_7 \\ \hat{j}_7 \\ \hat{k}_7 \end{pmatrix} = C(\varphi, \theta, \psi) B(-\psi) T(i, \Omega) \begin{pmatrix} \hat{i}_1 \\ \hat{j}_1 \\ \hat{k}_1 \end{pmatrix} = A \begin{pmatrix} \hat{i}_1 \\ \hat{j}_1 \\ \hat{k}_1 \end{pmatrix}.$$

So, $A'\bar{H}$ yields the spacecraft angular momentum components in S_1 . Hence,

$$\bar{T}_1 = \frac{d}{dt} (A'\bar{H}) = A'\dot{\bar{H}} + \dot{A}'\bar{H},$$

where \bar{T}_1 is the sum of the external torques resolved in S_1 .

$$\bar{T}_7 = A\bar{T}_1 = \dot{\bar{H}} + A\dot{A}'\bar{H}, \quad (6)$$

where \bar{T}_7 denotes the external torques resolved in S_7 . Now,

$$\begin{aligned} \dot{\bar{H}} &= \Phi(T, S_7) (\dot{\omega}_{17} + \dot{\omega}_{7m4}) + \dot{\Phi}(T, S_7) (\bar{\omega}_{17} + \bar{\omega}_{7m4}) \\ &- \begin{pmatrix} A_o & 0 & 0 \\ 0 & B_o & 0 \\ 0 & 0 & C_o + M_s H^2 \end{pmatrix} \dot{\omega}_{7m4} + \begin{pmatrix} \dot{D}_1 \\ \dot{D}_2 \\ \dot{D}_3 \end{pmatrix}; \end{aligned} \quad (7)$$

and from Appendix C,

$$A\dot{A}' = \begin{pmatrix} 0 & -\omega_3 & \omega_2 \\ \omega_3 & 0 & -\omega_1 \\ -\omega_2 & \omega_1 & 0 \end{pmatrix}, \quad (8)$$

where

$$\bar{\omega}_{17} = \omega_1 \hat{i}_7 + \omega_2 \hat{j}_7 + \omega_3 \hat{k}_7 .$$

Given $\Phi(T, S_7)$, $\bar{\omega}_{7m4}$, \bar{T}_7 , D_1 , D_2 , and D_3 , the Equations (6), (7), and (8) determine a sixth order system of differential equations in the variables ω_1 , ω_2 , ω_3 , φ , θ , and ψ .

In Appendix B, it is shown that

$$\Phi_s = \begin{pmatrix} \varphi_{11} & -\varphi_{12} & -\varphi_{13} \\ -\varphi_{12} & \varphi_{22} & -\varphi_{23} \\ -\varphi_{13} & -\varphi_{23} & \varphi_{33} \end{pmatrix},$$

with

$$\begin{aligned} \varphi_{11} &= c_1 + q_1 \cos 2\beta, \\ \varphi_{12} &= q_2 \cos \beta, \\ \varphi_{13} &= q_1 \sin 2\beta, \\ \varphi_{22} &= c_2, \\ \varphi_{23} &= -q_2 \sin \beta, \\ \varphi_{33} &= c_1 - q_1 \cos 2\beta, \end{aligned}$$

where c_1 , c_2 , q_1 , and q_2 are constants which depend on the dimensions and placement of the solar array and β is the solar panel rotation angle.

Thus,

$$\Phi(T, S_7) = \begin{pmatrix} A_1 + q_1 \cos 2\beta & -q_2 \cos \beta & -q_1 \sin 2\beta \\ -q_2 \cos \beta & B_1 & q_2 \sin \beta \\ -q_1 \sin 2\beta & q_2 \sin \beta & C_1 - q_1 \cos 2\beta \end{pmatrix}, \quad (9)$$

where

$$A_1 = A_0 + c_1,$$

$$B_1 = B_0 + c_2,$$

$$C_1 = C_0 + M_s H^2 + c_1, \text{ and}$$

$$\dot{\Phi}(T, S_7) = \dot{\beta} \begin{pmatrix} -2q_1 \sin 2\beta & q_2 \sin \beta & -2q_1 \cos 2\beta \\ q_2 \sin \beta & 0 & q_2 \cos \beta \\ -2q_1 \cos 2\beta & q_2 \cos \beta & 2q_1 \sin 2\beta \end{pmatrix}. \quad (10)$$

In the derivation of Equation (9) (Appendix B), it is assumed that the axis of rotation of the solar array is parallel to \hat{j}_7 (pitch axis).

Hence,

$$\bar{\omega}_{7m4} = \dot{\beta} \begin{pmatrix} 0 \\ 1 \\ 0 \end{pmatrix}. \quad (11)$$

Substituting Equations (7), (8), (9), (10), and (11) into Equation (6), one obtains

$$\begin{aligned} \bar{T}_7 = & \Phi(T, S_7) \dot{\omega}_{17} + (v_1 + \dot{\beta} v_2) \bar{\omega}_{17} + \begin{pmatrix} \dot{D}_1 \\ \dot{D}_2 \\ \dot{D}_3 \end{pmatrix} + \dot{\beta}^2 \begin{pmatrix} \sin \beta \\ 0 \\ \cos \beta \end{pmatrix} \\ & + \ddot{\beta} \begin{pmatrix} -q_2 \cos \beta \\ c_2 \\ q_2 \sin \beta \end{pmatrix} + \begin{pmatrix} 0 & -\omega_3 & \omega_2 \\ \omega_3 & 0 & -\omega_1 \\ -\omega_2 & \omega_1 & 0 \end{pmatrix} \Phi(T, S_7) \bar{\omega}_{17}, \end{aligned}$$

where

$$V_1 = \begin{pmatrix} 0 & D_3 & -D_2 \\ -D_3 & 0 & D_1 \\ D_2 & -D_1 & 0 \end{pmatrix},$$

$$V_2 = \begin{pmatrix} -2q_1 \sin 2\beta & 2q_2 \sin \beta & -2q_1 \cos 2\beta - c_2 \\ 0 & 0 & 0 \\ -2q_1 \cos 2\beta + c_2 & 2q_2 \cos \beta & 2q_1 \sin 2\beta \end{pmatrix}.$$

Hence,

$$\begin{pmatrix} \dot{\omega}_1 \\ \dot{\omega}_2 \\ \dot{\omega}_3 \end{pmatrix} = \Phi^{-1}(T, S_7) \left[\bar{T}_7 - (V_1 + \dot{\beta} V_2) \begin{pmatrix} \omega_1 \\ \omega_2 \\ \omega_3 \end{pmatrix} - \begin{pmatrix} \dot{D}_1 \\ \dot{D}_2 \\ \dot{D}_3 \end{pmatrix} - \dot{\beta}^2 \begin{pmatrix} q_2 \sin \beta \\ 0 \\ q_2 \cos \beta \end{pmatrix} \right. \\ \left. - \dot{\beta} \begin{pmatrix} -q_2 \cos \beta \\ c_2 \\ q_2 \sin \beta \end{pmatrix} - \begin{pmatrix} \omega_1(-q_1\omega_2 \sin 2\beta + q_2\omega_3 \cos \beta) + (C_1 - q_1 \cos 2\beta - B_1)\omega_2\omega_3 + q_2 \sin \beta (\omega_2^2 - \omega_3^2) \\ \omega_2(-q_2\omega_3 \cos \beta - q_2\omega_1 \sin \beta) + (A_1 - C_1 + 2q_1 \cos 2\beta)\omega_1\omega_3 - q_1 \sin 2\beta (\omega_3^2 - \omega_1^2) \\ \omega_3(q_2\omega_1 \sin \beta + q_1\omega_2 \sin 2\beta) + (B_1 - A_1 - q_1 \cos 2\beta)\omega_1\omega_2 - q_2 \cos \beta (\omega_1^2 - \omega_2^2) \end{pmatrix} \right] \quad (12)$$

It now remains to find the differential equations relating yaw, pitch, and roll to $\bar{\omega}_{17}$. This relationship may be found by using Equation (8) or an addition theorem for angular velocities. Using the second method, one can write

$$\bar{\omega}_{17} = \dot{\Omega} \hat{k}_1 - \dot{\psi} \hat{j}_4 + \dot{\psi} \hat{k}_5 + \dot{\theta} \hat{j}_6 + \dot{\phi} \hat{i}_7$$

$$\begin{aligned}
\begin{pmatrix} \omega_1 \\ \omega_2 \\ \omega_3 \end{pmatrix} &= \dot{\Omega} A \begin{pmatrix} 0 \\ 0 \\ 1 \end{pmatrix} - \dot{\psi} C(\varphi, \theta, \psi) \begin{pmatrix} 0 \\ 1 \\ 0 \end{pmatrix} + \psi C(\varphi, \theta, 0) \begin{pmatrix} 0 \\ 0 \\ 1 \end{pmatrix} \\
&+ \dot{\theta} C(\varphi, 0, 0) \begin{pmatrix} 0 \\ 1 \\ 0 \end{pmatrix} + \dot{\varphi} \begin{pmatrix} 1 \\ 0 \\ 0 \end{pmatrix} \\
&= C(\varphi, \theta, \psi) \begin{pmatrix} \dot{\Omega} \cos \nu \sin i \\ -\dot{\Omega} \cos i - \dot{\psi} \\ -\dot{\Omega} \sin \nu \sin i \end{pmatrix} \\
&+ \begin{pmatrix} -\dot{\psi} \sin \theta + \dot{\varphi} \\ \dot{\psi} \sin \varphi \cos \theta + \dot{\theta} \cos \varphi \\ \dot{\psi} \cos \varphi \cos \theta - \dot{\theta} \sin \varphi \end{pmatrix}.
\end{aligned}$$

Hence,

$$\begin{aligned}
\dot{\psi} &= \sec \theta (\omega_2 \sin \varphi + \omega_3 \cos \varphi) + \dot{\nu} \tan \theta \sin \psi \\
&+ \dot{\Omega} (-\theta \cos \nu + \sin \nu) \sin i,
\end{aligned}$$

$$\begin{aligned}
\dot{\theta} &= \omega_2 \cos \varphi - \omega_3 \sin \varphi + \dot{\nu} \cos \psi \\
&+ \dot{\Omega} (\psi \cos \nu \sin i + \cos i),
\end{aligned}$$

$$\begin{aligned}
\dot{\varphi} &= \omega_1 + \tan \theta (\omega_2 \sin \varphi + \omega_3 \cos \varphi) + \dot{\nu} \sec \theta \sin \psi \\
&+ \dot{\Omega} (\psi \cos i - \cos \nu \sin i).
\end{aligned} \tag{13}$$

Since $\dot{\Omega}$ is small ($\approx 1^\circ/\text{day}$), a small angle approximation is used in terms containing $\dot{\Omega}$ as a factor.

The equations (12) and (13) are a system of sixth order differential whose solution yields yaw, pitch, and roll as a function of time; given the constants c_1 , c_2 , c_3 , q_1 , and q_2 , and the functions of time \bar{T}_7 , β , D_1 , D_2 , and D_3 .

The flywheel angular momenta (which determine D_1 , D_2 , D_3) are not given functions of time, but are functions of the measured attitude and the control law. As stated in the introduction, an extensive effort has not been undertaken here to reproduce the actual mechanized attitude control. The control law used here will now be stated.

It is assumed that somehow roll, pitch, and yaw and their rates are measured. These measured values are used to determine the momenta of the flywheels so that the spacecraft's attitude is nearly that of zero roll, pitch, and yaw.

Since the angular velocity of S_{m4} (the solar array system) with respect to S_7 (the spacecraft system) can be written

$$\bar{\omega}_{7m4} = \bar{\omega}_{1m4} - \bar{\omega}_{17} ,$$

and since the solar array is driven so that it is nearly fixed with respect to the inertia system, S_1 ;

$$\bar{\omega}_{7m4} \approx -\bar{\omega}_{17} .$$

So, Equation (5) becomes

$$\bar{H} \approx \begin{pmatrix} A_o & 0 & 0 \\ 0 & B_o & 0 \\ 0 & 0 & C_o + M_s H^2 \end{pmatrix} \bar{\omega}_{17} + \begin{pmatrix} D_1 \\ D_2 \\ D_3 \end{pmatrix} .$$

Hence, this approximation reduces Equation (12) to

$$\begin{aligned} A_0 \dot{\omega}_1 &= T_1 - D_3 \omega_2 + D_2 \omega_3 - \dot{D}_1 + (B_0 - C_0 - M_s H^2) \omega_2 \omega_3 , \\ B_0 \dot{\omega}_2 &= T_2 + D_3 \omega_1 - D_1 \omega_3 - \dot{D}_2 + (C_0 + M_s H^2 - A_0) \omega_1 \omega_3 , \\ (C_0 + M_s H^2) \dot{\omega}_3 &= T_3 - D_2 \omega_1 + D_1 \omega_2 - \dot{D}_3 + (A_0 - B_0) \omega_1 \omega_2 , \end{aligned}$$

where

$$\bar{T}_7 = T_1 \hat{i}_7 + T_2 \hat{j}_7 + T_3 \hat{k}_7 .$$

Now, if the spacecraft is nearly correctly controlled, $\omega_1 \approx \omega_3 \approx 0$, $\omega_2 \approx -\dot{\psi}$ (orbital rate). Moreover, $\psi \approx \theta \approx \varphi \approx 0$. Hence, the approximate equations of motion become

$$\begin{aligned} A_0 \dot{\omega}_1 &= T_1 + D_3 \dot{\psi} - \dot{D}_1 - (B_0 - C_0 - M_s H^2) \dot{\psi} \omega_3 , \\ B_0 \dot{\omega}_2 &= -\dot{D}_2 + T_2 , \\ (C_0 + M_s H^2) \dot{\omega}_3 &= T_3 - D_1 \dot{\psi} - \dot{D}_3 - (A_0 - B_0) \dot{\psi} \omega_1 , \\ \dot{\psi} &= -\dot{\psi} \varphi + \omega_3 , \\ \dot{\theta} &= \omega_2 + \dot{\psi} , \\ \dot{\varphi} &= \omega_1 + \dot{\psi} . \end{aligned} \tag{14}$$

Now, let

$$\begin{aligned} \dot{D}_1 &= -(B_0 - C_0 + M_s H^2) \dot{\psi} \omega_{3m} + A_0 \dot{\psi} \dot{\psi}_m + \tau_1 , \\ \dot{D}_2 &= \tau_2 , \\ \dot{D}_3 &= -(A_0 - B_0) \dot{\psi} \omega_{1m} - (C_0 + M_s H^2) \dot{\psi} \dot{\varphi}_m + \tau_3 , \end{aligned}$$

where $\dot{\varphi}_m$, ω_{3m} , and ω_{1m} are determined from the measured attitude. Now,

$$A_0 \dot{\omega}_1 = (B_0 - C_0 - M_s H^2) \dot{(\omega_{3m} - \omega_m)} - A_0 \dot{\psi}_m + \dot{D}_3 - \tau_1 + T_1.$$

So,

$$A_0 \ddot{\varphi} \approx -\tau_1 + \dot{D}_3 + T_1.$$

Let

$$\tau_1 = A_0 (a \varphi_m + b \dot{\varphi}_m).$$

Hence,

$$\ddot{\varphi} + b \dot{\varphi}_m + a \varphi_m \approx \frac{1}{A_0} (T_1 + \dot{D}_3)$$

or

$$\ddot{\varphi} + b \dot{\varphi} + a \varphi \approx \frac{1}{A_0} (T_1 + \dot{D}_3).$$

So, if $4a > b^2$, a damped motion of roll can be expected. The term \dot{D}_3 can be nearly removed from the right-hand side by adding a "feed back" term which depends upon a measured flywheel momentum. This was not done here. In summary, the equations of motion are as follows:

(1) Given the parameters of the solar array (Appendix B) and the principal moments of inertia of the spacecraft without the array determine the inertia tensor of the spacecraft as follows:

$$c_1 = \left[\frac{\ell_1^2}{3} \left(1 - \frac{1}{2} \sin^2 \sigma \right) + \ell^2 + \frac{1}{24} \ell_2^2 + \ell \ell_1 \cos \sigma \right] M_s,$$

$$c_2 = \frac{1}{3} (\ell_1^2 \sin^2 \sigma + \frac{1}{4} \ell_2^2) M_s,$$

$$q_1 = \frac{1}{6} (-\ell_1^2 \sin^2 \sigma + \frac{1}{4} \ell_2^2) M_s,$$

$$q_2 = \ell_1 \sin \sigma (\frac{1}{3} \ell_1 \cos \sigma + \frac{1}{2} \ell) M_s,$$

$$A_1 = A_0 + c_1,$$

$$B_1 = B_0 + c_2,$$

$$C_1 = C_0 + M_s H^2 + c_1,$$

$$\Phi(T, S_7) = \begin{pmatrix} A_1 + q_1 \cos 2\beta & -q_2 \cos \beta & -q_1 \sin 2\beta \\ -q_2 \cos \beta & B_1 & q_2 \sin \beta \\ -q_1 \sin 2\beta & q_2 \sin \beta & C_1 - q_1 \cos 2\beta \end{pmatrix}.$$

(2)

$$V_1 = \begin{pmatrix} 0 & D_3 & -D_2 \\ -D_3 & 0 & D_1 \\ D_2 & -D_1 & 0 \end{pmatrix},$$

$$V_2 = \begin{pmatrix} -2q_1 \sin 2\beta & 2q_2 \sin \beta & -2q_1 \cos 2\beta - c_2 \\ 0 & 0 & 0 \\ -2q_1 \cos 2\beta + c_2 & 2q_2 \cos \beta & 2q_1 \sin 2\beta \end{pmatrix},$$

$$\bar{E} = \begin{pmatrix} \omega_1(-q_1\omega_2 \sin 2\beta + q_2\omega_2 \cos \beta) + (C_1 - q_1 \cos 2\beta - \beta_1)\omega_2\omega_3 + q_2 \sin \beta (\omega_2^2 - \omega_3^2) \\ \omega_2(-q_2\omega_3 \cos \beta - q_1\omega_1 \sin \beta) + (A_1 - C_1 + 2q_1 \cos 2\beta)\omega_1\omega_3 - q_1 \sin 2\beta (\omega_3^2 - \omega_1^2) \\ \omega_3(q_2\omega_1 \sin \beta + q_1\omega_2 \sin 2\beta) + (B_1 - A_1 - q_1 \cos 2\beta)\omega_1\omega_2 - q_2 \cos \beta (\omega_1^2 - \omega_2^2) \end{pmatrix}.$$

(3) The ninth order system of differential equations can now be written as

$$\begin{pmatrix} \dot{\omega}_1 \\ \dot{\omega}_2 \\ \dot{\omega}_3 \end{pmatrix} = \Phi^{-1}(T, S_7) \left[\bar{T}_7 - (V_1 + \dot{\beta} V_2) \begin{pmatrix} \omega_1 \\ \omega_2 \\ \omega_3 \end{pmatrix} - \begin{pmatrix} \dot{D}_1 \\ \dot{D}_2 \\ \dot{D}_3 \end{pmatrix} - \dot{\beta}^2 \begin{pmatrix} q_2 \sin \beta \\ 0 \\ q_2 \cos \beta \end{pmatrix} \right. \\ \left. + \ddot{\beta} \begin{pmatrix} -q_2 \cos \beta \\ c_2 \\ q_2 \sin \beta \end{pmatrix} - \bar{E} \right],$$

$$\dot{\psi} = \sin \theta (\omega_2 \sin \varphi + \omega_3 \cos \varphi) + \dot{\nu} \tan \theta \sin \psi$$

$$+ \dot{\Omega} (\theta \cos \nu - \sin \nu) \sin i,$$

$$\dot{\theta} = \omega_2 \cos \varphi - \omega_3 \sin \varphi + \dot{\nu} \cos \psi$$

$$- \dot{\Omega} (\psi \cos \nu \sin i + \cos i),$$

$$\dot{\varphi} = \omega_1 + \tan \theta (\omega_2 \sin \varphi + \omega_3 \cos \varphi) + \dot{\nu} \sec \theta \sin \psi$$

$$+ \dot{\Omega} (-\psi \sin i + \cos \nu \sin i),$$

$$\dot{D}_1 = A_0 (a \varphi_m + b \dot{\varphi}_m) + (A_0 - B_0 + C_0 + M_s H^2) \dot{\nu} \dot{\psi}_m,$$

$$\dot{D}_2 = B_0 (a \theta_m + b \dot{\theta}_m),$$

$$\dot{D}_3 = (C_0 + M_s H^2) (a \psi_m + b \dot{\psi}_m) - (A_0 - B_0 + C_0 + M_s H^2) \dot{\nu} \dot{\varphi}_m,$$

where a and b are constants; the initial conditions of $\omega_1, \omega_2, \omega_3, \psi, \theta, \varphi, D_1, D_2, D_3$ are given; the torque, \bar{T}_7 is a given function of ψ, θ, φ , and time (Appendix D).

SENSOR LOCATION ABOARD THE SPACECRAFT

An initial concern is the effect of extraneous background light upon the detectability of the stars whose magnitudes are near the design limit. The extraneous light has four sources:

- (1) direct sunlight,
- (2) earth reflected sunlight,
- (3) spacecraft reflected sunlight, and
- (4) moon reflected sunlight.

The planets do not contribute to the extraneous background, for indeed, they may be used as targets. In fact, where we speak of "stars", the brighter planets are included.

The influence of the first three sources of extraneous light may be minimized by a judicious choice of the sensor location and viewing direction. This minimization can be accomplished by using the following constraints:

- (1) roll, pitch, and yaw are maintained at nearly zero,
- (2) the orbit is sun-synchronous, and
- (3) the solar array is the only portion of the spacecraft which might reflect sunlight into the sensor.

Figure 3 is a schematic of the spacecraft which will be used to define the geometry of the problem. It is assumed that the roll, pitch, and yaw are zero so that S_7 coincides with the desired attitude S_4 . It is also assumed that the pitch axis, \hat{j}_7 , is the axis about which the solar array rotates.

Let the sensor have its origin at the terminus of \bar{Q} and let \bar{Q} be defined with respect to S_7 by

$$\bar{Q} = a \cos \gamma \hat{i}_7 + a \sin \gamma \hat{j}_7 + D \hat{k}_7,$$

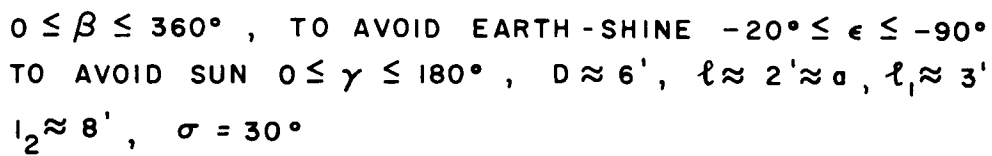


Figure 3: Geometry of Solar Panels, Optic Origin, and Optic Axis Direction.

where

- a radius of sensor mounting ring ($\approx 2'$),
- γ azimuth of the mounting position, measured about the yaw axis,
- D distance of mounting ring (which is perpendicular to the yaw axis) from solar array axis of rotation, \hat{j}_7 .

Because the orbit is "9:30 a.m." sun-synchronous on the average,

$$\Omega = 152.5^\circ + \text{right ascension of sun.}$$

The direction to the sun makes an angle of approximately 60° with the orbital normal. The sun's direction completes one rotation with respect to S_7 in an orbital period. Hence, to avoid direct sunlight, the sensor must be positioned so that $0 \leq \gamma \leq 180^\circ$.

Now, let \hat{O} denote the direction of the optical axis of the sensor, and let

$$\hat{O} = \cos \delta \cos \epsilon \hat{i}_7 + \sin \delta \cos \epsilon \hat{j}_7 + \sin \epsilon \hat{k}_7 ,$$

where

- ϵ elevation of optical axis with respect to \hat{i}_7, \hat{j}_7 plane
- δ azimuth, measured about the yaw axis, of the optical axis.

As ϵ increases, the sensor will point more toward the earth; and as ϵ decreases, the sensor will point more toward the panels. The elevation of the horizon is $25^\circ 30'$. Now, to avoid extraneous light reflected from the sunlit earth, the angle from the optical axis to any ray which terminates on the sunlight earth must be greater than 45° . This restriction is made so that a light shield of "reasonable size" can be designed for the sensor. The optical axis elevation is set at $\epsilon = -20^\circ$.

The problem which arises because of light reflected from the panels must now be considered. Let \bar{P} be a vector from the origin of S_7 (on the axis of panel rotation) to the closest corner of the panel (only one panel need be considered). Then,

$$\bar{P} = -\frac{l_2}{2} \sin \beta \hat{i}_7 + l \hat{j}_7 + \frac{l_2}{2} \cos \beta \hat{k}_7$$

where

- β panel rotation angle, $0 \leq \beta \leq 360^\circ$,
- l distance along \hat{j}_7 to panel $\approx 2'$,
- l_2 panel length $\approx 8'$.

Now let \hat{b} be a unit vector in the direction of the panel's edge.

Then

$$\hat{b} = \sin \sigma \cos \beta \hat{i}_7 + \cos \sigma \hat{j}_7 + \sin \sigma \sin \beta \hat{k}_7 ,$$

where

$$\sigma \text{ panel cant angle } \approx 30^\circ.$$

A vector from the origin of the optical system to a generic point on the panel's edge is then

$$\bar{u} + p \hat{b}, \quad 0 \leq p \leq l_2 ,$$

where

$$\bar{u} = \bar{Q} - \bar{P} = \left(\frac{l_2}{2} \sin \beta + a \cos \gamma\right) \hat{i}_7 + (a \sin \gamma - l) \hat{j}_7 + \left(D - \frac{l_2}{2} \cos \beta\right) \hat{k}_7 .$$

The cosine of the angle between the optical axis and a ray to a generic point on the panel's edge is thus,

$$\hat{O} \cdot \hat{d} = \frac{\hat{O} \cdot \bar{u} + p \hat{O} \cdot \hat{b}}{|\bar{u} + p \hat{b}|} = f(p) .$$

To maximize $f(p)$ (that is, minimum angle), choose

$$\begin{aligned} p &= \tilde{p} & \text{if } 0 \leq \tilde{p} \leq \ell_2, \\ &= 0 & \text{if } \tilde{p} < 0, \\ &= \ell_2 & \text{if } \tilde{p} > \ell_2, \end{aligned}$$

where

$$\tilde{p} = \frac{\hat{0} \cdot \hat{b} u^2 - (\bar{u} \cdot \hat{0})(\bar{u} \cdot \hat{b})}{(\hat{0} \cdot \hat{b})(\bar{u} \cdot \hat{b}) - \bar{u} \cdot \hat{0}},$$

$$\hat{0} \cdot \hat{b} = \cos \delta \cos \beta \cos \epsilon \sin \sigma + \sin \delta \cos \epsilon \cos \sigma + \sin \epsilon \sin \sigma \sin \beta,$$

$$u^2 = \ell^2 + D^2 + \frac{1}{4} \ell_2^2 + a^2 + a \ell_2 \sin \beta \cos \gamma - 2a \ell \sin \gamma - D \ell_2 \cos \beta,$$

$$\begin{aligned} \bar{u} \cdot \hat{0} &= \frac{1}{2} \ell_2 (\cos \delta \sin \beta \cos \epsilon - \cos \beta \sin \epsilon) + a \cos \epsilon \cos(\epsilon - \gamma) \\ &\quad + D \sin \epsilon - \ell \sin \delta \cos \epsilon, \end{aligned}$$

$$\bar{u} \cdot \hat{b} = a(\cos \gamma \sin \sigma \cos \beta + \sin \gamma \cos \sigma) + D \sin \sigma \sin \beta - \ell \cos \sigma.$$

It is difficult to proceed farther without the aid of numerical techniques. We now set

$$\begin{aligned} \epsilon &= -20^\circ, \\ D &= 6', \\ \ell &= a = 2', \\ \ell_1 &= 3', \\ \ell_2 &= 8', \\ \sigma &= 30^\circ, \end{aligned}$$

and consider all values of β , δ , and γ .

For any fixed value of δ and γ , the β which maximizes $\hat{0} \cdot \hat{d}$ may be found. This calculation yields the angle of closest approach to the panel envelope, that is, the surface formed by rotating the panel.

Figure 4 is a plot of the minimum angle between the optical axis and the solar panel envelope as a function of γ and δ . Note that to maximize this minimum, small γ and δ must be chosen. However, if δ is chosen too small, direct sunlight becomes a problem. Hence, $\delta = 30^\circ$ is recommended. With this choice of δ , it may be noted from Figure 4 that the minimum angle to the envelope is a weak function of γ . If $0^\circ \leq \gamma \leq 20^\circ$, then the minimum angle is between 38° and 40° . Suppose we choose $\gamma = 0$ (sensor origin in the roll-yaw plane), then the minimum angle is 38° .

Figure 5 is a plot of minimum angle between the optical axis and panel as a function of β . In this figure, two sensors are assumed, each symmetrically located with respect to the yaw-pitch plane.

Figure 6 is a representation of the viewing geometry as seen from S_7 (zero roll, pitch, and yaw are assumed). The location of the optical axis and field of view for each sensor is shown.

In summary, it is possible to locate two sensors on the spacecraft so that the angle from the optical axis of either sensor to the sun is greater than 50° , the angle to the horizon is greater than 46° , and the angle to the panel is greater than 38° . It is felt that an extraneous light shield of not unduly large size can be designed with these constraints. The angles β_i and σ_i which define the position of the i^{th} optical axis (these angles were defined in the section on coordinate systems) are

$$\beta_1 = 113^\circ$$

$$\beta_2 = 247^\circ$$

$$\sigma_1 = \sigma_2 = 62^\circ$$

β_i azimuth of i^{th} optical axis measured with respect to the pitch-yaw plane

σ_i coelevation of i^{th} optical axis with respect to the roll-yaw plane (Figure 2)

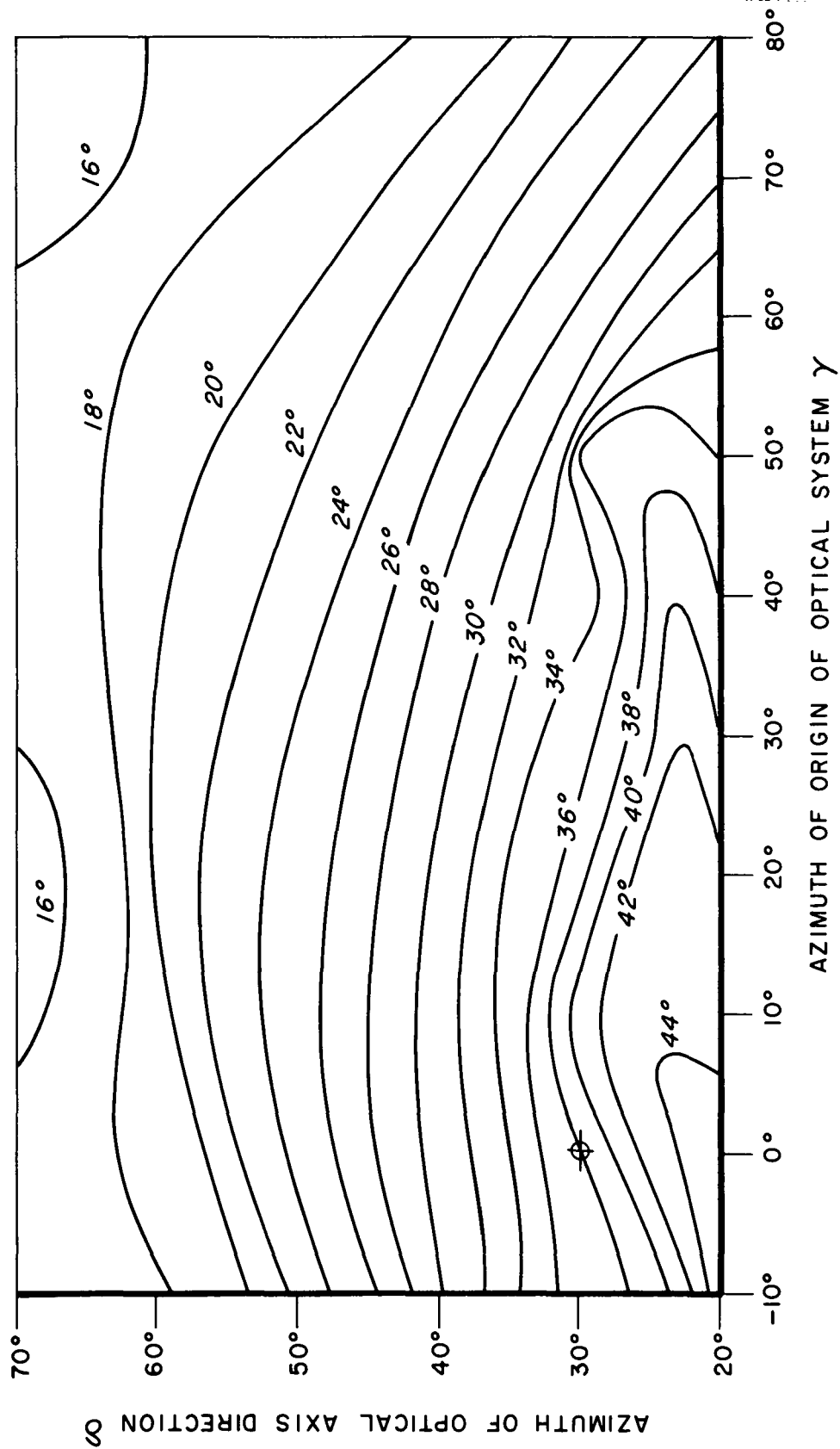


Figure 4: Minimum Angle Between Optical Axis and Solar Panel Envelope as a Function of γ and δ .

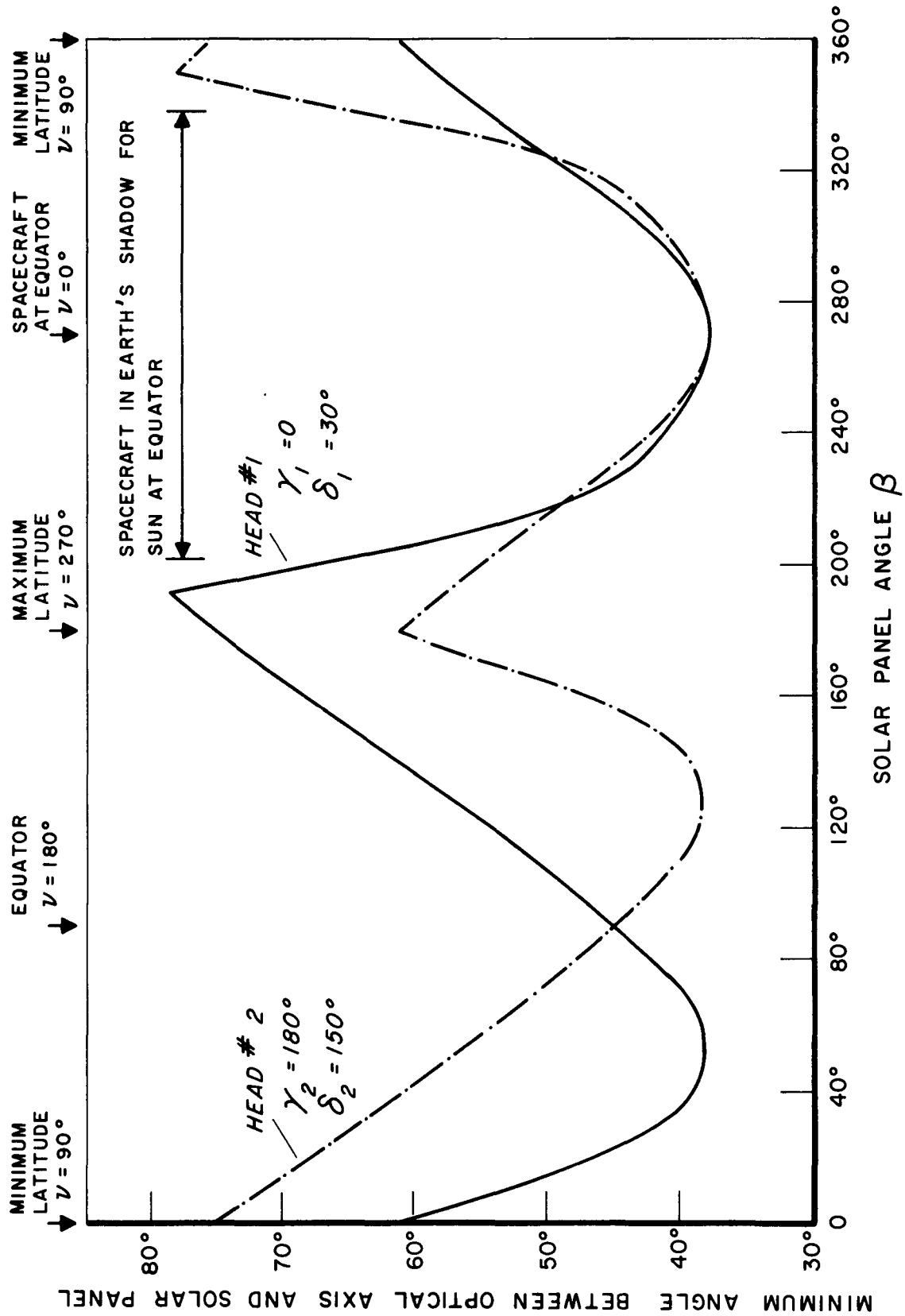


Figure 5: Minimum Angle Between Optical Axes of Each Head and Solar Panel as a Function of Solar Panel Angle.

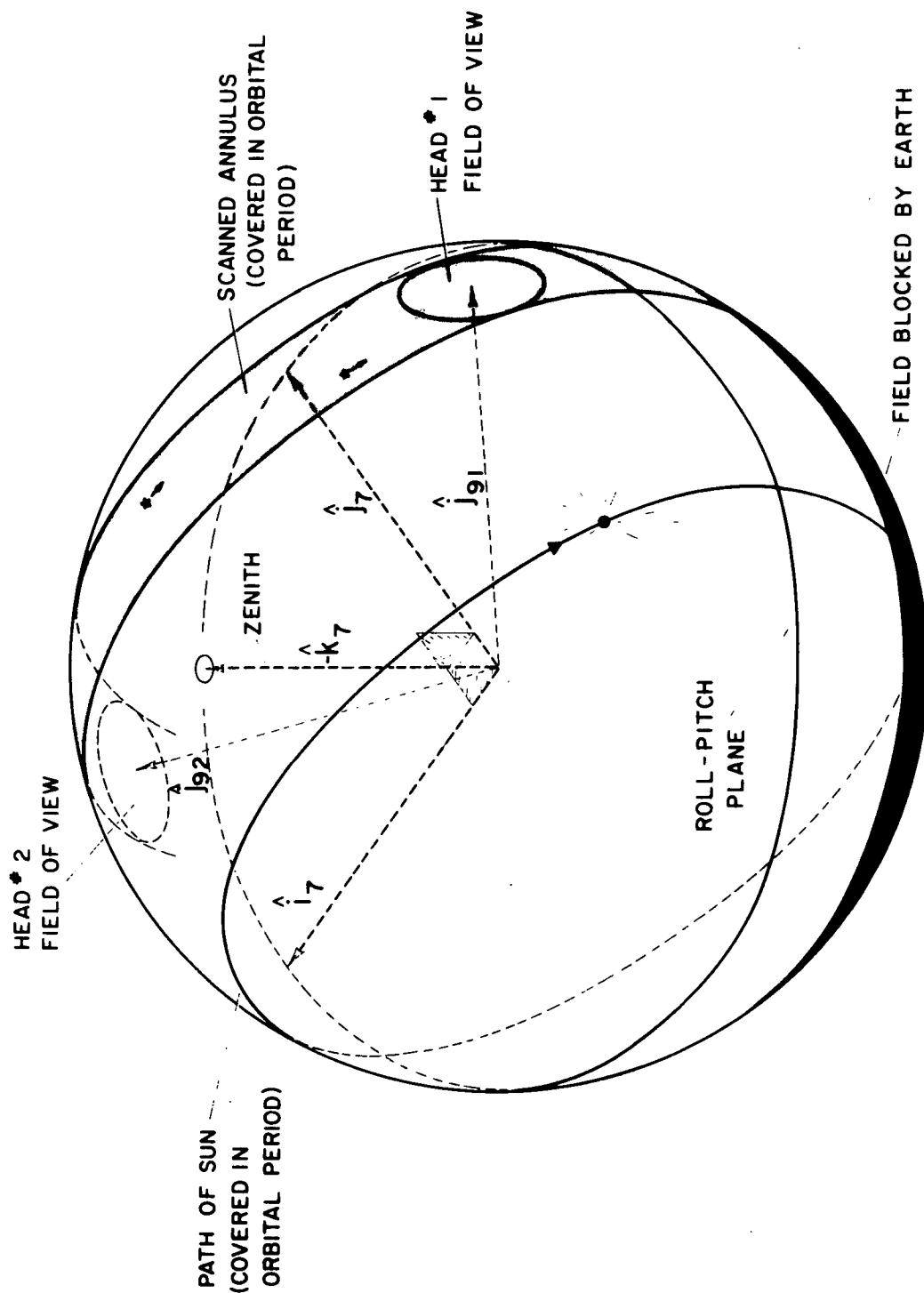


Figure 6: Viewing Geometry as seen from S_7 . \hat{i}_7 Roll, \hat{j}_7 Pitch, \hat{k}_7 Yaw. $-\hat{k}_7$ is the Zenith Direction.

EQUATIONS IMPLIED BY A MEASURED TRANSIT TIME

Recall that the system S_{10ij} is a coordinate system associated with the j^{th} slit of the i^{th} sensor, and the slit is in the $(\hat{j}_{9i}, \hat{k}_{10ij})$ plane. Hence, the instant a star is in the slit plane (that is, at a transit time), the direction to the star is given by

$$\hat{U}_{10} = \cos \eta \hat{j}_{9i} + \sin \eta \hat{k}_{10ij}.$$

The direction to the same star may be written as

$$\hat{U}_1 = \cos \delta \cos \alpha \hat{i}_1 + \cos \delta \sin \alpha \hat{j}_1 + \sin \delta \hat{k}_1,$$

where α and δ are the right ascension and declination, respectively, of the transited star. Hence, from Equation (1),

$$\begin{pmatrix} 0 \\ \cos \eta \\ \sin \eta \end{pmatrix} = B(v_{ij}) S(\sigma_i, \beta_i) C(\varphi, \theta, \psi) B(-v) T(i, \Omega) \begin{pmatrix} \cos \delta \cos \alpha \\ \cos \delta \sin \alpha \\ \cos \delta \end{pmatrix}. \quad (15)$$

The parameter, η , may be eliminated from the above systems by simply considering the first of the equations. Thus,

$$0 = B_1(v_{ij}) S(\sigma_i, \beta_i) C(\varphi, \theta, \psi) B(-v) \hat{h}, \quad (16)$$

where

B_1 = first row of B ,

$$\hat{h} = \begin{pmatrix} h_1 \\ h_2 \\ h_3 \end{pmatrix} = T(i, \Omega) \begin{pmatrix} \cos \delta \cos \alpha \\ \cos \delta \sin \alpha \\ \sin \delta \end{pmatrix}.$$

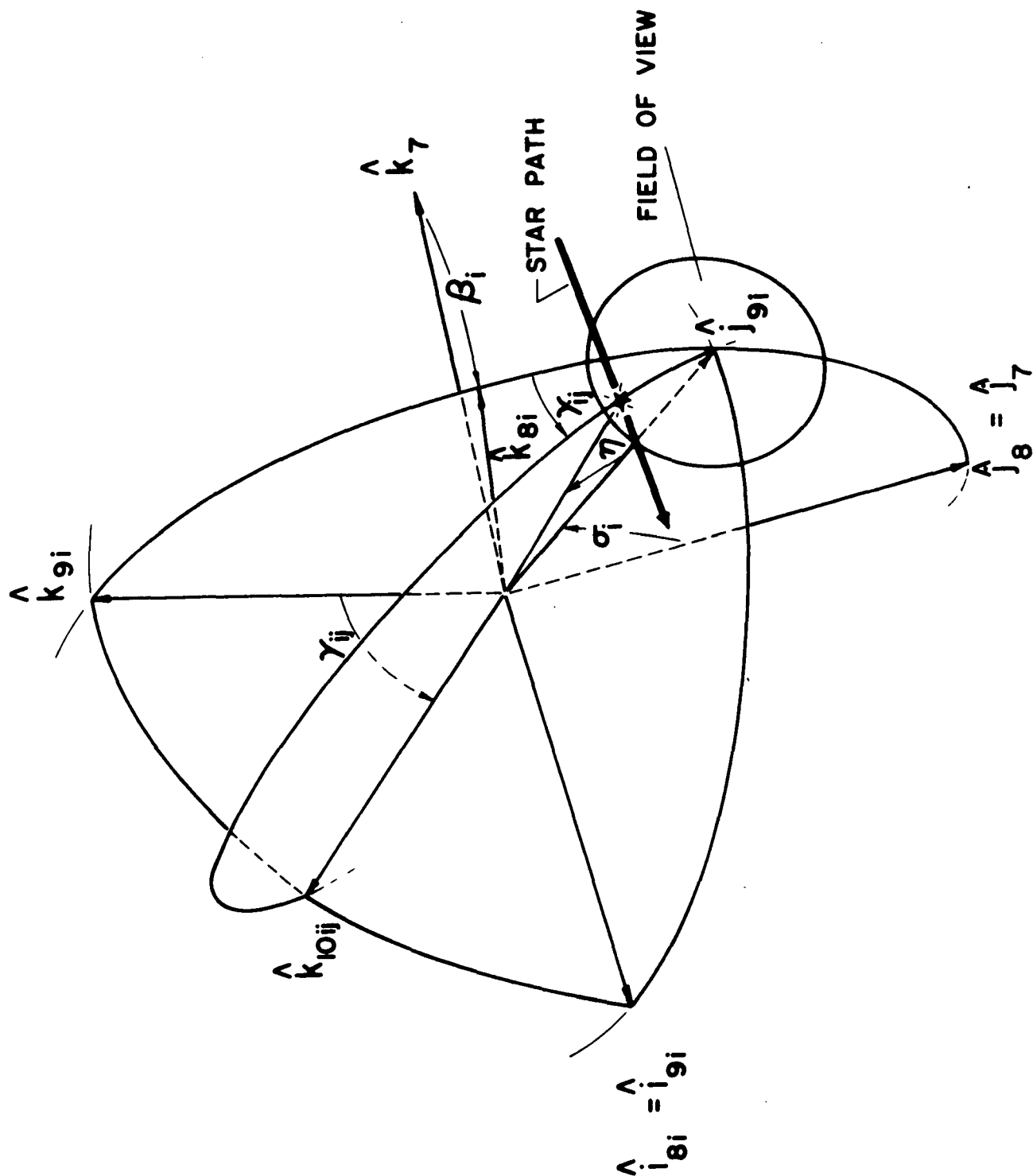


Figure 7: The Slit and Its Relationship to S_7 .

That is, h_1 , h_2 , and h_3 are the components of the star in S_3 .

Equation (16) represents one equation in the three unknowns $\varphi(t)$, $\theta(t)$, and $\psi(t)$, where t is the transit time. This equation is obtained from each transit of a known star. If no further information is given, each new equation simply adds one equation and three unknown angles - the roll, pitch, and yaw evaluated at each isolated transit time.

The physics which governs the motion of the spacecraft must be invoked to develop a time-dependent characterization of the attitude which involves just a few unknown parameters. This "attitude model" may then be used to internally couple roll, pitch, and yaw. This important point will now be considered in some detail.

THE ATTITUDE MODEL

Since attitude of the spacecraft as a function of time is completely determined by the spacecraft inertia tensor, flywheel angular momenta, external torque, and initial attitude, it is natural to attempt to use a set of simplified equations of motion to supply a model. Simplified equations rather than the more exact equations are necessary since the exact equation would require excessive computer running time to reduce operational data.

One simplification which seems necessary is that the solar array remains fixed with respect to an inertial system. This approximation yields the system of Equations (14). A comparison of the solution implied by this approximation and the true solution is given in Figure 8. Thus, the approximation produces an error of .03 degrees after 50 seconds. Such an error is on the border line of being acceptable.

To use the approximate equations as a model, additional assumptions must be made. The external torque, flywheel angular momenta, and flywheel torques must be somehow supplied. The flywheel angular momenta and torques can be measured (with errors). The external torque may be obtained¹ by assuming it constant in the data gathering interval. Such

¹The external torque may also be computed by assuming Equations (14) with roll, pitch, and yaw, on the average, zero. This yields

$$\begin{aligned}(t_2 - t_1) \langle T_1 \rangle &= \langle \dot{D}_1 \rangle - \dot{\psi} \langle D_3 \rangle, \\(t_2 - t_2) \langle T_2 \rangle &= \langle \dot{D}_2 \rangle, \\(t_2 - t_1) \langle T_3 \rangle &= \langle \dot{D}_3 \rangle + \dot{\psi} \langle D_1 \rangle,\end{aligned}$$

where

$$\begin{aligned}\langle T_i \rangle &\text{ average value of } T_i \text{ in } [t_1, t_2], \\(t_2 - t_1) \langle \dot{D}_i \rangle &= D_i(t_2) - D_i(t_1), \\ \langle D_i \rangle &\text{ average value of } D_i \text{ in } [t_1, t_2].\end{aligned}$$

The difficulty with this method of estimating the torque is that it tends to produce poor estimates if the external torque were to change suddenly or often.

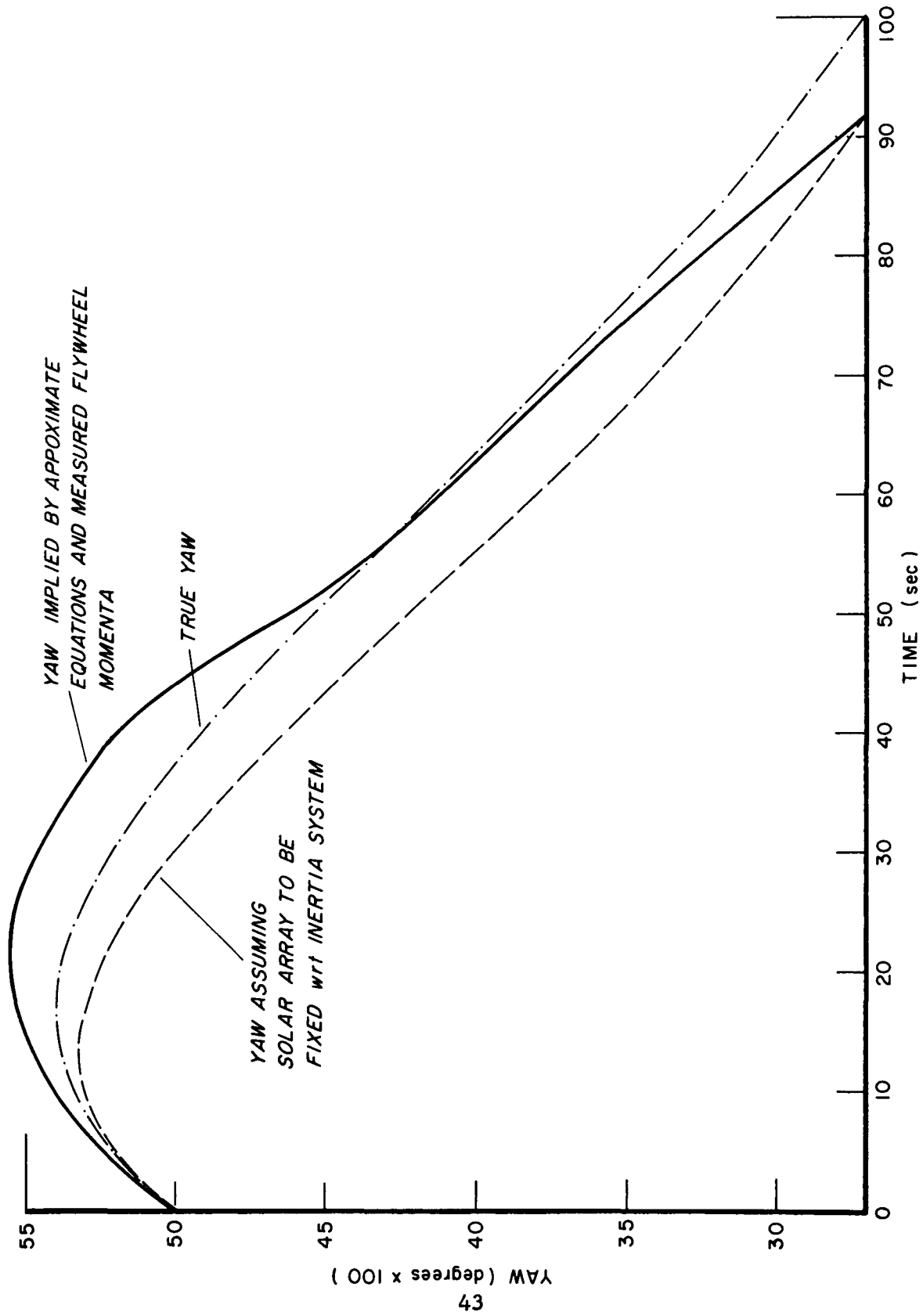


Figure 8: Yaw, and Two Approximations of Yaw as a Function of Time.

a model then contains 9 unknowns; so a minimum of 9 transit times must be held in the data reduction filter. To obtain a reliable attitude in the presence of typical transit time errors, approximately 20 transits must be held in the numerical filter. Later (pages 57-66), it will be shown that for the proposed instruments; transits are gathered at a rate of approximately 0.3 transit/sec. Thus, on the average, a data gathering interval of 60 seconds must be used to obtain 20 transits.

Figure 8 is a plot of yaw as implied by a solution of Equations (14), in which the flywheel momenta and torque are measured (10% RMS error) and the external torque is set equal to its average value.

Since a model which is based upon a set of simplified equations of motion implied a somewhat complicated data reduction scheme and may produce border line accuracies, such a model was abandoned. In retrospect, perhaps this was premature.

Constant Yaw, Pitch, and Roll Model

Instead of assuming a model which allows for a complicated attitude motion, an investigation was made as to the results attainable from a model which assumes yaw, pitch, and roll are constant during the data gathering interval. It turns out that if certain refinements are made, the constant model does generally provide a background from which quite accurate attitude estimates can be made. This general point will now be discussed.

Good Geometry

Assume an attitude estimate is required at some given time, T_p . Since only three transits are necessary to determine yaw, pitch, and roll, it seems natural to use the three measured transit times nearest to T_p . These three transit times will generally span an interval of about 10 seconds; so if the attitude is not changing rapidly, the constant model cannot introduce a large error.

A major difficulty with this approach, however, is that the geometry implied by the three measurements may be ill-conditioned. The nature and development of this ill-conditioning will now be discussed.

Consider the instant a star is in a slit. Three orthonormal directions may now be defined (Figure 9): \hat{s} , the direction to the star; \hat{r} , the slit normal; and $\hat{p} = \hat{r} \times \hat{s}$. The direction \hat{p} will be called the "preferred direction". Note that the spacecraft may be rotated with an arbitrarily large angle about \hat{s} or \hat{r} without causing the star to leave the slit. However, a rotation about \hat{p} causes \hat{s} to move in a direction perpendicular to the slit. Each transit thus establishes a preferred direction about which attitude motion is not allowed at the transit time. If only three relatively close transit times are measured, the best geometry would be such that the three preferred axis form an orthonormal triad. If the three preferred axis lie in a common plane, then the geometry is ill-contained.

Suppose a single head is used, then each preferred axis is approximately 90° from the optical axis (Figure 10). Hence, no preferred axis has a large component about the optical axis. This in turn implies that the single-head sensor yields a geometry which is inherently poorly conditioned since attitude about the optical axis is poorly defined.

If only three stars are used and the half-field-of-view angle is f , the placement of the stars which yields the optimum geometry is given in Figure 11. The optimum geometry is that which yields a maximum volume parallelepiped whose coterminal edges are the preferred axes. For $f = 10^\circ$ (the recommended half-field) the optimum configuration yields a parallelepiped of volume 0.202.

Now consider a two-headed sensor, for simplicity, and assume the angle between the optical axes is 90° (the recommended configuration, Figure 6, has a separation of $108^\circ 44'$). The configuration S_1, S_2 , and S_3 in Figure 12 will yield a well-conditioned geometry since the respective preferred axes of this triad are approximately $\hat{o}_1 \times \hat{o}_2, \hat{o}_2, -\hat{o}_1$. The configuration S_1, S_2 , and S_4 , however, will yield an ill-conditioned geometry since its respective preferred axes are approximately $\hat{o}_1 \times \hat{o}_2, \hat{o}_2, \hat{o}_1 \times \hat{o}_2$. Rotation about \hat{o}_1 is thus poorly determined by the configuration S_1, S_2 , and S_4 .

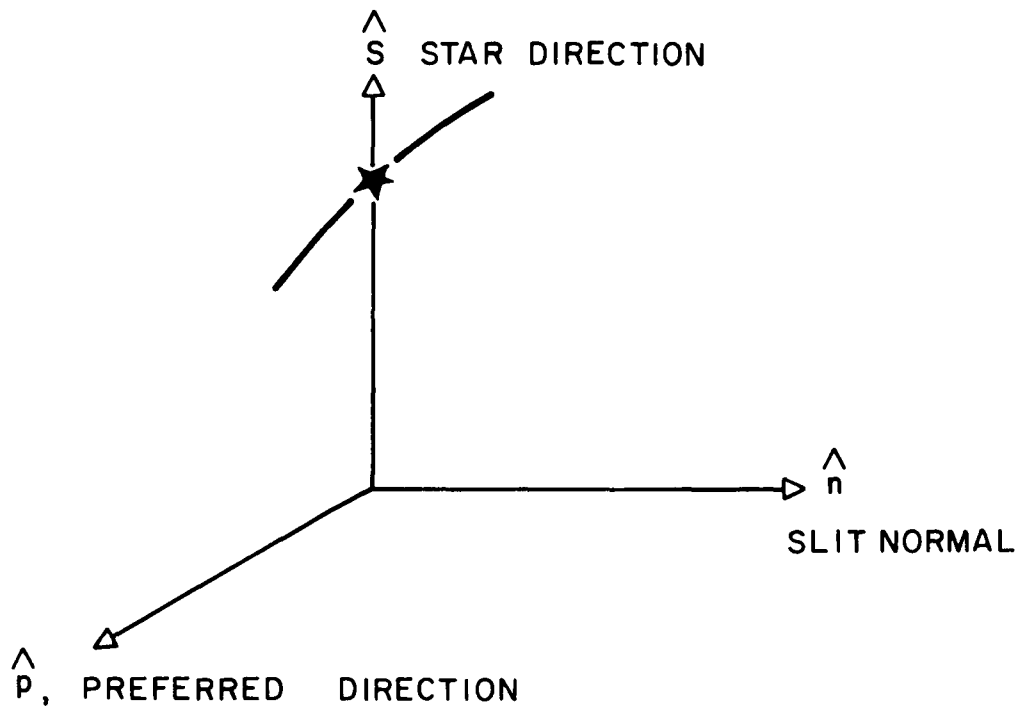


Figure 9: The Preferred Direction.

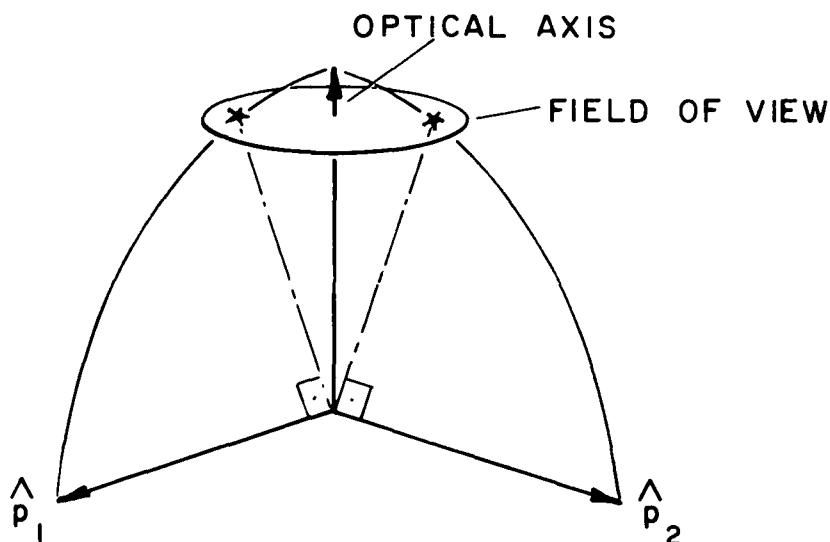


Figure 10: The Preferred Axes for the Single-Head Sensor. Note that Each Preferred Axis Has a Small Component on the Optic Axis; Hence, Attitude About the Optical Axis is Poorly Determined.

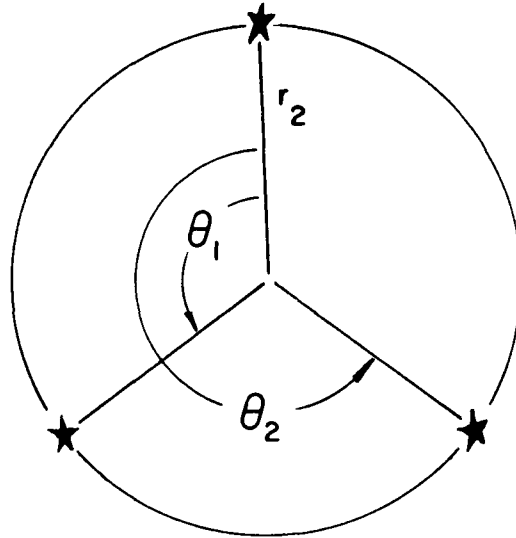


Figure 11: Placement of Three Stars to Yield the Optimum Geometry for the Single Head.

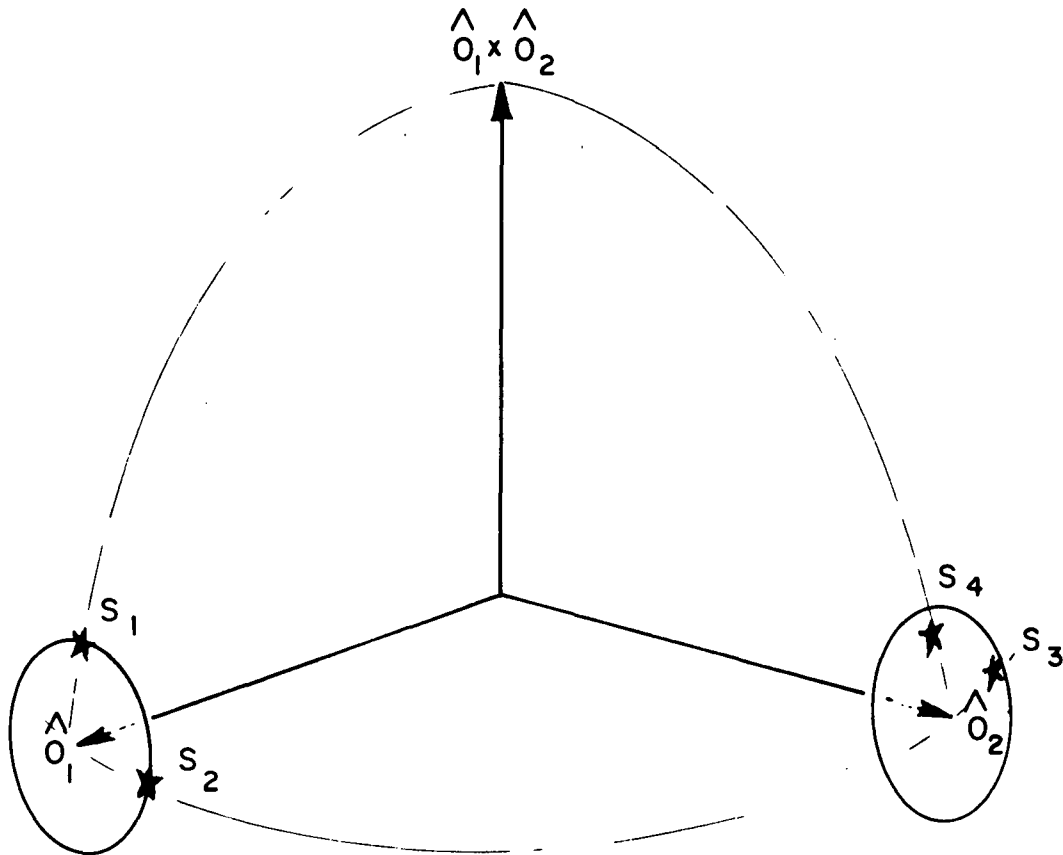


Figure 12: The Two-Head Sensor Geometry. Stars S_1 , S_2 , and S_3 Yield a Good Geometry, but S_1 , S_2 , and S_4 Yield a Poor Geometry.

For the recommended two-head sensor the optimum configuration of three stars yields a parallelepiped of volume 1.0 (compared to .202 for the one-head sensor). Hence, the two-head sensor has a significantly higher probability of providing a well-conditioned geometry with a small number of stars than does the single-head sensor.

In practice, all transits are not gathered simultaneously as was assumed in this discussion. Instead, they are typically gathered over a minute. This effect increases the directional region from which transits can be obtained and thus increases the probability of obtaining a good geometry.

The general method of choosing, from a given set $\{t_j\}$ of ordered times, the transit times used to compute the attitude at a given time, T_p , is as follows:

- (1) Choose three transit times, t_i , t_{i+1} , and t_k such that

$$t_i = \{t \mid \min_{t_j < T_p} (T_p - t_j)\},$$

$$t_k = \{t \mid \min_{j \neq i, i+1} |T_p - t_j|\}.$$

- (2) If these three times yield a good geometry, then the attitude is computed with these times. If they do not yield a good geometry, the next closest time to T_p is chosen. For example,

$$t_l = \{t_j \mid \min_{j \neq i, i+1, k} |T_p - t_j|\}.$$

The geometry with these four times is investigated, and the process continued.

A criterion as to whether or not a given set of transit times produces a good geometry can be obtained by examining the coefficient matrix of the linear system of equations, or by examining the star-slit position at each transit.

Weighting of Measurements

If the constant yaw, pitch, and roll models were accepted and the variance of each measurement transit time were known, the Gauss-Markoff theory from statistics (Reference [4]) gives a "weighting" of each equation.

It is known, however, that yaw, pitch, and roll are not constant; hence, those measurements which are nearer to the time at which the attitude is sought must be trusted more than those far removed. Unfortunately, there is no simple theory which gives a method of selecting the weights for the present problem. Instead, the weights were selected empirically.

Let T_p be a time at which an attitude estimate is desired. Also, let $\tau_{ip} = t_i - T_p$, where t_i is measured transit time. Let

$$f(\tau_{ip}) = w_0 - \frac{w_0 - 1}{10} |\tau_{ip}|.$$

A graph of $f(\tau)$ is given in Figure 13. It was felt that $f(\cdot)$ was undesirable to use as a correction to the weights since the first moment about T_p may not be zero. A correction was therefore added so that the first moment is zero, and the sum of the squares of the correction is a minimum. Thus, the weights are determined by

$$w_{ip} = f(\tau_{ip}) \left[1 - \tau_{ip} \frac{\sum_{i=1}^{n_p} \tau_{ip}}{\sum_{i=1}^{n_p} \tau_{ip}^2} \right],$$

where n_p is the number of measurements used to yield an estimate at T_p . It turned out that using the first-moment correction, on the average, did supply a slightly improved estimate.

Estimation of ω_{71} From Flywheel Outputs

For the nominal case, each flywheel rotates at an almost constant rate. The slow variations in their rates are caused by slow variations in the external torque. However, it may happen that the horizon sensor may supply an erroneous measurement due to a variation in the

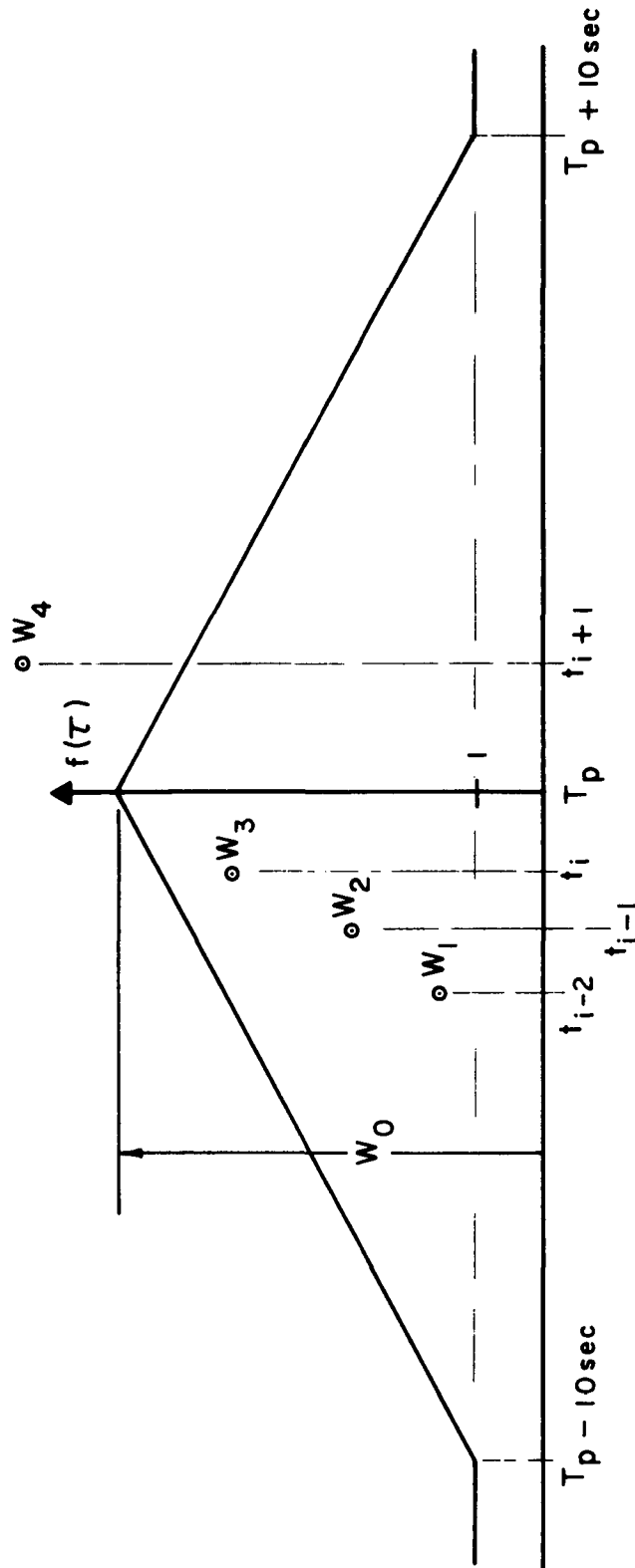


Figure 13: Method of Weighting to More Utilize Those Measurements Nearest to the Time at Which the Attitude is Desired.

earth's radiation output. These erroneous measurements will cause a more rapid change in the flywheel rotation rates, and hence in the angular velocity of the spacecraft fixed system, S_7 , with respect to the inertia system, S_1 . A method of estimating this angular velocity, $\bar{\omega}_{71}$, from the time history of the flywheel output will now be given.

Assume the following:

- (1) The solar panels are always at a fixed position with respect to an inertia system, S_1 ;
- (2) $\omega_1 \approx \omega_3 \approx 0$, and $\omega_2 \approx -\dot{\psi}$ (orbital rate); where ω_1 , ω_2 , and ω_3 are the components of $\bar{\omega}_{17}$ with respect to S_7 ;
- (3) Roll, pitch, and yaw are ≈ 0 .

Then, approximate equations of attitude motion were found to be (Equation (14)):

$$\begin{aligned} A_o \dot{\omega}_1 &= T_1 + D_3 \dot{\psi} - \dot{D}_1 - (B_o - C_o - M_s H^2) \dot{\psi} \omega_3, \\ B_o \dot{\omega}_2 &= -D_2 + T_3, \\ (C_o + M_s H^2) \dot{\omega}_3 &= T_3 - D_1 \dot{\psi} - \dot{D}_3 - (A_o - B_o) \dot{\psi} \omega_1, \end{aligned} \tag{17}$$

$$\begin{aligned} \dot{\psi} &= -\dot{\varphi} + \omega_3, \\ \dot{\theta} &= \omega_2 + \dot{\psi}, \\ \dot{\varphi} &= \omega_1 + \dot{\psi}, \end{aligned} \tag{18}$$

where A_o , B_o , and C_o are the principal moments of inertia without the panels, and

M_s mass of the panels,
 H distance between center of mass of the spacecraft with panels and the center of the mass of the panels,

- D_1, D_2, D_3 angular momentum components of the flywheels, measured with respect to the spacecraft system, S_7 ,
 T_1, T_2, T_3 components of the external torque resolved in S_7 ,
 ψ, θ, φ yaw, pitch, and roll, respectively.

First of all, the external torque may be estimated by assuming the following:

- (1) $\langle \omega_1 \rangle = \langle \omega_3 \rangle = 0$, $\langle \omega_2 \rangle = -\dot{\nu}$, where $\langle x \rangle$ is the average value of x in $[t_1, t_2]$;
(2) T_1, T_2 , and T_3 are slowly varying functions of time. Thus,

$$\langle T_1 \rangle (t_2 - t_1) = \langle \dot{D}_1 \rangle - \dot{\nu} \langle D_3 \rangle ,$$

$$\langle T_2 \rangle (t_2 - t_1) = \langle \dot{D}_2 \rangle ,$$

$$\langle T_3 \rangle (t_2 - t_1) = \langle \dot{D}_3 \rangle + \dot{\nu} \langle D_1 \rangle ,$$

where

$$(t_2 - t_1) \langle \dot{D}_i \rangle = D_i(t_2) - D_i(t_1).$$

Now, suppose there exists an interval of time $\tau_1 \leq t \leq \tau_2$ such that for t in this interval

$$T_1 + D_3 \dot{\nu} - \dot{D}_1 \approx T_2 - \dot{D}_2 \approx T_3 - D_1 \dot{\nu} - \dot{D}_3 \approx 0.$$

Then, we may assume $\omega_1 = \omega_3 = 0$, $\omega_2 = -\dot{\nu}$ in this interval. Let $t \geq \tau_2$, then the solution of the differential Equations (17) is

$$\begin{pmatrix} \omega_1(t) \\ \omega_3(t) \end{pmatrix} = \int_{\tau_2}^t \Phi(t-s) \begin{pmatrix} f_1(s) \\ f_3(s) \end{pmatrix} ds ,$$

$$\omega_2(t) = \frac{1}{B_o} \left[\int_{\tau_2}^t T_2(s) ds + D_2(\tau_2) - D_2(t) \right],$$

where

$$\Phi(t-s) = \begin{pmatrix} \cosh \lambda(t-s) & -\sqrt{\frac{a}{b}} \sinh \lambda(t-s) \\ -\sqrt{\frac{b}{a}} \sinh \lambda(t-s) & \cosh \lambda(t-s) \end{pmatrix},$$

$$A_o f_1(s) = T_1(s) + \dot{D}_3(s) - \dot{D}_1(s),$$

$$(C_o + M_s H^2) f_3(s) = T_3(s) - \dot{D}_1(s) - \dot{D}_3(s),$$

$$a = \frac{B_o - C_o - M_s H^2}{A_o} \approx .33,$$

$$b = \frac{A_o - B_o}{C_o + M_s H^2} \approx .29,$$

$$\lambda = \dot{\nu} \sqrt{ab} \approx .31 \dot{\nu} \approx 3.1 \times 10^{-4} \text{ rad/sec.}$$

If $t - \tau_2 \leq 500$ seconds, further approximations are possible so that

$$\omega_1(t) = \int_{\tau_2}^t f_1(s) ds,$$

$$\omega_3(t) = \int_{\tau_2}^t f_3(s) ds.$$

The yaw, pitch, and roll rates may then be approximated from Equations (18).

Because the D_i cannot be measured without error and various approximations were used, the estimates of ω_i have errors. Below, a graph is given which compares the true pitch rate with the estimated rate.

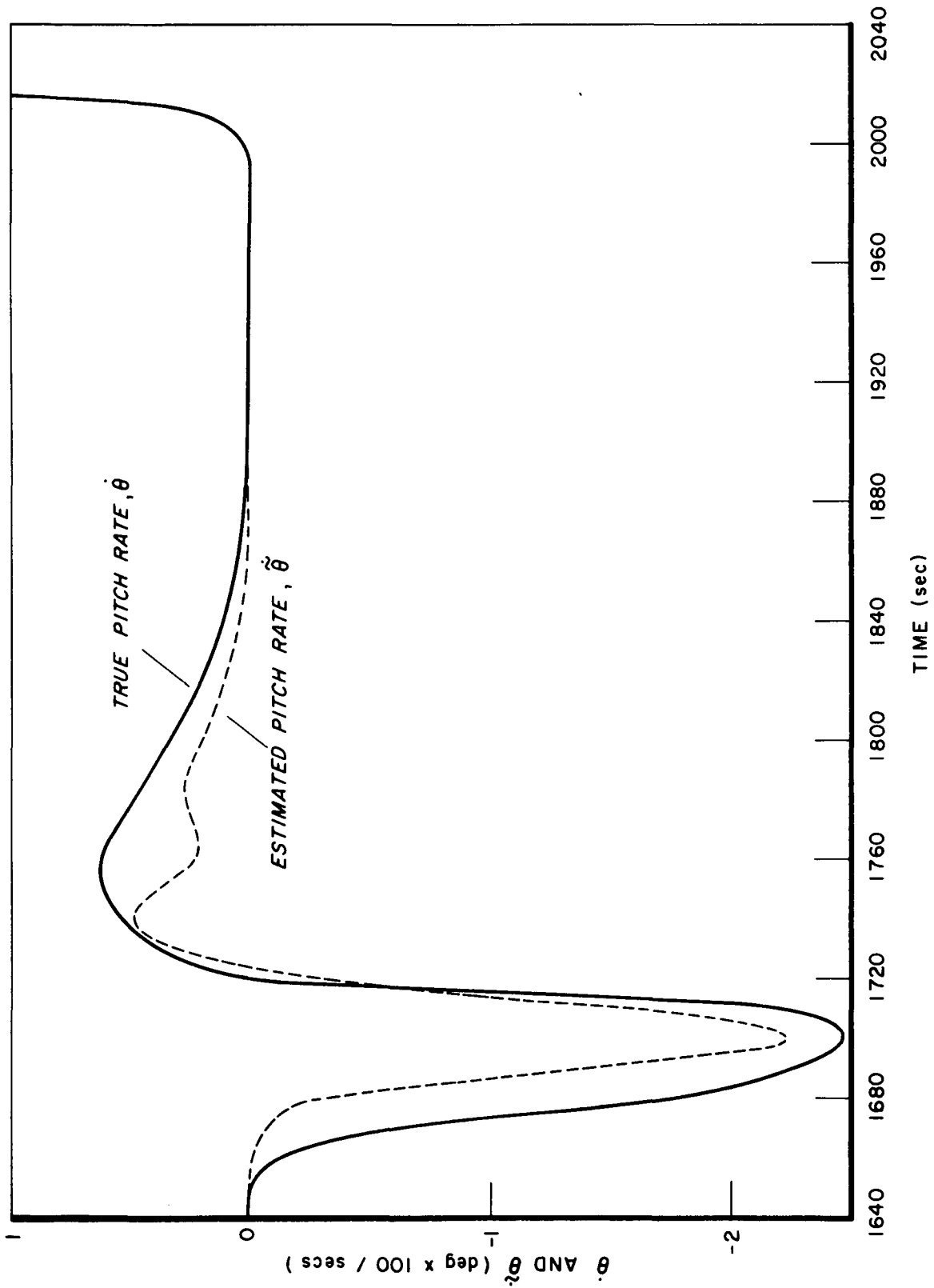


Figure 14: Estimated Pitch Rate and True Pitch Rate as a Function of Time.

$1640 \leq t \leq 2400$ Seconds

DETERMINATION OF ATTITUDE

In this section, the contents of the previous sections will be summarized and a final method of attitude determination will be given.

The basic constraint Equation (16) may be written

$$0 = \hat{D}(\gamma_{ij}, \sigma_i, \beta_i) C(\psi, \theta, \varphi) \hat{q} ,$$

where \hat{D} and \hat{q} are unit row and column vectors, respectively, and are given by

$$\hat{D}(\gamma_{ij}, \sigma_i, \beta_i) = B_1(\gamma_{ij}) S(\sigma_i, \beta_i)$$

$$\hat{q} = B(-v) \hat{h} .$$

So, for small yaw, pitch, and roll

$$a_\ell = A_\ell \begin{pmatrix} \psi(t_\ell) \\ \theta(t_\ell) \\ \varphi(t_\ell) \end{pmatrix}, \tag{19}$$

with

$$a_\ell = -\hat{D} \hat{q}, \text{ and}$$

$$A_\ell = d_1 q_2 - d_2 q_1, d_3 q_1 - d_1 q_3, d_2 q_3 - d_3 q_2 ,$$

where the q 's and d 's are the components of \hat{q} and \hat{D} , respectively.

If the components of the angular velocity, $\bar{\omega}_{17}$, are estimated from the flywheel output, then

$$\begin{aligned}\dot{\varphi} &\approx \tilde{\omega}_1 + \dot{\psi} \\ \dot{\theta} &\approx \tilde{\omega}_2 - \dot{\psi} \\ \dot{\psi} &\approx \tilde{\omega}_3 - \dot{\varphi}.\end{aligned}$$

The solution of this linear system of differential equations is

$$\varphi(t) = \varphi(T_p) \cos \lambda + \psi(T_p) \sin \lambda + \int_{T_p}^t [\tilde{\omega}_1(s) \cos \dot{\psi}(t-s) + \tilde{\omega}_3(s) \sin \dot{\psi}(t-s)] ds,$$

$$\theta(t) = -\dot{\psi}(t - T_p) + \int_{T_p}^t \tilde{\omega}_2(s) ds + \theta(T_p),$$

$$\psi(t) = \psi(T_p) \cos \lambda - \varphi(T_p) \sin \lambda + \int_{T_p}^t [-\tilde{\omega}_1(s) \sin \dot{\psi}(t-s) + \tilde{\omega}_3(s) \cos \dot{\psi}(t-s)] ds,$$

where

$$\lambda = (t - T_p) \dot{\psi}.$$

Since $\dot{\psi} \approx 10^{-3}$ rad/sec and $|t - T_p| < 100$ sec, $\lambda < .1$ rad. Hence, to a first order approximation,

$$\varphi(t) \approx \varphi(T_p) + (t - T_p) (\tilde{\omega}_1(T_p) + \dot{\psi}(T_p))$$

$$\theta(t) \approx (\tilde{\omega}_2(T_p) - \dot{\psi}) (t - T_p) + \theta(T_p)$$

$$\psi(t) \approx \psi(T_p) + (t - T_p) (\tilde{\omega}_3(T_p) - \dot{\varphi}(T_p)).$$

Substituting these results into Equation (19), one obtains

$$a_{\ell} + (T_p - t_{\ell}) A_{\ell} \begin{pmatrix} \tilde{\omega}_3 \\ \tilde{\omega}_2 - \dot{\nu} \\ \tilde{\omega}_1 \end{pmatrix} = (A_{\ell 1} + \lambda_{\ell} A_{\ell 3}, A_{\ell 2}, A_{\ell 3} - \lambda_{\ell} A_{\ell 1}) \begin{pmatrix} \psi(T_p) \\ \theta(T_p) \\ \varphi(T_p) \end{pmatrix}.$$

If a number of measurements are to be processed to obtain the attitude at T_p , a system of equations can be written as follows:

$$\bar{b} = B \begin{pmatrix} \psi(T_p) \\ \theta(T_p) \\ \varphi(T_p) \end{pmatrix}, \quad \bar{b} (n_p \times 1), \quad B (n_p \times 3).$$

These equations are then weighted by the criterion discussed in the previous section to obtain

$$W\bar{b} = WB \begin{pmatrix} \psi(T_p) \\ \theta(T_p) \\ \varphi(T_p) \end{pmatrix},$$

where W is a diagonal matrix $(n_p \times n_p)$.

STELLAR AVAILABILITY AND DETECTABILITY

At this point, only the direction of the sensor's optical axis with respect to S_7 has been specified. A number of other parameters must, however, be specified in order to discuss the probability and accuracy of stellar detections. These as-of-yet unspecified parameters are listed in Table V. Also listed in Table V are numerical values of these parameters. The procedure employed in choosing these numerical values is obtained through the iterative process shown in Figure 15. The total process is described in References [5], [6], and [7] and will not be repeated here.

In Table V, the parameters above the double line are independent. Those below the double line are a function of the orbit, distribution of position and magnitude of the stars, and the independent parameters.

Figures 16 and 17 give the slit pattern for the passive and active systems. Note that the passive system has a much smaller central dead zone than does the active. Also, note (Table V) that the width of the slit on the mask of the passive system is greater, by a factor of 5, than that of the active. Each of these effects occurs for the following reason: In order to make the transit duration independent of the star position along the slit, the mask for each slit is wedged-shape (Figure 16) with vertex at the spin axis projection upon the plane of the mask (focal plane). For the passive system, the spin axis is (approximately) the satellite pitch axis which is 62° from the optical axis. Hence, within the field of view, the sides of the slit projection are nearly parallel. The active system, however, is such that the spin axis and the optical axis are (approximately) the same. Hence, the active system must possess a relatively large dead zone and rotational slit width to avoid the convergence of the slit sides near the optical axis.

Consider the following instrument parameters as given: aperture diameter, area of slits on the photodetector, solid angle subtended

TABLE V
INSTRUMENTATION PARAMETERS

Parameter	Numerical Value
Aperture	Passive 1", Active 2"
Field of View	20° with central dead zone (see Figs. 16 and 17)
Rotational Slit Width	Passive 2 arc min., Active 6 arc min.
Cathode Diameter	1"
Number of Slits	Passive 5 (see Figure 16) Active 1 (see Figure 17)
Photodetector	Photomultiplier
Optical System	Refractive
Electrical Filter	Four-pole Paynter followed by a differentiator to detect peak of filter output
Threshold Level	Function of spin period, set to yield sufficient number of detections
Focal Length	2.836"
F Number	Passive 2.836, Active 1.418
Min. Width of Slit on Mask	Passive .0013", Active .00026"
Max. Width of Slit on Mask	Passive .0014", Active .00087"
Max. Blur Spot	Passive 1.58 arc min., Active 0.31 arc min.
Average Time of Star in FOV	365 Seconds
Maximum Time of Star in FOV	389 Seconds
Probability of Detection	Figure 18
Accuracy of Detection	Equation (20)
Expected Number of Detections	Figure 19

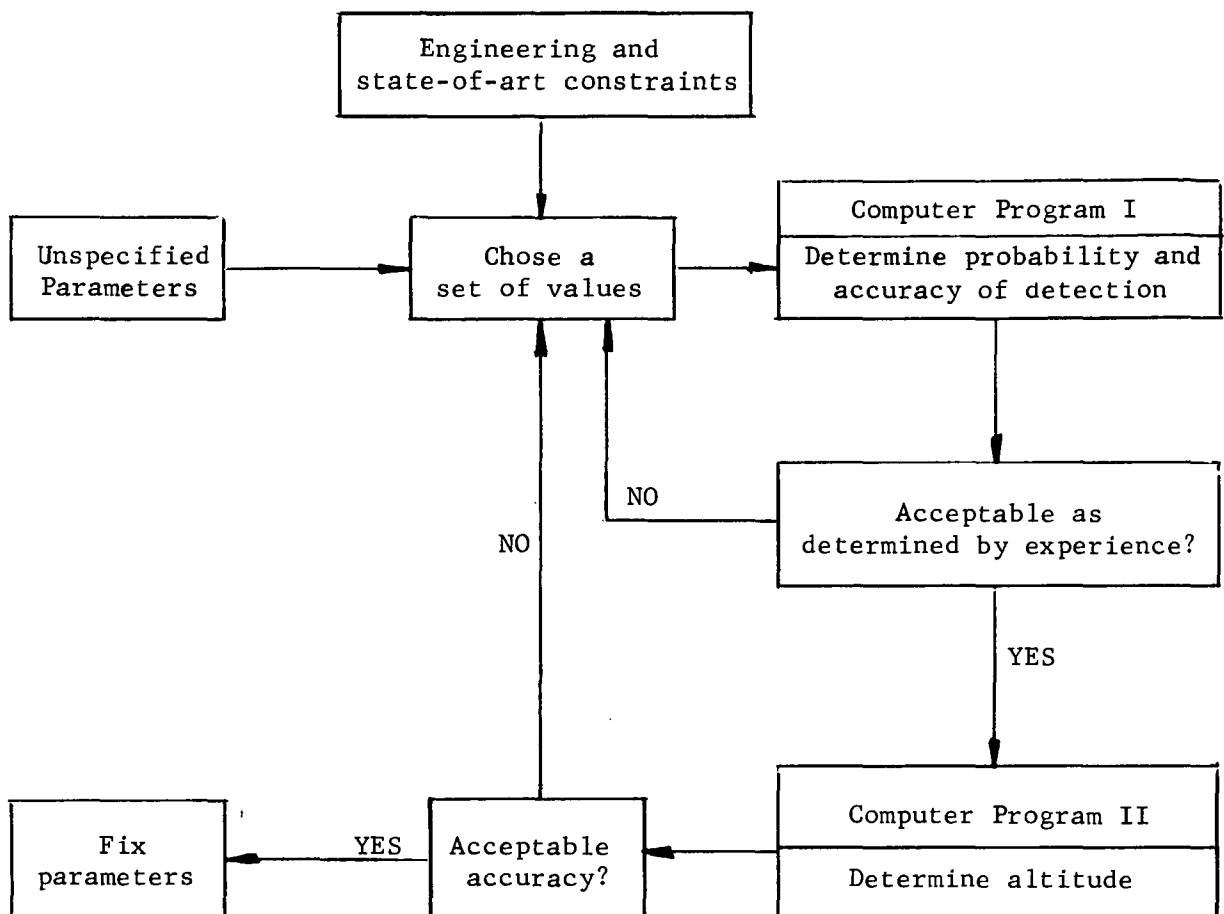


Figure 15: Iterative method of obtaining instrumentation parameters. The computer program I is an outgrowth of that reported in [7]. The program II is that discussed in the previous section.

by the slits, optical efficiency, photocathode sensitivity, slit geometry, and electrical filter. These inputs, together with the directional and intensity distribution of the stars allow the computation of the following outputs as a function of the instrument spin period: background noise at filter output, scanning noise* at filter output, signal noise at filter output, signal-to-noise ratio, standard deviation of the transit time error, expected number of false transits per unit time due to scanning and background effects, number of primary photoelectrons which arrive at the photodetector as a function of stellar magnitude, and probability of detection as a function of stellar magnitude. The method of computation is explained quite completely in Reference [8].

One output from Program I (Figure 15) is the stellar detection probability as shown in Figure 18. This output is obtained again by completion of the iteration indicated in Figure 15. A second output is the estimated transit time error.

The standard deviation of the measured transit time may be found as follows:

$$\sigma(m, P) = \sigma_T(m_T(P)) 10^{.4(m - m_T(P))}, \quad (20)$$

where

m	magnitude of star being detected,
$m_T(P)$	magnitude of star detected at the threshold level, this level being a function of the instrument spin period,
$\sigma_T(m_T(P))$	standard deviations of the measured transit time if a star were detected at the threshold level**.

Values of $\sigma_T(m_T(P))$ are given in Table VI.

*Noise due to dim stars which are close to the slit at the time a target star is detected. This noise source may be eliminated by rejection of such contaminated target stars.

**The threshold level is chosen so that the probability of detecting a star of magnitude $m_T(P)$ is 0.5.

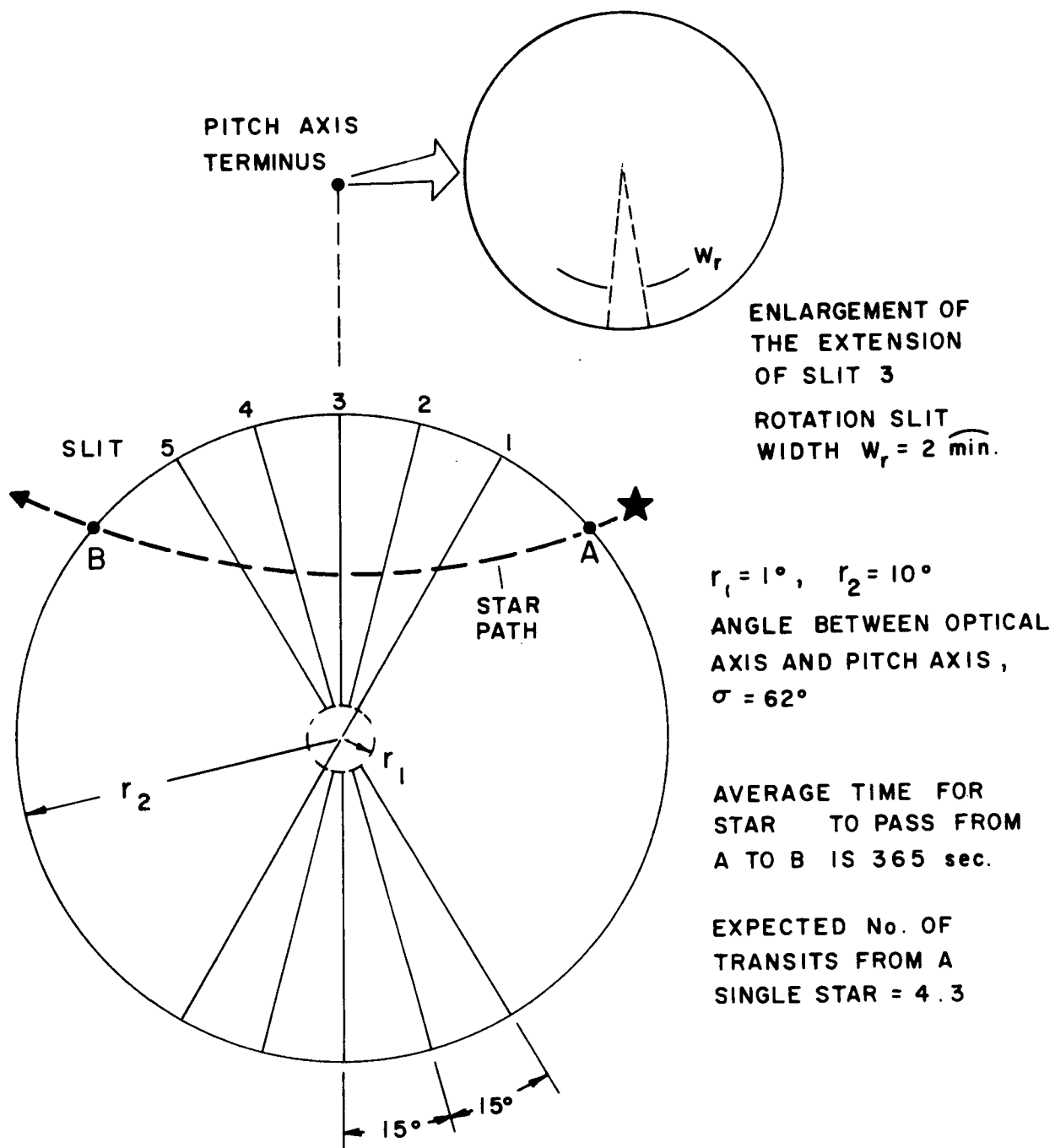


Figure 16: Slit Pattern for Passive System. If Two Heads are Used, Slit 5 is Continuous in Second Head.

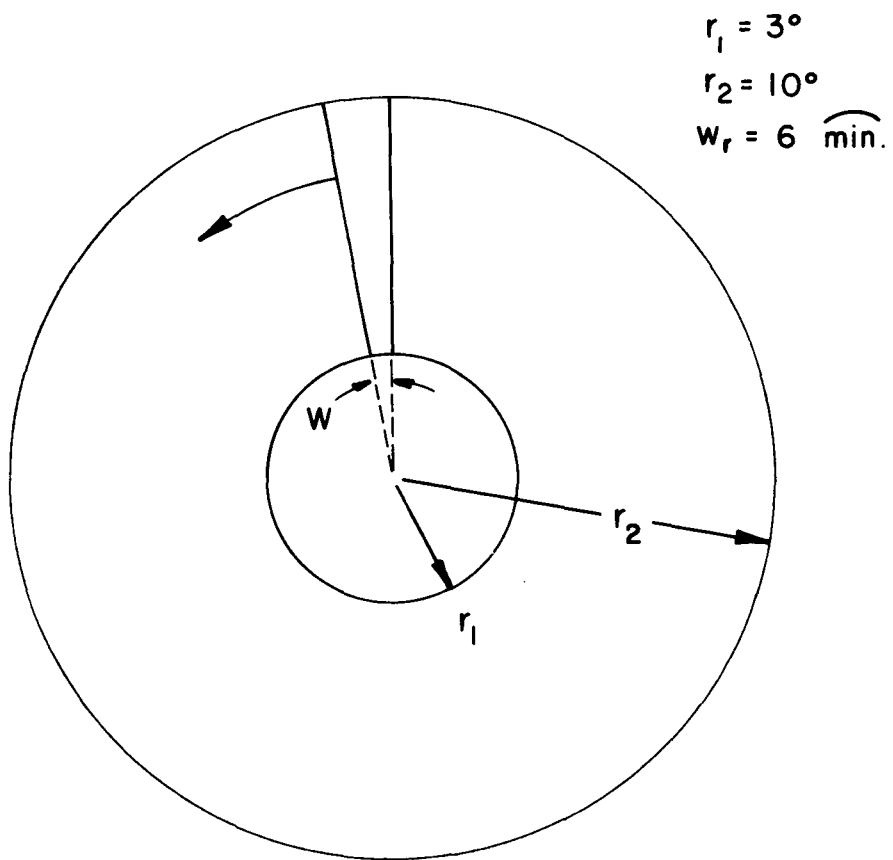


Figure 17: Slit Pattern for Active System.

TABLE VI

$m_T(P)$ and $\sigma_T(m_T(P))$

P (Seconds)	$m_T(P)$	$\sigma_T(m_T(P))$ (Seconds)
5	3.5	.000081
10	4.0	.00012
20	4.5	.00035
30	4.75	.00053
6200	5.00	.041

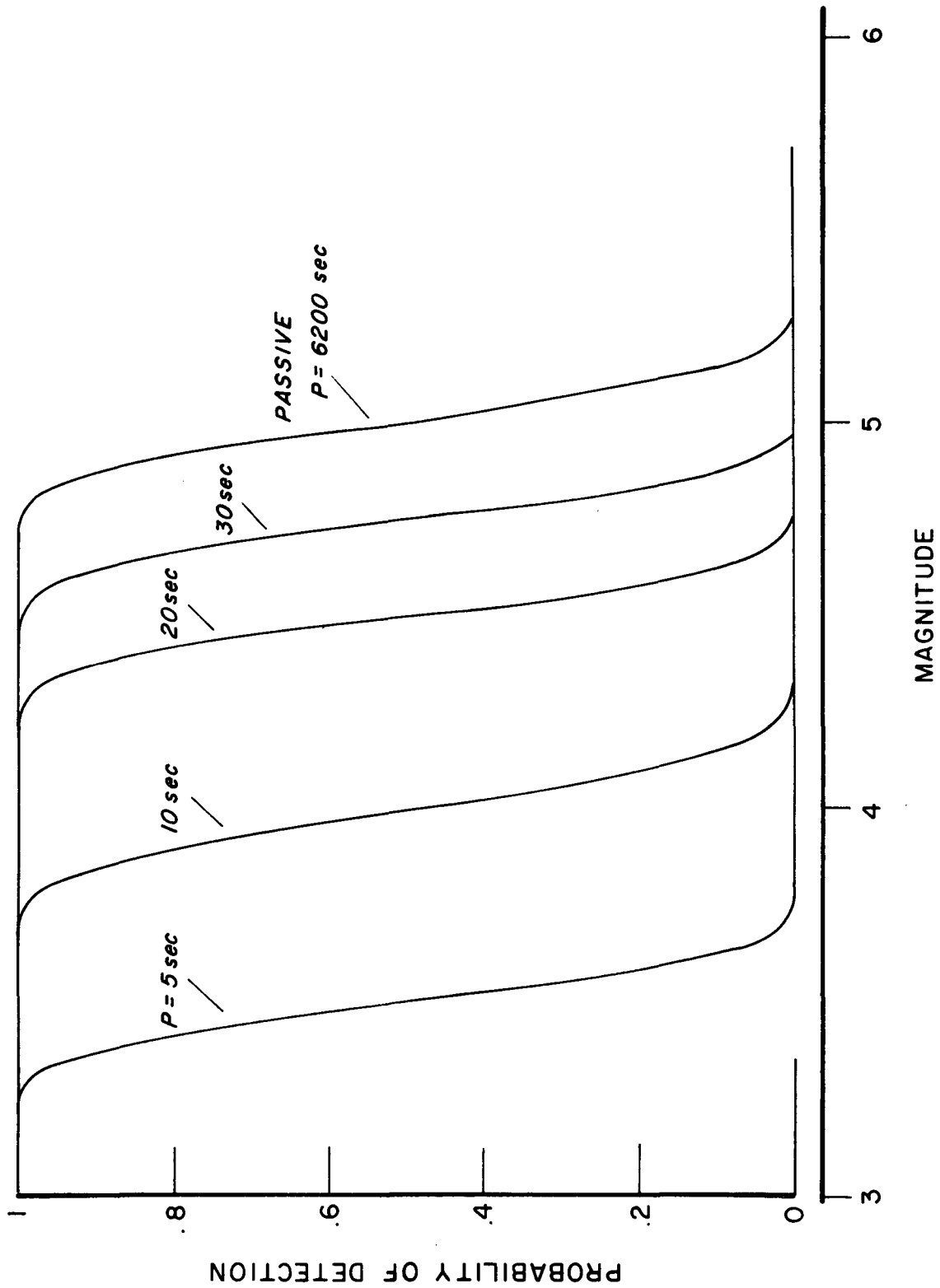


Figure 18: Detection Probability as a Function of Stellar Magnitude and Instrumentation Spin Period. $P = 5, 10, 20, 30$ (2" Aperture), and 6200 Seconds (1" Aperture).

All orbital elements except the longitude of the ascending node, Ω , have been specified. Hence, if this element is given, the orbit is completely specified and thus stellar background is known. This information together with the detection probabilities given in Figure 18 are sufficient to compute the expected number of stellar detections per second. This information is given in Figure 19.

First note (Figure 19) that the average number of stellar detections depends more strongly on Ω as the instrument spin period is decreased. This occurs because the shorter periods imply detections of the brighter stars only (also, of course, more detections per detected star), but the brighter stars tend to be distributed in clusters. That is, the dimmer stars tend to be more uniformly distributed than the brighter stars.

Next, note that 0.2 transits/sec will be obtained with the passive system and 0.4 transits/sec will be obtained with 30 sec spin period active system. A first thought might be that the 30 sec active system yields attitude whose errors are one-half those of the passive system. It will be shown that this is, in general, not a good approximation. This point will be discussed in detail later.

Recall that the apertures of the passive and active systems were fixed at 1" and 2", respectively (Table V). Thus, the active system demands a larger instrument. Of course, it may be argued that a smaller active instrument (than 2") can provide more transits/sec than the proposed passive system. It seems, however, that if one is to pay for the added instrumentation necessary for the active system, the resulting attitude estimate must be better than a marginal improvement over that afforded by the passive system. This criterion fixes the aperture of the active system at 2" and the maximum spin period of the active system at 30 seconds.

Finally, note from Figure 19 that, except for a certain set of Ω , little or no improvement in number of transits/sec is obtained from spin periods less than 10 seconds.

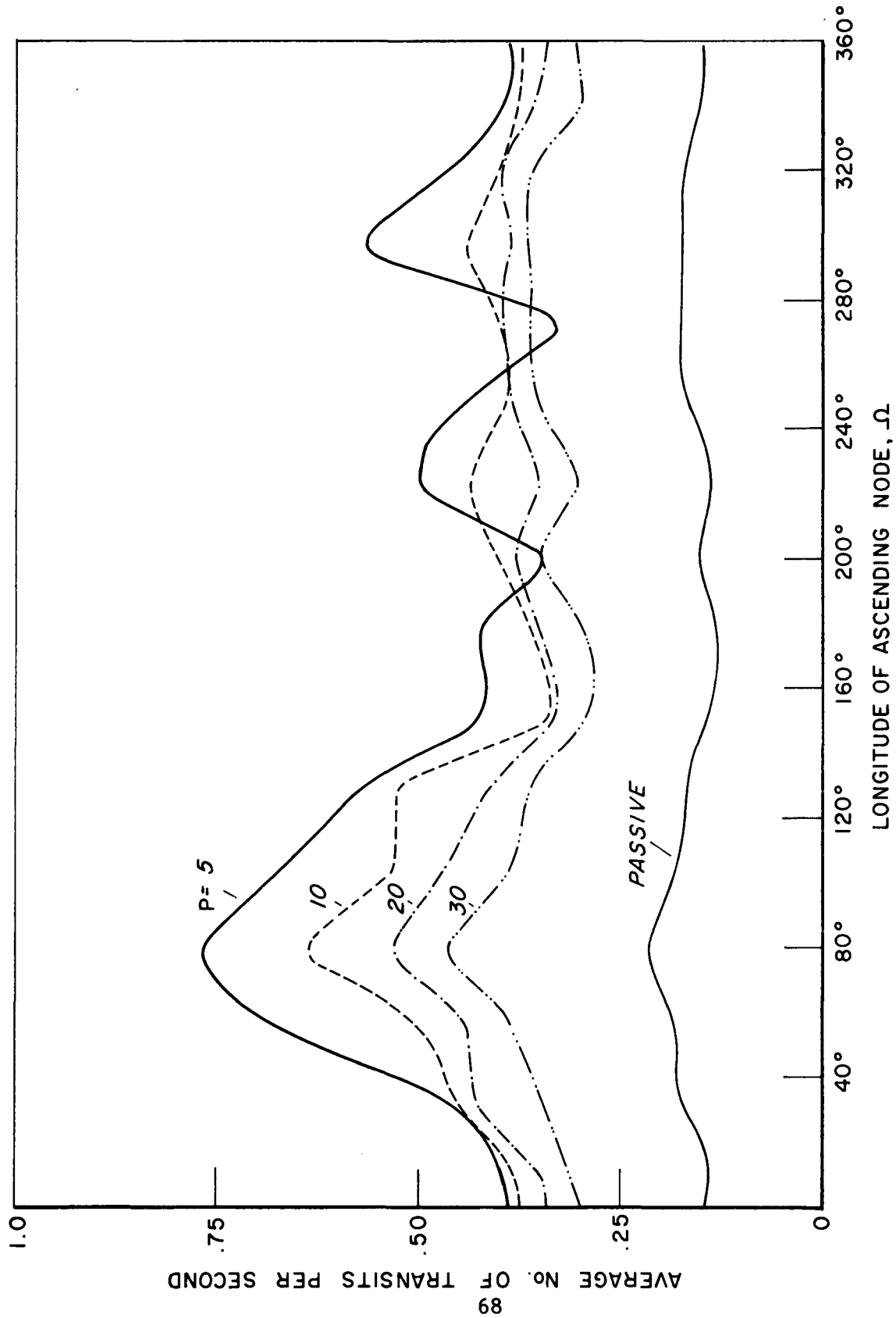


Figure 19: Average Number of Transits/Second for Passive System and Active System with Spin Periods of 5, 10, 20, and 30 Seconds. Two Sensors of the Recommended Configurations.

RESULTS

Figure 20 gives the general method used in this study to determine the accuracy to which the stellar transits determine the spacecraft's yaw, pitch, and roll. Note that four distinct attitudes are used.

- (1) The attitude as measured by the onboard attitude control system. This attitude estimate is used to drive the flywheel, and in this study it is considered a somewhat poor estimate of the true attitude. The parameters used to drive the flywheels are thus

$$\begin{aligned}\psi_m &= \psi + \Delta\psi \\ \theta_m &= \theta + \Delta\theta \\ \varphi_m &= \varphi + \Delta\varphi \\ \dot{\psi}_m &= \dot{\psi} + \Delta\dot{\psi} \\ \dot{\theta}_m &= \dot{\theta} + \Delta\dot{\theta} \\ \dot{\varphi}_m &= \dot{\varphi} + \Delta\dot{\varphi}\end{aligned}$$

where $\Delta\psi$, $\Delta\theta$, $\Delta\varphi$, $\Delta\dot{\psi}$, $\Delta\dot{\theta}$, and $\Delta\dot{\varphi}$ are chosen (as a function of time) input errors. In this study, the error in control attitude rates were chosen as $\Delta\dot{\psi} = \Delta\dot{\theta} = \Delta\dot{\varphi} = 0$, and the errors in control attitude were chosen as the functions

$$\begin{aligned}\Delta\psi(t) &= 2C_i, & t_{i-1} + \epsilon \leq t \leq t_i; \\ \Delta\theta(t) &= C_i + .05^\circ \sin 2\pi t, & t_{i-1} + \epsilon \leq t \leq t_i; \\ \Delta\varphi(t) &= C_i, & t_{i-1} + \epsilon \leq t \leq t_i.\end{aligned}$$

In the interval $t_i < t < t_i + \epsilon$, a smoothing formula was used so that the error in control attitude is continuous. Numerical values of the C's and t's are given in Table VII.

These errors were chosen to simulate constant bias errors in the horizon sensor. These constant bias errors change rapidly to simulate changes in the observed radiation output of the earth as the spacecraft orbits the earth. The sinusoidal term was added to the control pitch error to simulate an uncompensated error due to the earth oblateness.

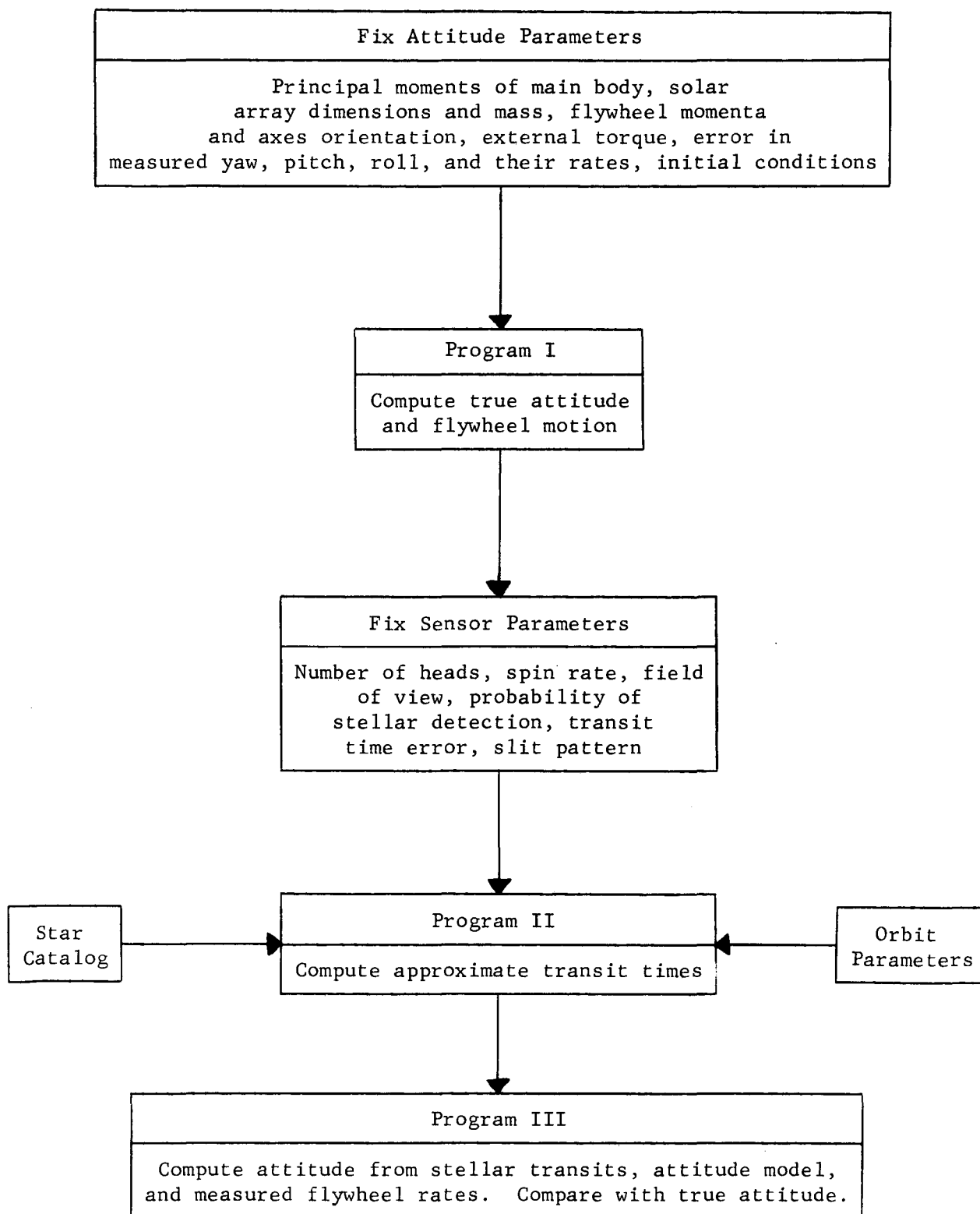


Figure 20: Method Used to Compute True Attitude and Star Sensor Attitude.

TABLE VII

PARAMETERS WHICH DEFINE THE CHOSEN ERROR IN THE
CONTROL ATTITUDE ($t_o = 0$)

i	t_i (sec)	C_i (deg x 100)
1	170	- 8
2	410	- 2
3	1000	2
4	1670	-10
5	2000	12
6	2670	4
7	3330	6
8	4170	- 4
9	5000	2
10	∞	0

- (2) The true attitude. This attitude is obtained as a solution of the differential equations with chosen initial conditions and chosen input parameters as previously given. A plot of resulting yaw and pitch is given in Figure 21. An explanation of its behavior is in order. To do so, let us concentrate on yaw in the time interval $450 \leq t \leq 2000$ seconds.

In the interval $450 \leq t \leq 1000$ seconds, $\Delta\psi = .04^\circ$. The control law is designed to drive $\psi_m = \psi + \Delta\psi$ to zero; hence, $\psi \approx -\Delta\psi = -.04^\circ$ as is shown in Figure 22. At $t = 1670$ seconds, the error in control yaw jumps to $\Delta\psi = -.10^\circ$. However, ψ does not immediately jump to 0.10° . Instead, there is considerable overshoot and a value of $\psi = 0.80^\circ$ is reached. After about 300 seconds, the jump in the control yaw error is damped out so that in the interval $1200 \leq t < 2000$ seconds, $\psi \approx -\Delta\psi = 0.10^\circ$. At $t = 2000$ seconds, another jump in the control yaw error occurs. The process is then repeated, this time with more overshoot because of the greater jump in control yaw error.

- (3) The model attitude. This attitude is the functional form assumed for yaw, pitch, and roll over the data gathering time interval. This model attitude has been discussed previously.
- (4) Finally, there is the attitude as estimated by the transit time and the flywheel outputs. This attitude is denoted by $\tilde{\psi}$, $\tilde{\theta}$, and $\tilde{\varphi}$. In this study, an attitude estimate will be supplied every 20 seconds over one orbital period. An attitude estimate could be supplied more often with no difficulty.

The accuracy with which the attitude can be determined by use of the stellar transits will now be considered. The passive system and various spin rates for the active system will be investigated. For both the passive system and the active system, the stellar field implied by $\Omega = 0$ was chosen. This choice was made because $\Omega = 0$ generally gives the smallest number of transits per orbital period over all choices of Ω (Figure 19). This choice thus, on the average, will yield larger attitude errors than other choices of Ω .

Passive System

Salient error results for the determination of attitude with the passive system are given in Figures 23, 24, and 25. Figure 23 gives cumulative distribution of the roll error. To obtain this figure, 310 cases were

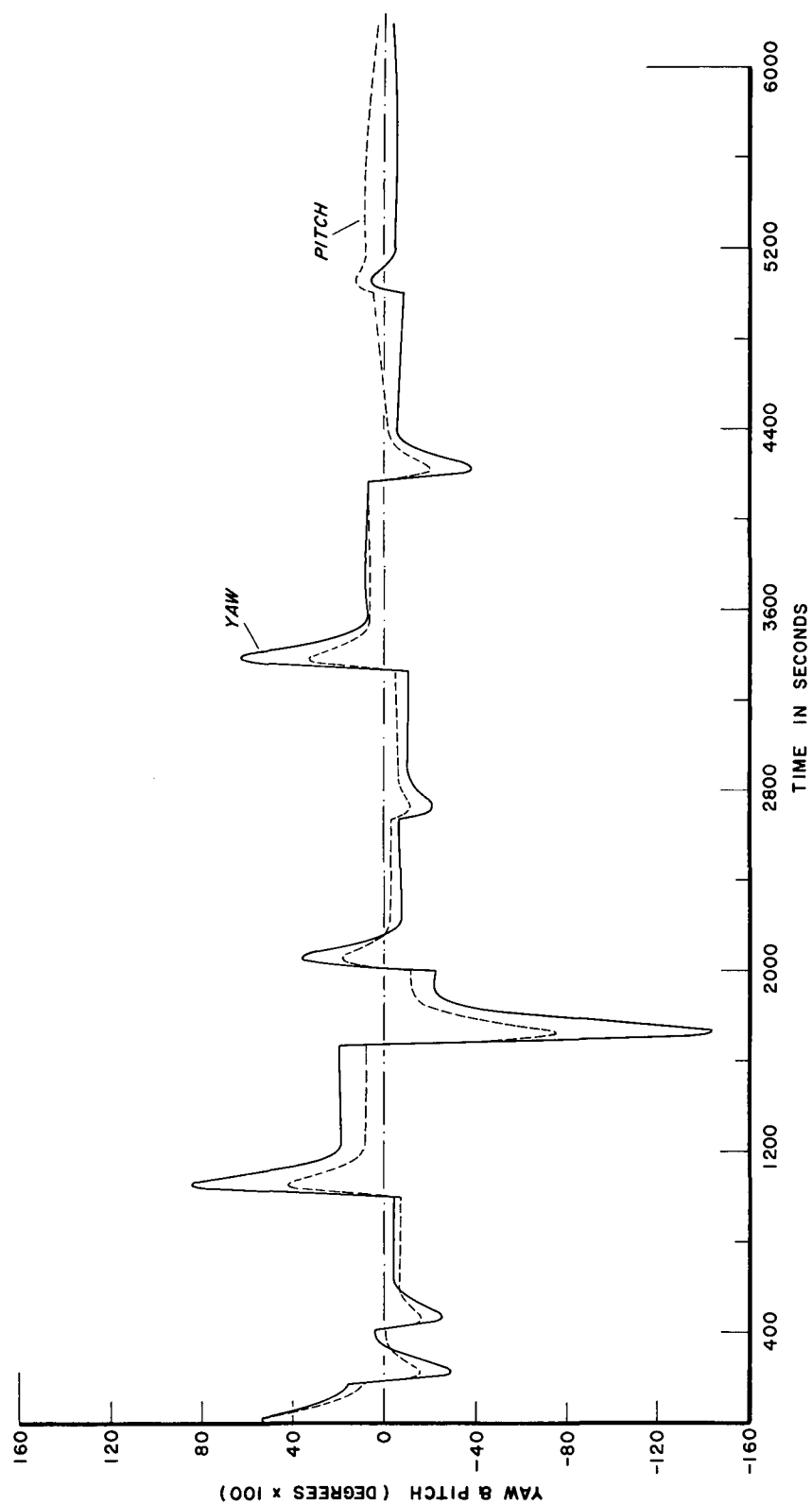


Figure 21: True Yaw and Pitch as a Function of Time.

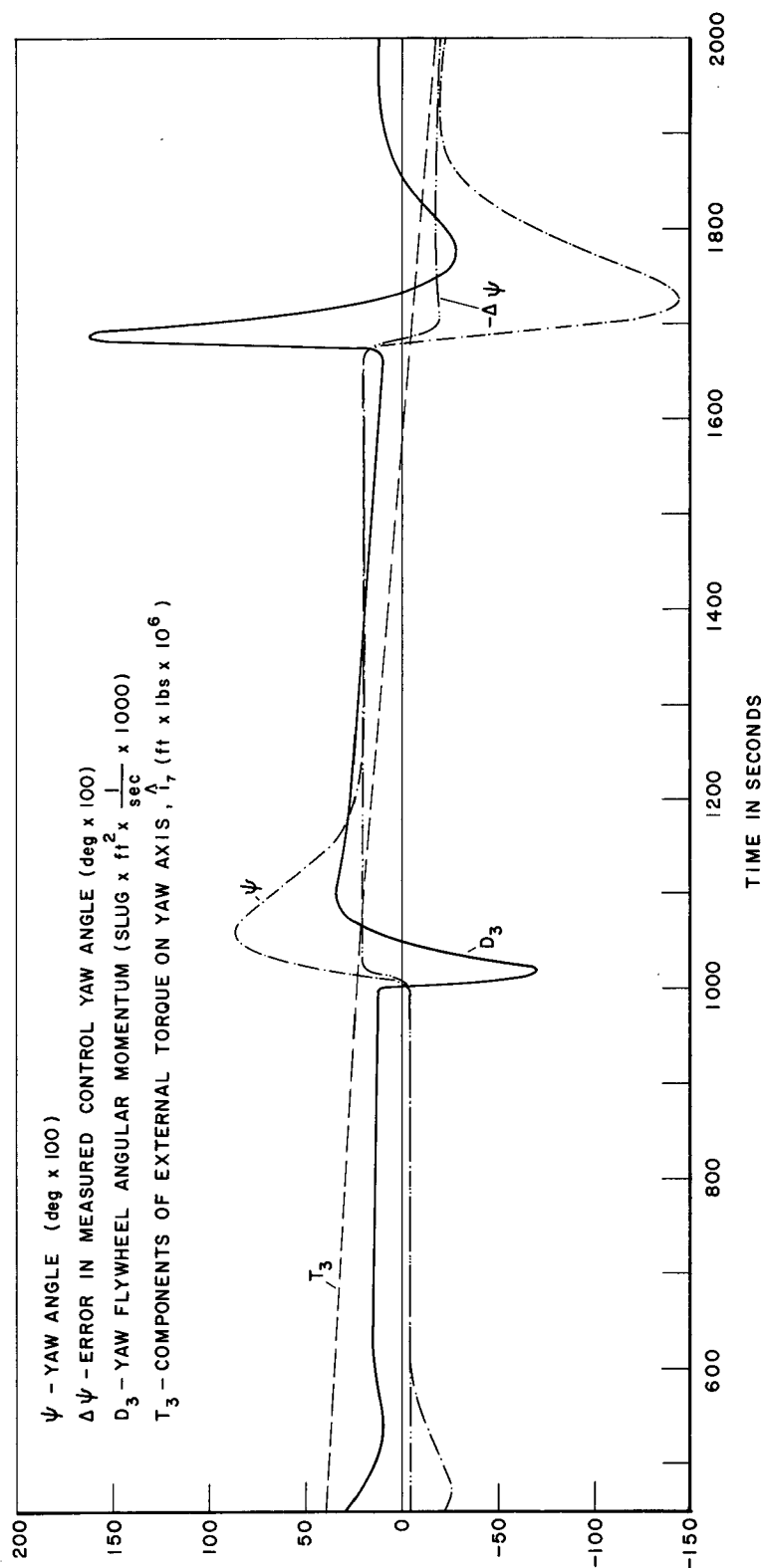


Figure 22: True Yaw, Error in Control Yaw, Yaw Flywheel Angular Momentum, and Yaw External Torque for $450 \leq t \leq 2000$ Seconds. Control Law is Such that $\psi + \Delta\psi$ is Driven to Zero.

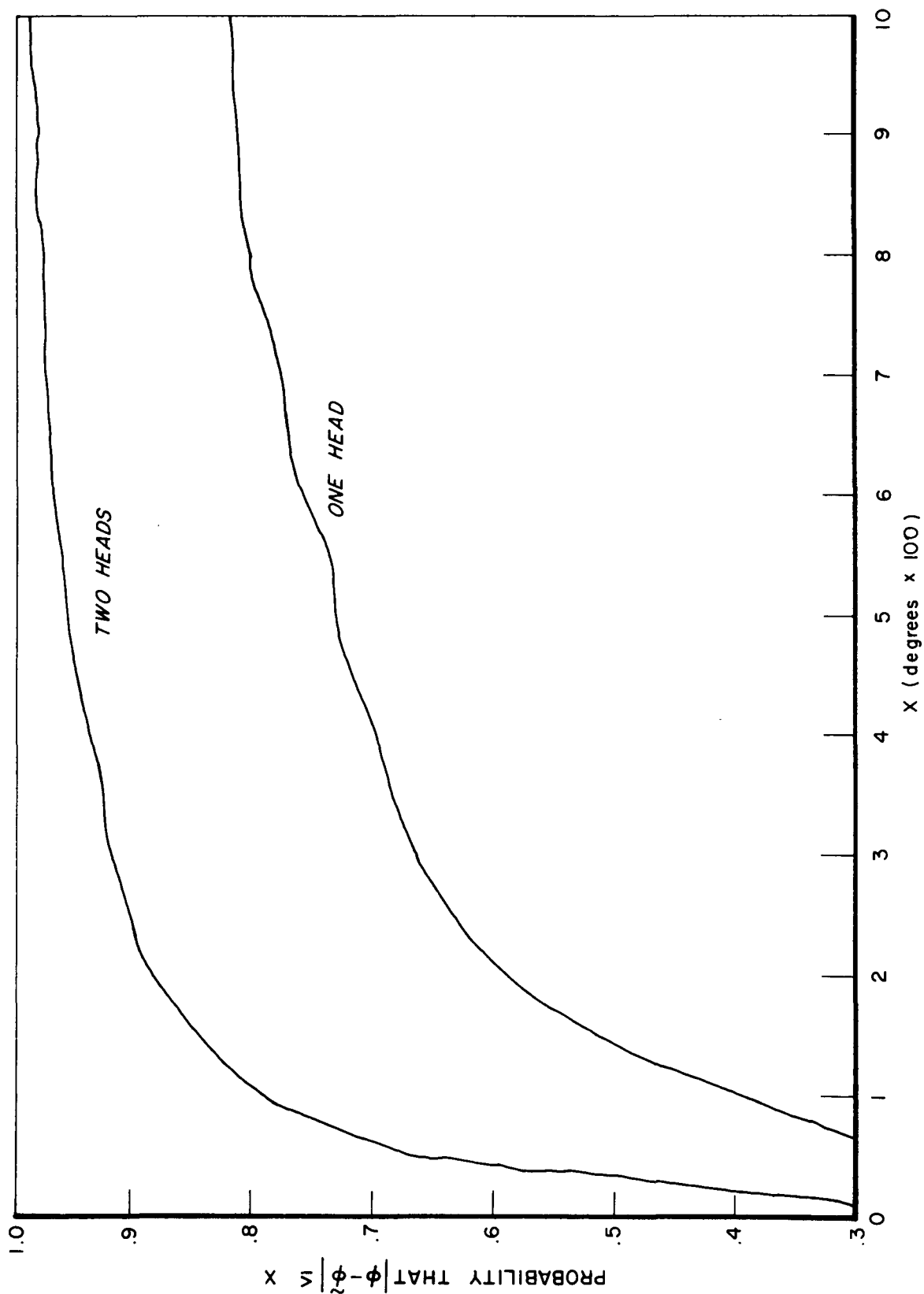


Figure 23: Cumulative Distribution Function of Roll Error. Passive System, One and Two Heads, Aperture 1". Errors in Yaw and Pitch are Slightly Smaller than the Roll Error.

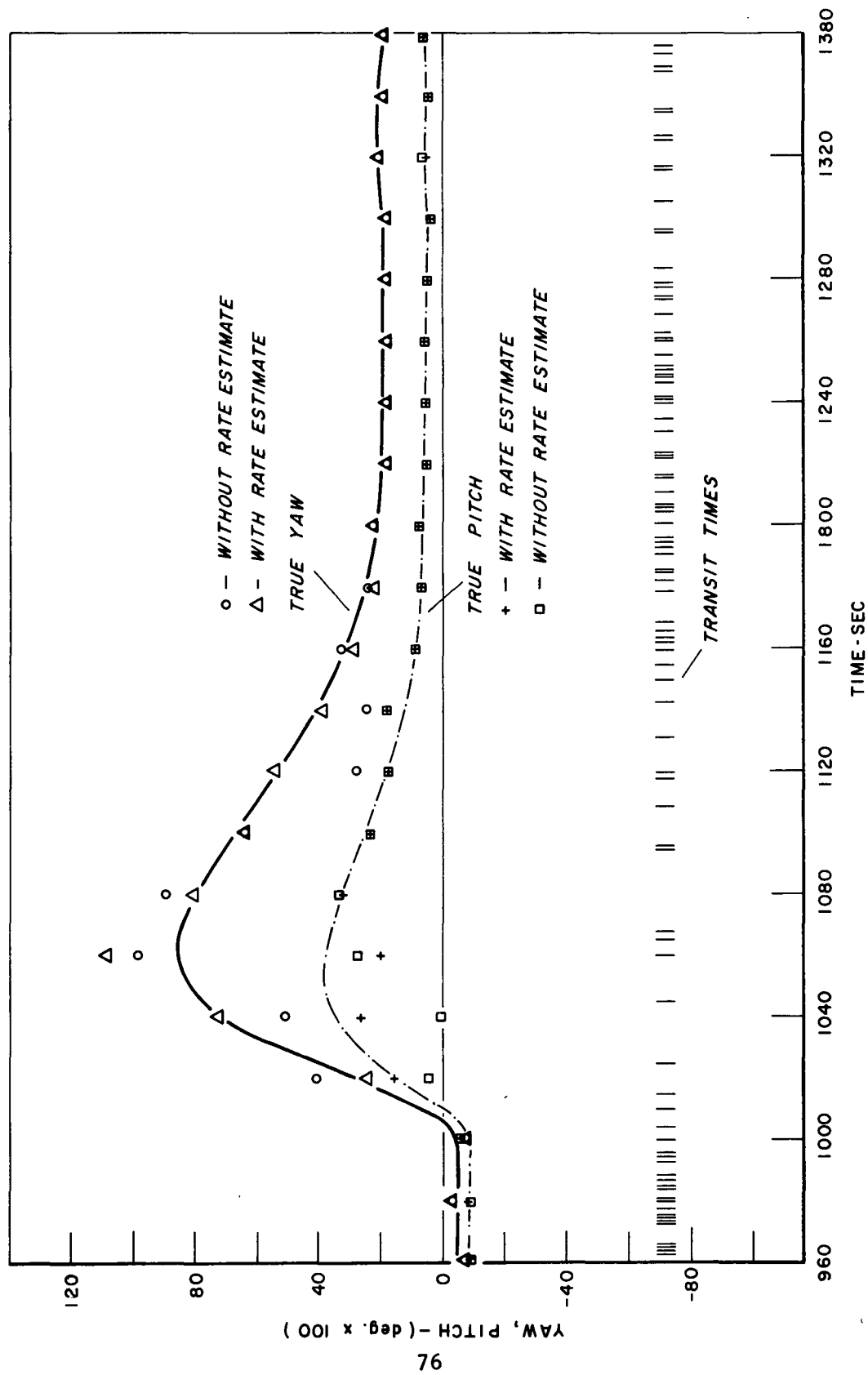


Figure 24: Yaw and Pitch, and Two Estimates of Yaw and Pitch for $960 \leq t \leq 1380$ Seconds.

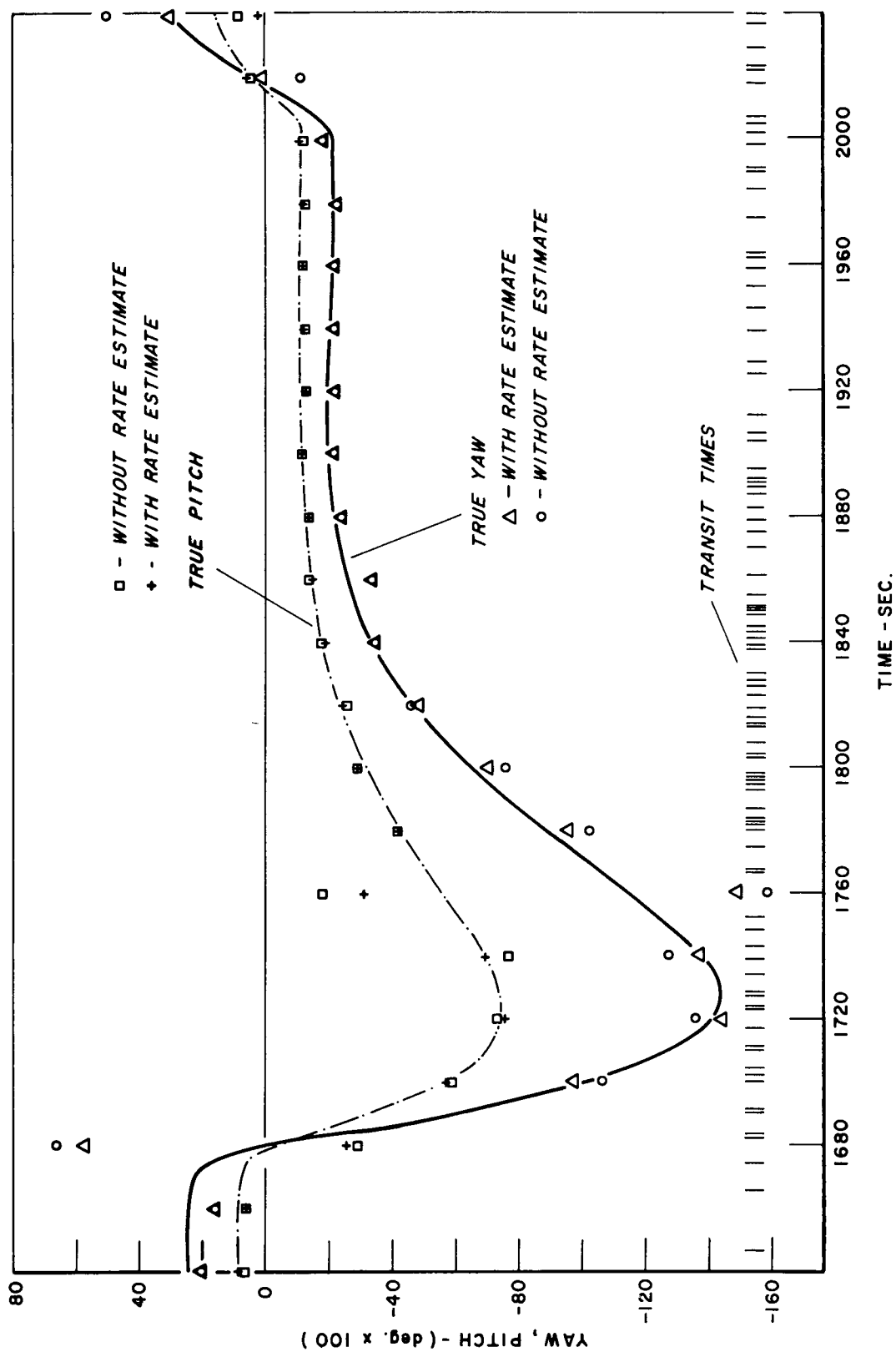


Figure 25: Yaw and Pitch, and Two Estimates of Yaw and Pitch for $1640 \leq t \leq 2040$ Seconds.

examined (an estimate every 20 seconds over the orbital period). Note that the passive system yields a roll error of less than 0.02° in 87 percent of the cases if a two-headed sensor is used. The corresponding number for the single-headed sensor is 58 percent.

Figures 24 and 25 compare two estimates of yaw and pitch with the true yaw and pitch in two different time intervals. Note that the attitude obtained with the aid of the rate estimates as described previously yield a significant improvement over that which simply used a constant model attitude. Roll estimates are not shown in Figures 24 and 25, but they are quite similar to the errors shown.

Active System

Results derived from active system parameters with spin periods of 10, 20, and 30 seconds are summarized in Figures 26, 27, and 28. Figure 26 shows the cumulative distribution function of the absolute value of the roll and yaw errors for the two-headed active system. The corresponding function for the pitch errors is not given, but it is quite similar to the plotted functions. From this figure, one notes that the errors are somewhat independent of the spin period. Also, the errors are quite small in that the probability is 0.96; that the error in any attitude angle is less than 0.03° .

Figure 27 is of the same format as Figure 26 except it is obtained from the parameters of the single-head system. Note that there is a significant change as the spin period is varied. For the single-head, the 10 second period yields larger errors than that of the 30 or 20 second periods. This increase in error occurs even though the data rate (Figure 19 and Table VIII) is approximately the same as that of the 30-20 second period. It occurs because at the faster spin rate only the brighter stars can be detected; hence, there may exist relatively long intervals of time over which only one or two stars are detected. This state implies large errors and is more probable with one head than with two heads.

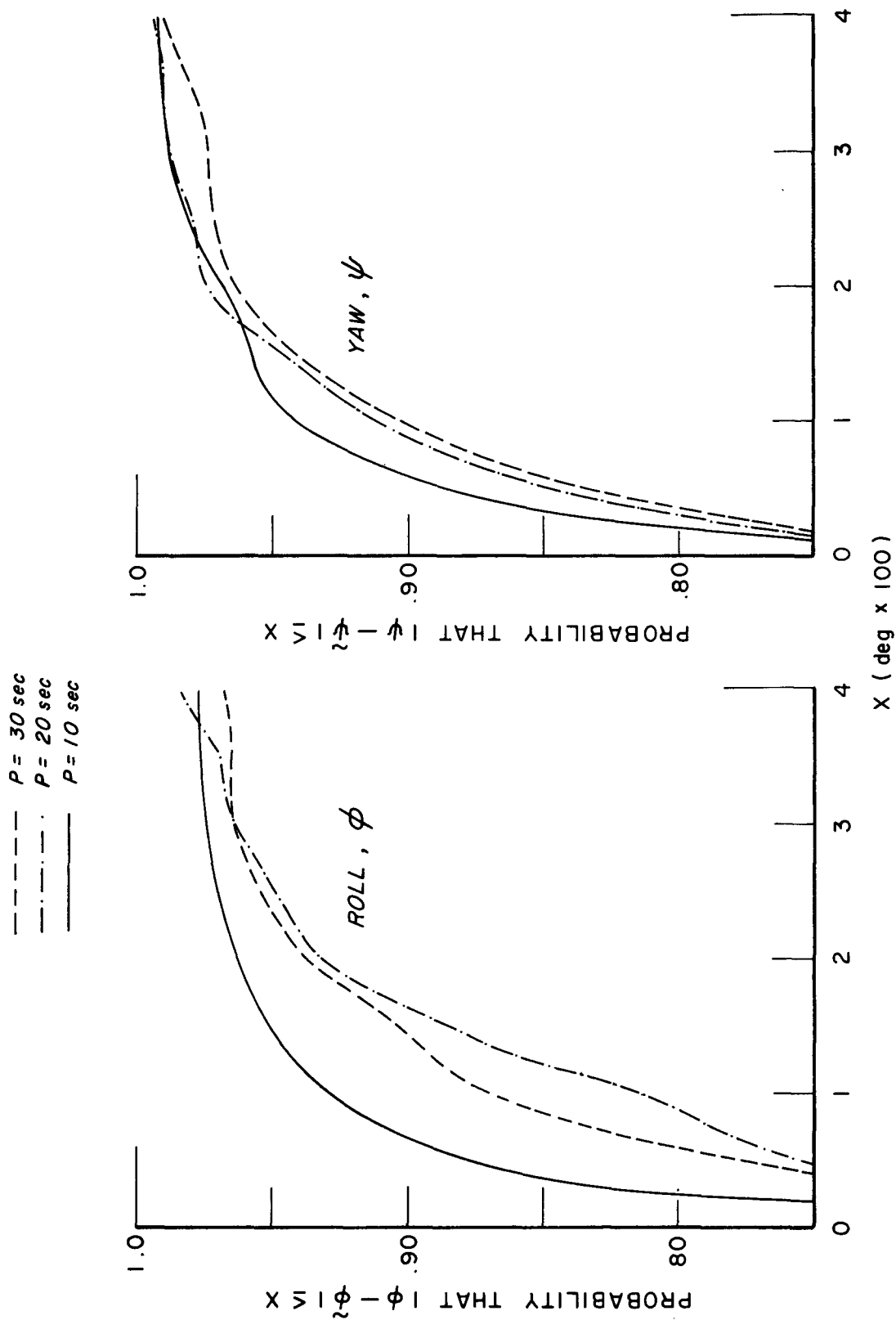


Figure 26: Cumulative Distribution Functions of Roll and Yaw Errors 30, 20, and 10 Second Periods. Two Heads, 2" Aperture, Active System.

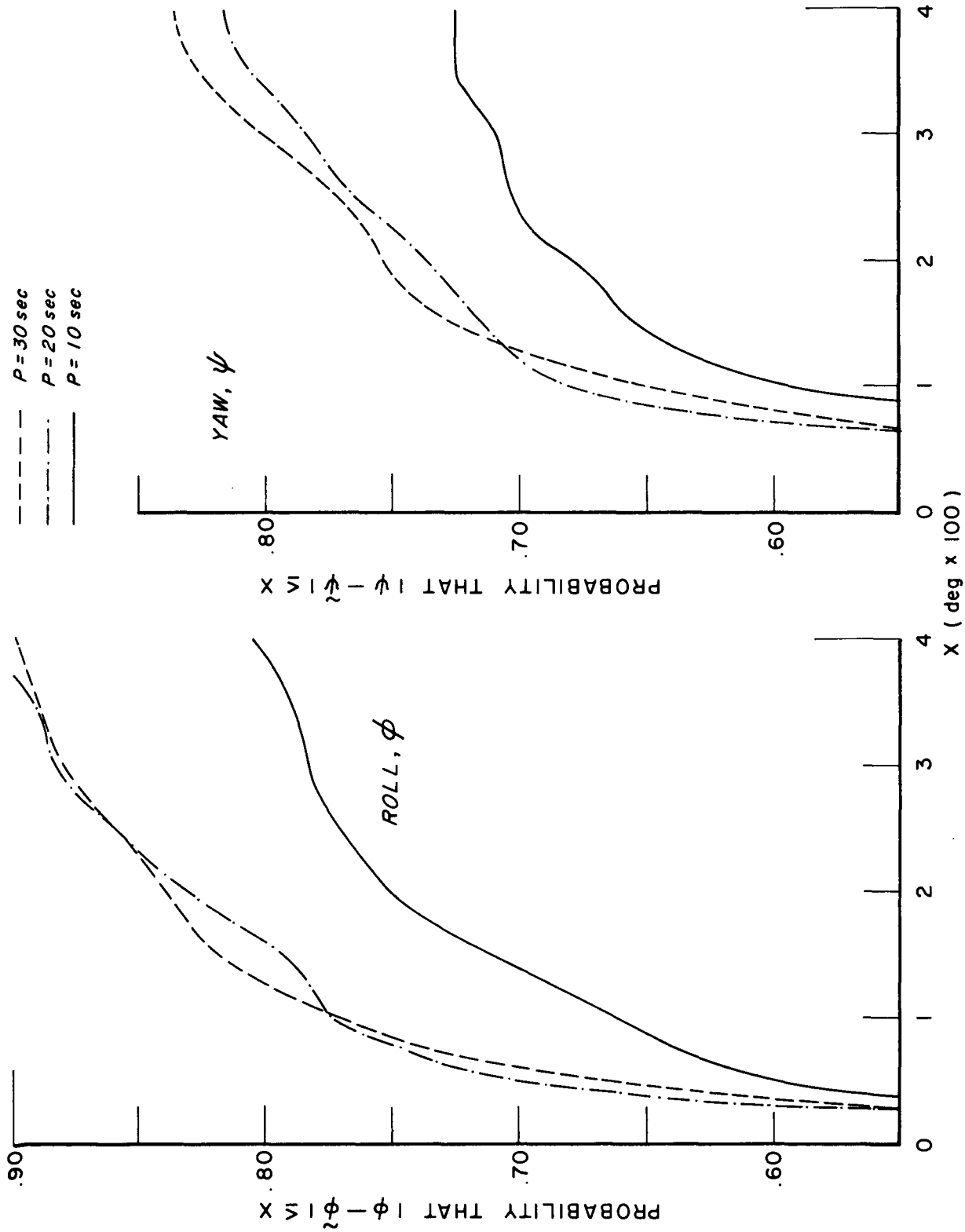


Figure 27: Cumulative Distribution Functions of Roll and Yaw Errors 30, 20, and 10 Second Periods. Sinble Head, 2" Aperture, Active System.

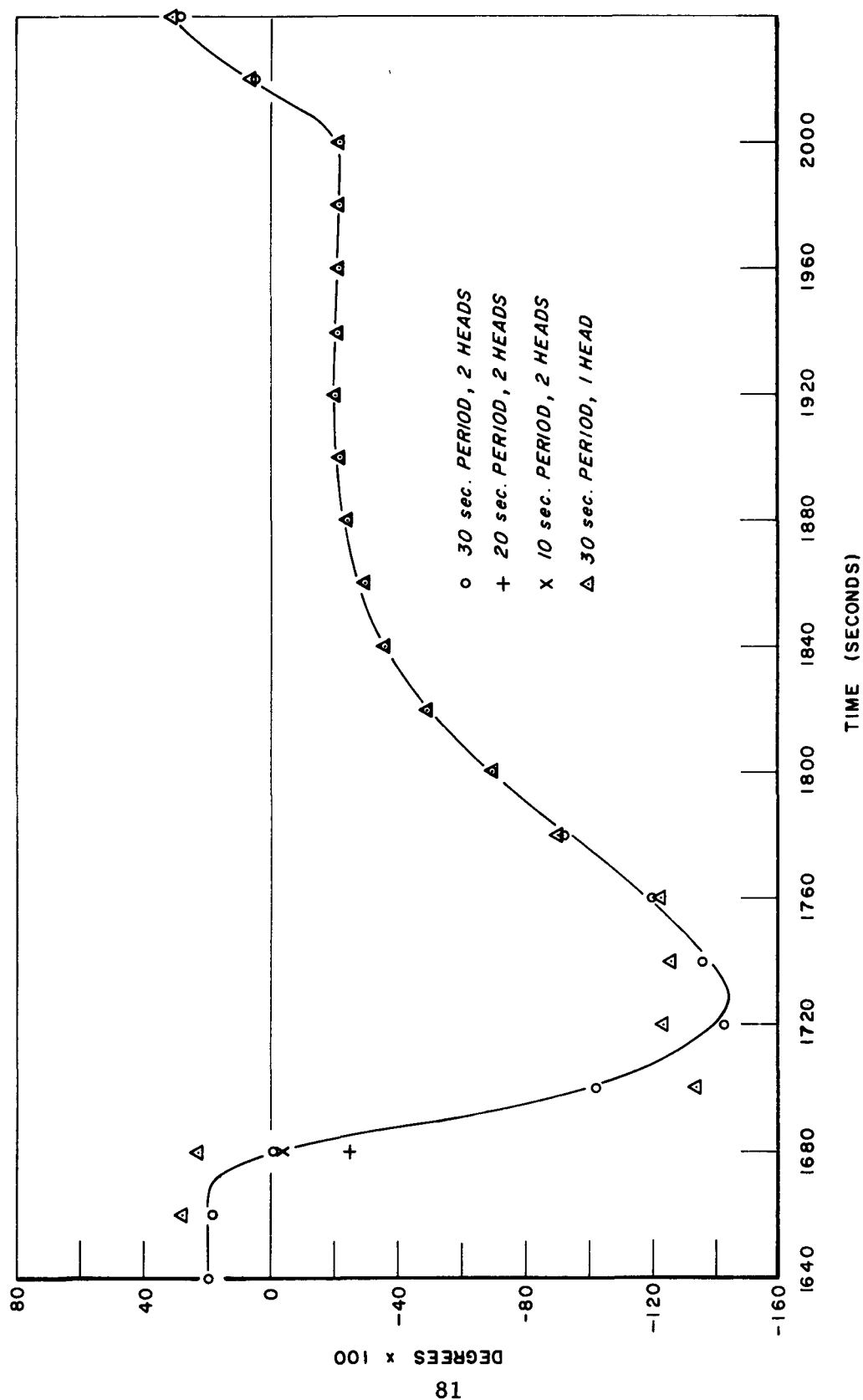


Figure 28: Estimated Yaw, $\tilde{\psi}$, and ψ in the Time Interval $1640 \leq t \leq 2040$ Seconds. $\tilde{\psi}$ Obtained from the 30 Second Period Two Head and Single Head System is Shown. Also Shown are the Poorest Estimates Obtained by Use of the 20 and 10 Second Period (at $T_p = 1680$ Seconds).

A central question which was to be answered by this study is:

If an active instrument is to be used, what is the optimum spin rate?

An answer may now be given.

Suppose, for the moment, that optical aperture diameter is fixed at two inches and the field of view is fixed at 20° , then periods much longer than 30 seconds should not be considered. In this case, the accuracy of the system approaches that of the passive system. Why consider an active system if a small passive system yields a comparable accuracy? Periods much shorter than 10 seconds should not be considered. In this case, time intervals can exist in which only one or two stars are detected if a single-head sensor is used. But, even if the spacecraft is fitted with a two-headed sensor, periods will exist in which the moon will cause one head to be inoperative. Hence, single-head operation must be considered. Shorter spin periods could be considered if the aperture diameter were greater than two inches or the field of view were greater than 20° , for each of these changes would imply that more stars would be detectable. The first change implies a larger instrument, and the second implies a more difficult optical and stray-light shielding problem. Neither change is recommended. Our recommendation for an active system is one which consists of two heads, each with a spin period between 20 and 30 seconds.

Additional results are given in Table VIII. This table lists the standard deviation of each estimated attitude angle, the number of stars which were detected in an orbital period, and the total number of transits gathered in an orbital period. This information is given for the two-head and single-head sensor and for three active systems.

TABLE VIII

STANDARD DEVIATION OF YAW, PITCH, AND ROLL ERRORS,
NUMBER OF STARS TRANSITED, AND NUMBER OF TRANSITS.
ATTITUDE ERRORS IN DEGREES $\times 100$. $\Omega = 0$.

Period	Two Heads				Single Head			
	$\sigma(\delta\psi)$	$\sigma(\delta\theta)$	$\sigma(\delta\phi)$	Transits	$\sigma(\delta\psi)$	$\sigma(\delta\theta)$	$\sigma(\delta\psi)$	Transits
10 secs	.75	1.17	2.05	2927	18.6	22.7	36.4	1450
20 secs	1.81	1.82	3.87	3455	5.1	7.9	13.7	1723
30 secs	1.01	1.38	2.20	2881	4.7	7.4	11.8	1448
Passive	4.72	2.75	3.84	1808	12.1	25.4	36.7	910

AREAS FOR ADDITIONAL INVESTIGATIONS

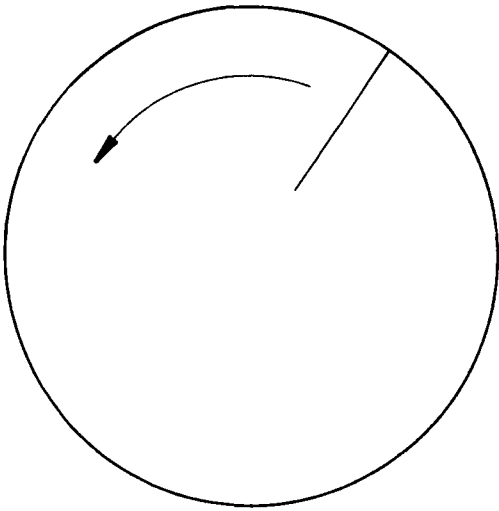
This study may be considered as a fairly complete analysis of the feasibility of providing a high accuracy, operational, near real-time attitude determination system for the ERTS spacecraft. However, several areas have been uncovered during the study in which system changes may improve the accuracy of the system. These points and additional areas for study will now be commented upon.

Instrumentation

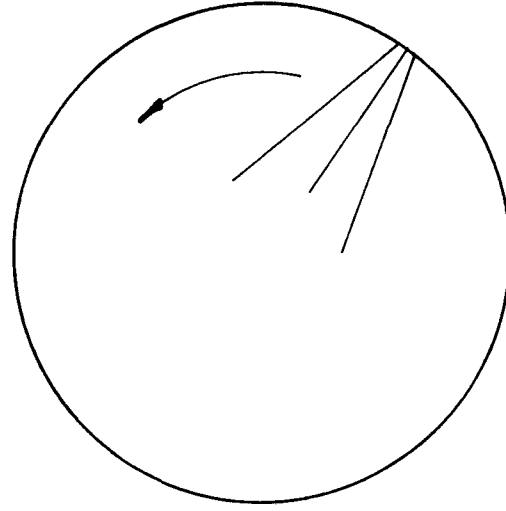
It is possible to consider different slit patterns for both the passive and active systems which should yield smaller attitude errors at the expense of more difficult optical designs. Smaller errors may not be of importance for the two-headed active system, for the present system does provide quite satisfactory results. However, it may be desirable to improve the accuracy performance of the passive and single-head active systems.

A possible slit pattern improvement for the active system is shown in Figure 29. This figure shows a three-slit configuration similar to that successfully used by CDC on the ATS-III spacecraft (Reference [9]). This configuration provides a coelevation measurement (angle between a star's direction and the optical axis) as well as the azimuth measurement obtained with the single slit. The coelevation measurement is obtained because the time between successive transits of the same star is a function of the coelevation. That is, three closely occurring transits will characterize a star far from the optical axis. As the star is moved toward the optical axis, the transits will become more widely spaced.

This three slit configuration also makes possible a simpler star identification problem than that implied by a single slit. This simplification occurs because more information is obtained concerning each star's direction so that each candidate star is required to pass a more severe test before it is paired to the transited star. The disadvantage of the three-

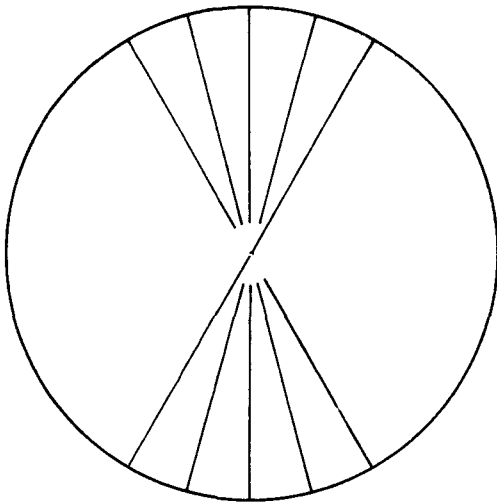


**PRESENT ACTIVE
SLIT PATTERN**

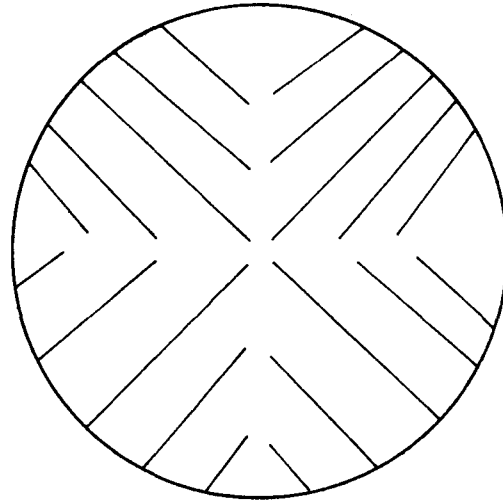


POSSIBLE IMPROVEMENT

Figure 29: Possible Improvement of Slit Pattern for the Active System.



**PRESENT PASSIVE
SLIT PATTERN**



POSSIBLE IMPROVEMENT

Figure 30: Possible Improvement of Slit Pattern for the Passive System.

slit configuration is that the optical system must possess small radial distortion as well as small tangential distortion. For the single-slit configuration, radial distortion does not give rise to errors. Also, the background noise is greater for the three-slit configuration than the single slit configuration.

Figure 30 gives the present passive slit pattern and a possible improvement. The suggested improvement will provide more transits per star and thus a more accurate system. Moreover, it could ease the star identification problem. This can be done by designing the pattern so that the time between successive transits of the same star is constant if yaw, pitch, and roll are zero. Again, the optical design problems are greater with the suggested change.

Star Identification

The star identification problem has not been considered in this study. Each slit pattern presents a separate problem. It is most difficult for the present passive slit pattern, for in this case the star as well as the slit must be identified. The problem may be considered solved for the suggested change to the active slit pattern.

Analysis

It may be possible to improve system performance in the presence of low data and rapid changes in attitude. This could be done by use of approximate equations of motion and a Kalman-type filter instead of the model and filter used in the present study. The disadvantage of this suggested approach is that systems of differential equations must be solved numerically in the data reduction process. Thus, a longer computer running time will be required. Perhaps this more time-consuming reduction should be used only if a low data rate is coupled with a rapid change in attitude.

CONCLUDING REMARKS

Instrumentation

Two classes of instrumentation were considered, a passive system and an active system. The passive system consists of five radial slits which are fixed with respect to the spacecraft. Stars transit the slits due to the slow orbital motion of the spacecraft. For this system, a one-inch diameter optical aperture can be used and fifth magnitude stars detected. The system is very attractive from the instrumentation view point since a small, light weight, low power consumption, reliable instrumentation with no moving parts is possible.

The active system consists of a single radial slit (three times wider than each slit of the passive system) which is made to rotate about the sensor optical axis. This rotation is produced by simply rotating the small thin reticle upon which the slit is photoetched. Thus, the active system gathers stellar transits at a greater average rate than the passive system. However, its optical aperture must be larger (two-inch diameter) and a method must be provided to measure the orientation of the slit about its rotation axis (angle encoder or constant drive motor). The recommended spin period of the reticle is 20 to 30 seconds. At these periods, stars of magnitude 4.5 to 4.75 will be reliably detected.

For both systems, the recommended detector is a photomultiplier. This recommendation is made simply to make possible a smaller optical aperture than if a solid state detector were used.

Two sensor heads are recommended for both the passive and active systems. Two heads provide a stronger measurement geometry, greater data rate, redundancy, and system operation in the presence of the moon (the moon can saturate only one of the two heads at a time). The field of view of each head is 20° with a central dead zone of 3° for the active system and 1° for the passive system.

To yield maximum angular distance from the earth (which may be sunlit), sun, and solar array, the following head placement should be used. Each head should be placed 62° from the pitch axis. The projection of the first head's optical axis on the yaw-roll plane is 113° ; the second head's, 247° (see Figure 2). For this case, the angle from the optical axis of either sensor to the sun is greater than 50° , the angle to the horizon is greater than 46° , and the angle to the panel is greater than 38° .

Data Reduction

A batch processing, least squares estimator is recommended. The model attitude is of the form

$$\varphi(t) = \varphi(T_p) + (t - T_p) (\tilde{\omega}_1(T_p) + \dot{\nu}\psi(T_p)),$$

$$\theta(t) = \theta(T_p) + (t - T_p) (\tilde{\omega}_2(T_p) - \dot{\nu}),$$

$$\psi(t) = \psi(T_p) + (t - T_p) (\tilde{\omega}_3(T_p) - \dot{\nu}\varphi(T_p)),$$

where T_p is a time at which an attitude estimate is desired, $\dot{\nu}$ is the orbital true anomaly rate, and $\tilde{\omega}$'s are estimated angular velocity components of the spacecraft system with respect to an inertial system. These components are estimated from the measured time history of the flywheel momenta, and by assuming the spacecraft is "on the average" local-vertical stabilized and such that the external torque is a slowly varying function of time.

The transits closest to T_p which yield a strong geometry (not ill-conditioned) are then chosen to be used in the least squared solution. The resulting linear equations in $\varphi(T_p)$, $\theta(T_p)$, and $\psi(T_p)$ are weighted, with greater weights (generally) for transits near T_p . The computer running time to provide one attitude estimate is approximately 0.1 seconds on the CDC 6400.

Error Analysis

The greatest error source does not originate in the instrumentation, but in the attitude model. However, the estimated attitude is quite good even in the presence of a poorly controlled spacecraft and a poor stellar field. The active system has a greater accuracy than that of the passive system. One -sigma values of the absolute value of the error in the active or passive and single-head or two-head systems are:

	Two-Heads			Single-Head		
	Yaw	Pitch	Roll	Yaw	Pitch	Roll
Active (30 sec)	.010°	.014°	.022°	.047°	.074°	.118°
Passive	.047°	.027°	.038°	.121°	.254°	.367°

These values were obtained from the poorest stellar field over all orbital Ω 's and a rather poorly controlled spacecraft attitude.

REFERENCES

1. Grosch, C. B., et.al., The SCNS Attitude Determination Experiment on ATS-III. Proceedings of the Symposium on Spacecraft Attitude Determination, Vol. 1, Oct. 1969, pp. 212-214.
2. Final Report: Computer Program for OSO-H Star Sensor, prepared by CDC for NASA-Goddard Space Flight Center, Greenbelt, Maryland, Contract No. NAS5-11286, March 1971, pp. 40-45.
3. Pringle, Ralph Jr., On the Stability of a Body with Connected Moving Parts, AIAA Journal, Vol. 4, No. 8, August 1966.
4. Scheffe, Henry, The Analysis of Variance, Wiley, New York, 1967, pp. 14-15.
5. Final Report: Study of a Scanning Celestial Attitude Determination System (SCADS) for a Synchronous Satellite, prepared by CDC for NASA-Goddard Space Flight Center, Greenbelt, Maryland, Contract No. NAS5-10372, February 1968.
6. Final Report: Feasibility Study for a Scanning Celestial Attitude Determination System (SCADS) on the IMP Spacecraft, prepared by CDC for NASA-Goddard Space Flight Center, Greenbelt, Maryland, Contract No. NAS5-9439, June 1967.
7. Final Report: Computer Programs for Scanning Celestial Attitude Determination Systems, prepared by CDC for NASA-Goddard Space Flight Center, Greenbelt, Maryland, Contract No. NAS5-10495, February 1970.
8. Nickel, D. F., Internal CDC report: TM 1021, Compilation of Equations Describing Starmapper Signal and Noise Components, July 1970.
9. Final Report: Self-Contained Navigational Experiment, prepared by CDC for NASA-Goddard Space Flight Center, Greenbelt, Maryland, Contract No. NAS5-9683, July 1969.

APPENDIX A

ANGULAR MOMENTUM OF A BODY COMPOSED OF
CONNECTED RIGID SECTIONS

APPENDIX A

ANGULAR MOMENTUM OF A BODY COMPOSED OF
CONNECTED RIGID SECTIONS

Assume the body is composed of two rigid sections such that these sections have at least one point in common (see Figure 1A). Denote the set of points in one rigid section as s and the set of points in the other as m . Assume one point of s is fixed with respect to an inertial system, and let;

S_1 be an inertial system,

S_s be a system fixed in s at its center of mass,

\bar{c} be a vector from the center of mass of s to a common point of s and m ,

S_m be a system fixed in m at the terminus of \bar{c} .

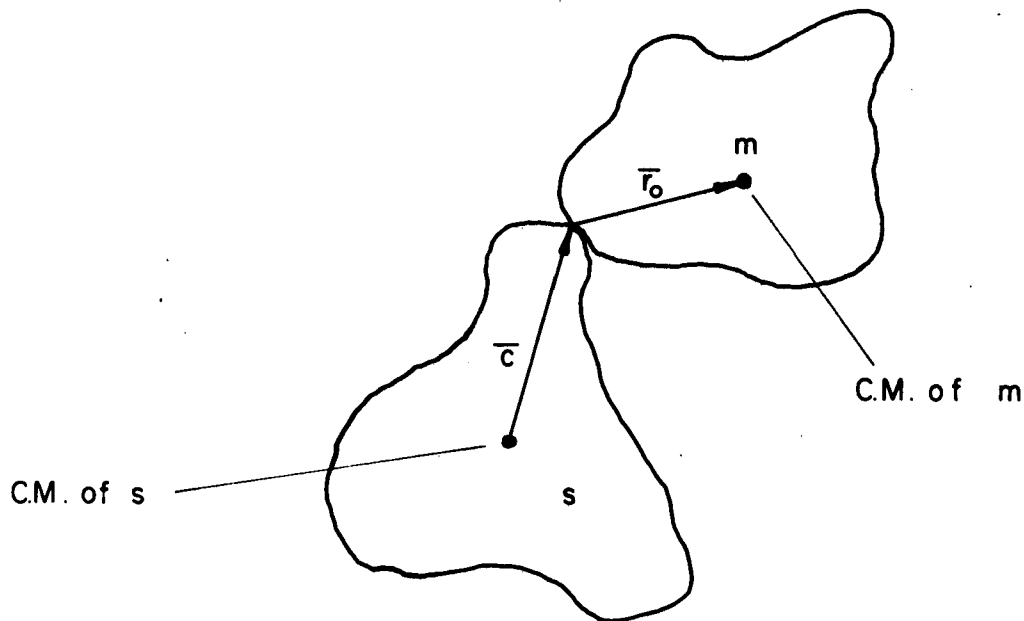


Figure 1A: The Connected Rigid Bodies s and m .

Now,

$$\bar{H} = \sum_T \bar{R}_i \times m_i \frac{d\bar{R}_i}{dt} = \sum_T \bar{R}_i \times m_i \left(\frac{d\bar{R}_i}{dt} + \bar{\omega}_{1s} \times \bar{R}_i \right),$$

where

$$T = s + m,$$

\bar{H} angular momentum of the body,

\bar{R}_i position vector of the i^{th} point in the body, the origin of \bar{R}_i is the center of mass of s ,

m_i is the mass of the i^{th} point,

$$\frac{d\bar{R}_i}{dt} = \dot{x}_j \hat{i}_j + \dot{y}_j \hat{j}_j + \dot{z}_j \hat{k}_j$$

$$(\text{with } \bar{R} = x_j \hat{i}_j + y_j \hat{j}_j + z_j \hat{k}_j),$$

$\bar{\omega}_{ij}$ is the angular velocity of S_j with respect to S_i .

Thus,

$$\bar{H} = \sum_m \bar{R}_i \times m_i \frac{d\bar{R}_i}{dt} + \sum_T m_i \bar{R}_i \times (\bar{\omega}_{1s} \times \bar{R}_i),$$

since

$$\frac{d\bar{R}_i}{dt} = 0 \quad \text{for } \bar{R}_i \subset s.$$

Also,

$$\sum_T m_i \bar{R}_i \times (\bar{\omega}_{1s} \times \bar{R}_i) = \phi(T, S_s) \bar{\omega}_{1s},$$

where

$\Phi(T, S_s)$ is the inertia tensor of the total body computed with respect to S_s .

For $\bar{R}_i \subset m$, let $\bar{R}_i = \bar{c} + \bar{r}_i$. So,

$$\begin{aligned} \sum_m \bar{R}_i \times m_i \frac{d \bar{R}_i}{dt} &= \sum_m (\bar{c} + \bar{r}_i) \times m_i \left(\frac{d \bar{c}}{dt} + \frac{d \bar{r}_i}{dt} + \bar{\omega}_{sm} \times \bar{r}_i \right) \\ &= \sum_m (\bar{c} + \bar{r}_i) \times m_i (\bar{\omega}_{sm} \times \bar{r}_i) \\ &= \sum_m \bar{c} \times m_i (\bar{\omega}_{sm} \times \bar{r}_i) + \Phi(m, S_m) \bar{\omega}_{sm} . \end{aligned}$$

Hence,

$$\bar{H} = \Phi(T, S_s) \bar{\omega}_{1s} + \Phi(m, S_m) \bar{\omega}_{sm} + M_m \bar{c} \times (\bar{\omega}_{sm} \times \bar{r}_o) ,$$

where

\bar{r}_o vector from the terminus of \bar{c} (origin of S_m) to the center of mass of m ,

M_m mass of m .

If several systems, m_i , are present, then

$$\bar{H} = \Phi(T, S_s) \bar{\omega}_{1s} + \sum_i \left(\Phi(m_i, S_{mi}) \bar{\omega}_{smi} + M_{mi} \bar{c}_i \times (\bar{\omega}_{smi} \times \bar{r}_{oi}) \right) .$$

If each of the systems are connected to s at their center of mass, then $\bar{r}_{oi} = 0$. So, in this case,

$$\bar{H} = \Phi(T, S_s) \bar{\omega}_{1s} + \sum_i \Phi(m_i, S_{mi}) \bar{\omega}_{smi} .$$

APPENDIX B
INERTIA TENSOR OF THE SOLAR ARRAY

APPENDIX B

INERTIA TENSOR OF THE SOLAR ARRAY

Figure 1B represents the approximation of the dynamic configuration of the spacecraft which will be used to compute its inertia tensor. The solar array is represented by two rectangular thin plates which are both tipped out of the plane defined by \hat{k}_7 and the rotation axis of the array. This tip angle, σ , is used to position the panels more nearly in the sun's direction. The angle, σ , is a constant, but β increases by 360° in an orbital period.

To aid in the computation of the solar array inertia tensor, introduce a system, S_p , with origin at the center of mass of the right-hand panel as pictured. Let \hat{i}_p be normal to the panel, and let \hat{j}_p and \hat{k}_p be parallel to its edges. Then,

$$\Phi(R, S_p) = \frac{M_s}{24} \begin{pmatrix} \ell_1^2 + \ell_2^2 & 0 & 0 \\ 0 & \ell_2^2 & 0 \\ 0 & 0 & \ell_1^2 \end{pmatrix}$$

is the inertia tensor of the right-hand panel, computed with respect to S_p . Here,

- M_s total solar array mass,
- ℓ_1 panel width,
- ℓ_2 panel length.

Recall that \hat{j}_7 is a principal direction of the spacecraft without the solar array. This direction is nominally that of the pitch axis, which, in turn, is nominally that of the axis of rotation of the array.

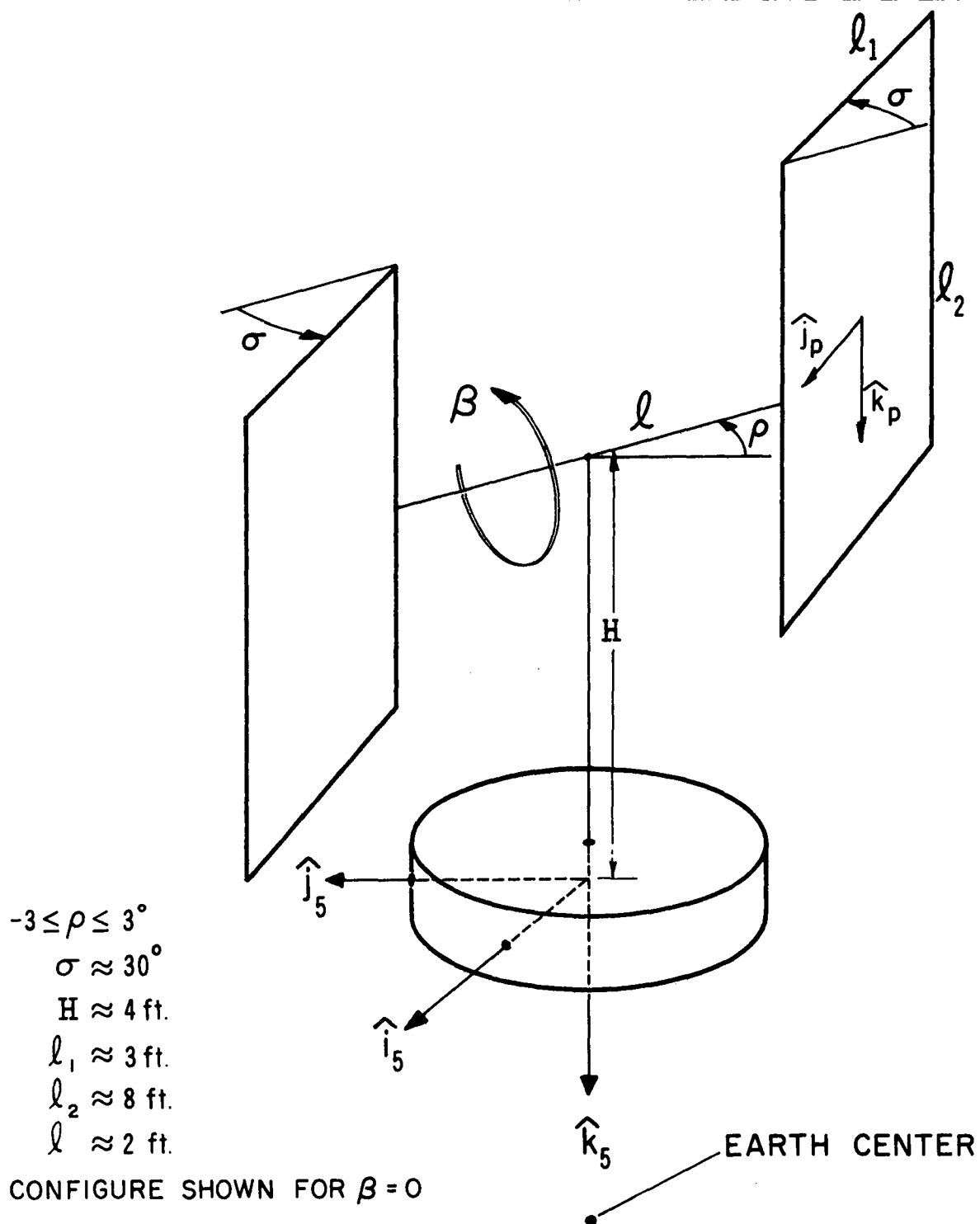


Figure 1B: Dynamic Configuration of the Spacecraft.

Now the orientation of S_p with respect to S_7 is defined by the angles ρ , β , and σ as follows:

$$\begin{aligned}\hat{j}_7 &\rightarrow \hat{j}_7' && \text{rotation } -\rho \text{ about } \hat{k}_7 = \hat{k}_7', \\ \hat{k}_7' &\rightarrow \hat{k}_7'' && \text{rotation } \beta \text{ about } \hat{j}_7' = \hat{j}_7'', \\ \hat{i}_7'' &\rightarrow \hat{i}_p && \text{rotation } -\sigma \text{ about } \hat{k}_7'' = \hat{k}_p.\end{aligned}$$

Hence,

$$\begin{aligned}\begin{pmatrix} \hat{i}_p \\ \hat{j}_p \\ \hat{k}_p \end{pmatrix} &= \begin{pmatrix} \cos \sigma & -\sin \sigma & 0 \\ \sin \sigma & \cos \sigma & 0 \\ 0 & 0 & 1 \end{pmatrix} \begin{pmatrix} \cos \beta & 0 & -\sin \beta \\ 0 & 1 & 0 \\ \sin \beta & 0 & \cos \beta \end{pmatrix} \begin{pmatrix} \cos \rho & -\sin \rho & 0 \\ \sin \rho & \cos \rho & 0 \\ 0 & 0 & 1 \end{pmatrix} \begin{pmatrix} \hat{i}_7 \\ \hat{j}_7 \\ \hat{k}_7 \end{pmatrix} \\ &= S \begin{pmatrix} \hat{i}_7 \\ \hat{j}_7 \\ \hat{k}_7 \end{pmatrix}, \quad S = (s_{ij}).\end{aligned}$$

As before, let S_{m4} be parallel to S_7 , but with origin at the center of mass of the array. Then, a vector from the origin of S_{m4} to the origin of S_p is (Figure 1B)

$$-\ell \hat{j}_7' - \frac{\ell_1}{2} \hat{j}_p = -\left(\frac{\ell_1}{2} s_{21} + \ell \sin \rho\right) \hat{i}_7 - \left(\frac{\ell_1}{2} s_{22} + \ell \cos \rho\right) \hat{j}_7 - \frac{\ell_1}{2} s_{23} \hat{k}_7$$

$$\Phi(R, S_{m4}) = \frac{M_s}{2} \begin{pmatrix} h_2^2 + h_3^2 & -h_1 h_2 & -h_1 h_3 \\ -h_1 h_2 & h_1^2 + h_3^2 & -h_2 h_3 \\ -h_1 h_3 & -h_2 h_3 & h_1^2 + h_2^2 \end{pmatrix}$$

$$+ S' \Phi(R, S_p) S$$

where

$$S' = S^T,$$

$$h_1 = -\left(\frac{\ell_1}{2} s_{21} + \ell \sin \rho\right),$$

$$h_2 = -\left(\frac{\ell_1}{2} s_{22} + \ell \cos \rho\right),$$

$$h_3 = -\frac{\ell_1}{2} s_{23}.$$

The above expressions yield the inertia tensor for the right-hand panel. For the left-hand panel, the function is obtained by evaluation at $-\ell, -\ell_1$. The same matrix, S , is assumed for both panels (that is, the panels are assumed to remain parallel). Hence,

$$\Phi_S = \Phi(R, S_{m4}) + \Phi(L, S_{m4}) = \Phi(m_4, S_{m4})$$

$$= \frac{M_s \ell_1^2}{3} \begin{pmatrix} 1 - s_{21}^2 & -s_{21} s_{22} & -s_{21} s_{23} \\ & 1 - s_{22}^2 & -s_{22} s_{23} \\ & & 1 - s_{23}^2 \end{pmatrix}$$

$$+ \frac{M_s \ell_2^2}{12} \begin{pmatrix} 1 - s_{31}^2 & -s_{31} s_{32} & -s_{31} s_{33} \\ & 1 - s_{32}^2 & -s_{32} s_{33} \\ & & 1 - s_{33}^2 \end{pmatrix}$$

$$+ M_s \ell \begin{bmatrix} \cos \rho (\ell \cos \rho + \ell_1 a_{22}) & -\frac{\ell_1}{2} \cos \beta \sin \sigma + \ell \sin \rho \cos \rho & -\frac{\ell_1}{2} a_{23} \sin \rho \\ & \sin \rho (\ell \sin \rho + \ell_1 a_{21}) & -\frac{\ell_1}{2} a_{23} \cos \rho \\ & & \ell + \ell_1 \cos \sigma \end{bmatrix}$$

If it is assumed that $\rho = 0$, then the above expression can be greatly simplified. This simplification has been used. Hence,

$$\Phi_s = \begin{pmatrix} c_1 + q_1 \cos 2\beta & -q_2 \cos \beta & -q_1 \sin 2\beta \\ & c_2 & q_2 \sin \beta \\ & & c_1 - q_1 \cos 2\beta \end{pmatrix},$$

where

$$c_1 = \left[\frac{\ell_1^2}{3} \left(1 - \frac{1}{2} \sin^2 \sigma \right) + \ell^2 + \frac{1}{24} \ell_2^2 + \ell \ell_1 \cos \sigma \right] M_s,$$

$$c_2 = \frac{1}{3} (\ell_1^2 \sin^2 \sigma + \frac{1}{4} \ell_2^2) M_s,$$

$$q_1 = \frac{1}{6} (-\ell_1^2 \sin^2 \sigma + \frac{1}{4} \ell_2^2) M_s,$$

$$q_2 = \ell_1 \sin \sigma \left(\frac{1}{3} \ell_1 \cos \sigma + \frac{1}{2} \ell \right) M_s.$$

APPENDIX C
THE SKEW-SYMMETRIC MATRIX $\dot{A}A'$ AND THE ANGULAR VELOCITY

APPENDIX C

THE SKEW-SYMMETRIC MATRIX $\dot{A}A'$ AND THE ANGULAR VELOCITY

In the derivation of the equations of motion, it was expedient to trace the following path:

- (1) Write the angular momentum of the body with components in the body-fixed system, S_7 .
- (2) Transform this vector into one with components in the inertial system, S_1 .
- (3) Set the time derivative of the transformed vector equal to the external torque (components in S_1).
- (4) Transform both members of the equality obtained in step 3 into vectors with components in the body-fixed system.

This process introduced a matrix of the form $\dot{A}A'$, where A is a 3×3 orthonormal matrix. Since the form of this matrix may not be well known, a short discussion concerning its relationship to angular velocity is now given.

Theorem 1:

For any position \bar{R} , there exists a unique \bar{q} , independent of \bar{R} , such that

$$\frac{d_i \bar{R}}{dt} = \frac{d_j \bar{R}}{dt} + \bar{q} \times \bar{R},$$

where

$$\frac{d_i \bar{R}}{dt} = \dot{x}_i \hat{i}_i + \dot{y}_i \hat{j}_i + \dot{z}_i \hat{k}_i.$$

Here x_i , y_i , and z_i are the component of \bar{R} in S_i .

Proof of Existence

Let

$$\begin{pmatrix} \hat{i}_j \\ \hat{j}_j \\ \hat{k}_j \end{pmatrix} = A \begin{pmatrix} \hat{i}_i \\ \hat{j}_i \\ \hat{k}_i \end{pmatrix},$$

where A may be a non-constant function of time. Hence,

$$\begin{pmatrix} x_i \\ y_i \\ z_i \end{pmatrix} = A' \begin{pmatrix} x_j \\ y_j \\ z_j \end{pmatrix}, \quad A' = A^T,$$

$$\begin{pmatrix} \dot{x}_i \\ \dot{y}_i \\ \dot{z}_i \end{pmatrix} = A' \begin{pmatrix} \dot{x}_j \\ \dot{y}_j \\ \dot{z}_j \end{pmatrix} + \dot{A}' \begin{pmatrix} x_j \\ y_j \\ z_j \end{pmatrix},$$

$$A \begin{pmatrix} \dot{x}_i \\ \dot{y}_i \\ \dot{z}_i \end{pmatrix} = \begin{pmatrix} \dot{x}_j \\ \dot{y}_j \\ \dot{z}_j \end{pmatrix} + \dot{A}A' \begin{pmatrix} x_j \\ y_j \\ z_j \end{pmatrix}.$$

Now, the matrix $\dot{A}A'$ is skew-symmetric for

$$AA' = I, \text{ the } 3 \times 3 \text{ identity,}$$

$$\dot{A}A' + \dot{A}A' = 0,$$

$$\dot{A}A' + (A'A)' = 0,$$

which proves the skew-symmetry. Hence,

$$A \begin{pmatrix} \dot{x}_i \\ \dot{y}_i \\ \dot{z}_i \end{pmatrix} = \begin{pmatrix} \dot{x}_j \\ \dot{y}_j \\ \dot{z}_j \end{pmatrix} + \begin{pmatrix} 0 & -q_3 & q_2 \\ q_3 & 0 & -q_1 \\ -q_2 & q_1 & 0 \end{pmatrix} \begin{pmatrix} x_j \\ y_j \\ z_j \end{pmatrix}.$$

Expressing this result in vector notation completes the existence.

Proof of Uniqueness

Suppose there exists $\bar{q}_1 \neq \bar{q}_2$, then $(\bar{q}_1 - \bar{q}_2) \times \bar{R} = 0$ for all \bar{R} ; but this is impossible. This completes the proof of this classical theorem.

Notation:

\bar{q} is written $\bar{q} = \bar{\omega}_{ij}$, and is called the angular velocity of S_j with respect to S_i .

Corollary:

If

$$\begin{pmatrix} \hat{i}_j \\ \hat{j}_j \\ \hat{k}_j \end{pmatrix} = A \begin{pmatrix} \hat{i}_i \\ \hat{j}_i \\ \hat{k}_i \end{pmatrix},$$

then

$$\dot{A}A' = \begin{pmatrix} 0 & -\omega_3 & \omega_2 \\ \omega_3 & 0 & -\omega_1 \\ -\omega_2 & \omega_1 & 0 \end{pmatrix} \Rightarrow \dot{A} = - \begin{pmatrix} 0 & -\omega_3 & \omega_2 \\ \omega_3 & 0 & -\omega_1 \\ -\omega_2 & \omega_1 & 0 \end{pmatrix} A,$$

where

$$\bar{\omega}_{ij} = \omega_1 \hat{i}_j + \omega_2 \hat{j}_j + \omega_3 \hat{k}_j .$$

The proof is contained in the proof of Theorem 1.

The corollary gives a constructive method of computing the components of $\bar{\omega}_{ij}$, but in practice this method is cumbersome. A second method will now be given (the standard method) which is a result of two simple theorems.

Theorem 2:

$$\bar{\omega}_{ik} = \bar{\omega}_{ij} + \bar{\omega}_{jk} .$$

Proof

$$\frac{d_i \bar{R}}{dt} = \frac{d_j \bar{R}}{dt} + \bar{\omega}_{ij} \times \bar{R} .$$

$$\frac{d_j \bar{R}}{dt} = \frac{d_k \bar{R}}{dt} + \bar{\omega}_{jk} \times \bar{R} .$$

So,

$$\frac{d_i \bar{R}}{dt} = \frac{d_k \bar{R}}{dt} + (\bar{\omega}_{ij} + \bar{\omega}_{jk}) \times \bar{R} .$$

Hence,

$$\bar{\omega}_{ik} = \bar{\omega}_{ij} + \bar{\omega}_{jk} .$$

Theorem 3:

If

$$\begin{pmatrix} \hat{i}_j \\ \hat{j}_j \\ \hat{k}_j \end{pmatrix} = \begin{pmatrix} \cos \theta & \sin \theta & 0 \\ -\sin \theta & \cos \theta & 0 \\ 0 & 0 & 1 \end{pmatrix} \begin{pmatrix} \hat{i}_i \\ \hat{j}_i \\ \hat{k}_i \end{pmatrix},$$

then

$$\bar{\omega}_{ij} = \dot{\theta} \hat{k}_i = \dot{\theta} \hat{k}_j.$$

Proof

$$\dot{A}A' = \dot{\theta}A \begin{pmatrix} -\sin \theta & -\cos \theta & 0 \\ \cos \theta & -\sin \theta & 0 \\ 0 & 0 & 0 \end{pmatrix} = \dot{\theta} \begin{pmatrix} 0 & -1 & 0 \\ 1 & 0 & 0 \\ 0 & 0 & 0 \end{pmatrix},$$

so the corollary implies the stated result.

Example

$$\hat{i}_1 \rightarrow \hat{i}_2 \text{ rotation } \varphi \text{ about } \hat{k}_1 = \hat{k}_2.$$

$$\hat{k}_2 \rightarrow \hat{k}_3 \text{ rotation } \theta \text{ about } \hat{i}_2 = \hat{i}_3.$$

What is $\bar{\omega}_{13}$?

Solution 1

$$\bar{\omega}_{13} = \bar{\omega}_{12} + \bar{\omega}_{23} = \dot{\varphi} \hat{k}_1 + \dot{\theta} \hat{i}_3 = \dot{\theta} \hat{i}_3 + \dot{\varphi}(\sin \theta \hat{j}_3 + \cos \theta \hat{k}_3).$$

Solution 2

$$A = \begin{pmatrix} \cos \varphi & \sin \varphi & 0 \\ -\cos \theta \sin \varphi & \cos \theta \cos \varphi & \sin \theta \\ \sin \theta \sin \varphi & -\sin \theta \cos \varphi & \cos \theta \end{pmatrix}.$$

$$\dot{A} = \dot{\varphi} \begin{pmatrix} -\sin \varphi & \cos \varphi & 0 \\ -\cos \theta \cos \varphi & -\cos \theta \sin \varphi & 0 \\ \sin \theta \cos \varphi & \sin \theta \sin \varphi & 0 \end{pmatrix}$$

$$+ \dot{\theta} \begin{pmatrix} 0 & 0 & 0 \\ \sin \theta \sin \varphi & -\sin \theta \cos \varphi & \cos \theta \\ \cos \theta \sin \varphi & -\cos \theta \cos \varphi & -\sin \theta \end{pmatrix}.$$

So

$$\dot{A}A' = \dot{\varphi} \begin{pmatrix} 0 & -\cos \theta & \sin \theta \\ \cos \theta & 0 & 0 \\ -\sin \theta & 0 & 0 \end{pmatrix} + \dot{\theta} \begin{pmatrix} 0 & 0 & 0 \\ 0 & 0 & -1 \\ 0 & 1 & 0 \end{pmatrix}.$$

Hence,

$$\bar{\omega}_{13} = \dot{\theta} \hat{i}_3 + \dot{\varphi} \sin \theta \hat{j}_3 + \dot{\varphi} \cos \theta \hat{k}_3.$$

APPENDIX D
THE EXTERNAL TORQUE

APPENDIX D

THE EXTERNAL TORQUE

The formulas which are used to compute the external torques will now be stated without derivation. Three sources of torques are assumed; namely, solar pressure, gravity gradient, and magnetic.

Solar Pressure

$$\bar{T}_7 \text{ (solar pressure)} = 2.0 \times 10^{-5} \begin{pmatrix} \sin \sigma \\ \cos \sigma \cos \nu \\ 0 \end{pmatrix} \text{ lb force - ft}$$

if $0 \leq \nu \leq 112.5^\circ$
or $247.5^\circ \leq \nu \leq 472.5^\circ$,

= 0 elsewhere.

In deriving this expression, it was assumed the sun is at the equator, and sunlight only impinges upon the solar panels. The following numerical values were assumed:

$$\begin{aligned} P &= 9.4 \times 10^{-8} \text{ lb force/ft}^2 \text{ (solar pressure constant),} \\ \epsilon_0 &= .1 \text{ (panel albedo),} \\ H &= 4 \text{ ft,} \\ l_1 &= 3 \text{ ft,} \\ l_2 &= 8 \text{ ft (see Figure 1B).} \end{aligned}$$

Gravity Gradient

$$\bar{T}_7 \text{ (gravity gradient)}$$

$$= 3\nu^2 \begin{pmatrix} (C_1 - B_1 - q_1 \cos 2\beta)\varphi - q_2 \theta \cos \beta - q_2 \sin \beta \\ (C_1 - A_1 - 2q_1 \cos 2\beta)\theta - q_2 \varphi \cos \beta - q_1 \sin 2\beta \\ q_2 \varphi \cos \beta - q_2 \theta \sin \beta \end{pmatrix}.$$

Magnetic Moment Torque \bar{T}_7 (magnetic moment)

$$= K \begin{pmatrix} \cos \dot{\nu} t (-\theta M_2 - \psi M_3) + 2 \sin \dot{\nu} t (M_2 + \varphi M_3) \\ \cos \dot{\nu} t (M_3 + \theta M_1) + 2 \sin \dot{\nu} t (\theta M_3 - M_1) \\ \cos \dot{\nu} t (\psi M_1 - M_2) + 2 \sin \dot{\nu} t (-\varphi M_1 - \theta M_2) \end{pmatrix},$$

where

$$-M_2 = M_1 = M_3 = 3,000 \text{ pole-cm},$$

$$K = 1.477 \times 10^{-8} \text{ lb force - ft/pole-cm}.$$

The expression was obtained from an unpublished G. E. document.

APPENDIX E

DETERMINATION OF APPROXIMATE INGRESS, EGRESS, AND TRANSIT TIME

APPENDIX E

DETERMINATION OF APPROXIMATE INGRESS, EGRESS, AND TRANSIT TIME

As an aid to the star identification, it is desirable to compute the approximate time any star enters the field of view (ingress), leaves the field of view (egress), and transits the slit. These approximate times may be obtained by assuming the spacecraft has its nominal attitude, that is, roll, pitch, and yaw are zero.

In this study, each star is assumed identified, so the identification problem is not considered. The approximate ingress, egress, and transit times are needed since initial estimates are required to obtain the exact transit times (necessary for a simulation since measurements are not made) via a recursive method.

Approximate Transit Time

If $\psi = \theta = \varphi = 0$, then from Equation (16)

$$0 = B_1(\gamma) S(\sigma, \beta) B(-\nu) \hat{h}$$

at the instant the star transits the slit (the subscripts i and j have been dropped). This equation is simply one equation in the unknown transit time. The true anomaly, ν , and the slit orientation angle, γ , are given functions of time. So,

$$0 = (\cos \gamma, 0, \sin \gamma) S(\sigma, 0) \begin{pmatrix} \cos(\nu - \beta)h_1 + \sin(\nu - \beta)h_3 \\ h_2 \\ -\sin(\nu - \beta)h_1 + \cos(\nu - \beta)h_3 \end{pmatrix} \quad (1E)$$

or

$$0 = a \cos(\nu - \beta) + b \sin(\nu - \beta) + c,$$

where

$$a = \cos \gamma h_1 - \sin \gamma \cos \sigma h_3,$$

$$b = \sin \gamma \cos \sigma h_1 + \cos \gamma h_3,$$

$$c = \sin \gamma \sin \sigma h_3 \stackrel{\Delta}{=} v h_3.$$

Hence,

$$\begin{aligned} \sin (\nu-\beta) &= \frac{-b v h_2 \pm a \sqrt{1-v^2-h_2^2}}{(1-h_2^2)(1-v^2)}, \\ \cos (\nu-\beta) &= \frac{-a v h_2 \mp b \sqrt{1-v^2-h_2^2}}{(1-h_2^2)(1-v^2)}. \end{aligned} \quad (2E)$$

A problem remains as to which of the above signs are to be used in Equation (2E). This choice may be resolved by determining $\cos \eta$ and $\sin \eta$ from Equation (15). Hence,

$$\cos \eta = B_2 S(\sigma, 0) \begin{pmatrix} \cos (\nu-\beta) h_1 + \sin (\nu-\beta) h_3 \\ h_2 \\ -\sin (\nu-\beta) h_1 + \cos (\nu-\beta) h_3 \end{pmatrix}$$

or

$$(1-v^2) \cos \eta = h_2 \cos \sigma \mp \sin \sigma \cos \gamma \sqrt{1-v^2-h_2^2}.$$

Similarly,

$$(1-v^2) \sin \eta = -h_2 \cos \gamma \sin \sigma \mp \cos \sigma \sqrt{1-v^2-h_2^2}.$$

Now all transits must be such that $0 \leq \eta \leq 90^\circ$; also, the cant angle, σ , will be chosen such that $0 \leq \sigma \leq 90^\circ$. So, if $\cos \gamma > 0$, the lower sign must be chosen. If $\cos \gamma < 0$, the upper sign must be chosen if $\sigma > r_2 = \eta_{\max}$ (one-half the field of view).

Hence, if γ is a given constant (passive system), the approximate time of transit may be obtained as follows:

$$t = t_0 + \frac{1}{\dot{\gamma}} \tan^{-1} \frac{-b v h_2 \pm a \sqrt{1 - v^2 - h_2^2}}{-a v h_2 \mp b \sqrt{1 - v^2 - h_2^2}}, \quad (3E)$$

where the upper sign is chosen if $\cos \gamma > 0$, and the lower sign if $\cos \gamma < 0$ and $\sigma > r_2$. The quadrant is chosen by the sign of the numerator and denominator. A circular orbit is assumed (that is, $\dot{v} = \text{constant}$).

If γ is not given (active system), then Equation (3E) is not a solution for the transit time. In this case, we assume

$$\gamma = \gamma_0 + \dot{\gamma} t,$$

where γ_0 and $\dot{\gamma}$ are given constants and $\dot{\gamma} \gg \dot{v}$. Equation (1E) may be written

$$0 = A \cos \gamma + B \sin \gamma,$$

where

$$A = h_1 \cos (v - \beta) + h_3 \sin (v - \beta),$$

$$B = \cos \sigma (-h_3 \cos (v - \beta) + h_1 \sin (v - \beta)) + \sin \sigma h_3.$$

Hence,

$$\sin \gamma = \frac{\pm A}{\sqrt{A^2 + B^2}},$$

$$\cos \gamma = \frac{\mp B}{\sqrt{A^2 + B^2}}.$$

But,

$$\sin n = \pm \sqrt{A^2 + B^2},$$

therefore,

$$\tan \gamma = \frac{A}{-B}.$$

Thus, the transit time may be found from the recursive relationship

$$t_{i+1} = -\gamma_0 + \frac{1}{\dot{\gamma}} \tan^{-1} \frac{A(t_i)}{-B(t_i)},$$

which converges for $\dot{\gamma} \gg \dot{v}$.

Approximate Ingress and Egress

At ingress or egress, the angle between the star and \hat{j}_9 is r_2 , the half field of view angle. Hence,

$$\cos r_2 = (0, \cos \sigma, \sin \sigma) \begin{pmatrix} \cos (v-\beta)h_1 + \sin (v-\beta)h_3 \\ h_2 \\ -\sin (v-\beta)h_1 + \cos (v-\beta)h_3 \end{pmatrix}.$$

So, at an ingress or egress,

$$\sin (v-\beta) = \frac{-h_1 c \pm h_3 \sqrt{(p-h_2)(h_2-q)}}{\sin \sigma (1-h_2^2)},$$

$$\cos (v-\beta) = \frac{-h_3 c \pm h_1 \sqrt{(p-h_2)(h_2-q)}}{\sin \sigma (1-h_2^2)},$$

where

$$c = \cos \sigma h_2 - \cos r_2 ,$$

$$p = \cos (\sigma + r_2) ,$$

$$q = \cos (\sigma - r_2) .$$

Note from Figure 2 that for $0 \leq \sigma \leq 90^\circ$, $\hat{i}_9 \cdot \hat{h} \leq 0$ at ingress, and $\hat{i}_9 \cdot \hat{h} \geq 0$ at egress. But,

$$\hat{i}_9 \cdot \hat{h} = \frac{\pm \sqrt{(p-h_2)(h_2-q)}}{\sin \sigma} .$$

So, choose lower sign for ingress, upper for egress.